Advanced Control Methodology for Biomass Combustion

Stefan Bjornsson

A thesis submitted in partial fulfillment of the requirements for the degree of

Master of Science in Mechanical Engineering

University of Washington

2014

Committee:

Igor V. Novosselov, Chair
Philip C. Malte
John C. Kramlich

Program Authorized to Offer Degree:
Department of Mechanical Engineering

Table of Contents

List of Figures

List of Tables

Abstract

This thesis presents a feasibility study for a low cost sensor-based combustion control system using a predictive chemical kinetic model that captures efficiencies and pollution emissions during biomass combustion. Low cost sensor module was developed, the sensors were calibrated to measure carbon monoxide and particulate matter (PM) in combustion exhaust. Major combustion species in the exhaust of a commercial biomass furnace, operating with white oak, were measured. The species concentrations were measured using the low cost sensors and commercially available diagnostics. The low cost sensor outputs compare well with the reference instruments and the sensors can be employed to measure varying concentration of CO and particulate matter in combustion exhaust.

A predictive chemical kinetic model was generated to simulate biomass processes. The model uses a four element chemical reactor network (CRN) and successfully simulates smoldering, ignition and flaming combustion events. The model agrees with concentration of CO and particulate matter from experiments.

The sensors and CRN model can be integrated in a control system for biomass combustion that can potentially improve combustion efficiency and reduce emissions of particulate matter, CO and unburned hydrocarbons that have been linked to urban and rural air pollution resulting in adverse health effects.

Chapter 1
Introduction

1.1 Motivation

The demand for energy is increasing and continues to contribute to a steady rise in carbon dioxide (CO_2) concentrations in the atmosphere. Energy derived from biomass combustion holds the promise of reducing net carbon dioxide emissions. Biomass growth by photosynthesis absorbs CO_2, so the overall process is generally considered CO_2-neutral. Biomass power plants are less efficient (14,000 Btu/kWh)[1] compared to plants operating with fossil fuels such as coal (10,500 Btu/kWh), petroleum (11,000 Btu/kWh) or natural gas (8,000 Btu/kWh)[2] and authorities continue to implement more stringent emissions limits, forcing development of more advanced systems.

Small-scale biomass furnaces are considered a significant source of particulate matter (PM) since well-proven and established PM emission reduction technologies are prohibitively expensive and only economically viable for medium- to large-scale applications. In addition, for a specific furnace technology, the biomass combustion process depends on multiple factors such as fuel composition, format, and placement in the combustion furnace and air distribution. An overview of factors influencing combustion efficiency is shown in Figure 1.1. This multivariable dependence complicates meeting continuously decreasing emission limits for operation when using a diversity of fuel types. Different combustion technologies are available for fuels of varying qualities, with low-quality and inexpensive fuels requiring sophisticated combustion systems. Therefore, only medium-scale and large-scale systems are presently appropriate for burning cheap, low-quality biomass fuels. This motivates

developing a new inexpensive and effective combustion control solutions for small scale and residential biomass furnaces to be operated with a variety of fuels.

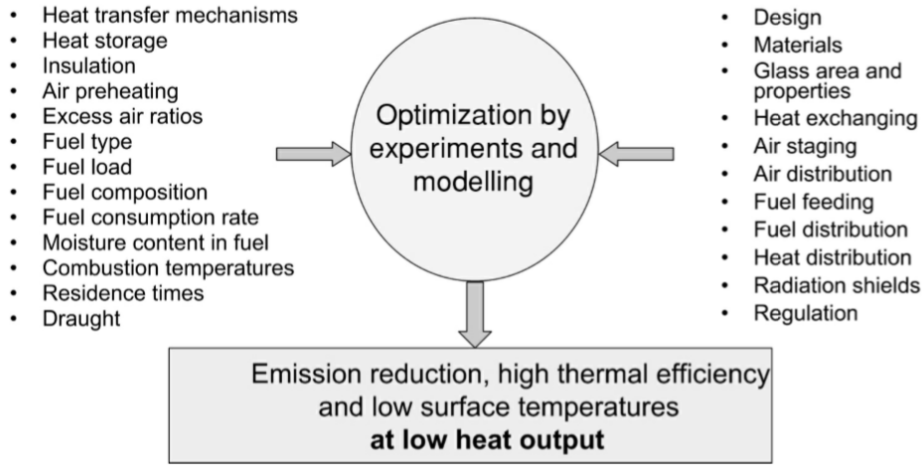

Figure 1.1: Overview of factors influencing biomass combustion [3].

In this study, batch combustion of white oak in a biomass furnace under various operating conditions is described in detail and compared to the predictions of the CRN model. In a separate part of the study, low-cost sensor outputs are compared to outputs of reference instruments.

1.2 Objectives

The objectives of this study are:

1. Develop a sensor module consisting of low-cost sensors to be employed in a biomass control system. Calibrate the CO and particulate matter sensors and deploy sensor module to measure combustion exhaust.
2. Perform burns in a biomass furnace and measure gases and particulate matter with commercial instruments and inexpensive sensors.

3. Compare measurement obtained by commercial combustion diagnostics to low-cost sensor outputs.
4. Analyze combustion processes in the experimental furnace.
5. Develop a chemical reactor network (CRN) to simulate combustion processes.
6. Evaluate feasibility of integrating the sensor module and CRN model to an advanced biomass combustion control algorithm to be employed in residential and small-scale industrial biomass combustion furnaces.

Chapter 2
Literature Review & Fundamental Concepts

This chapter reviews fundamental biomass combustion processes, previous biomass combustion studies, chemical kinetics, chemical kinetic modeling, and pollutant formation in biomass combustion. These fundamental concepts and results from previous studies are used to analyze combustion processes in this study and to design a CRN model for a biomass furnace.

2.1 Biomass

This section reviews chemical components of biomass and briefly discusses its role in the energy portfolio.

Biomass is created by the process of photosynthesis where water and carbon dioxide react to form glucose ($C_6H_{12}O_6$) and oxygen. This reaction occurs in living plants and in some bacteria. Photosynthesis and plant respiration are responsible for producing a complex array of carbohydrates and other compounds, including cellulose, hemicelluloses, lignin, lipids, proteins, simple sugars, starches, hydrocarbons, ash and water. The major chemical constituents of woody biomass are cellulose, hemicellulose and lignin. Figure 2.1 (right) demonstrates the cellulose chain - a polysaccharide consisting of long chains of glucose molecules which are attached by glycosidic bonds. Hydroxyl (OH) and hydroxymethyl (CH_2OH) groups reside on each glucose site. These groups are highly reactive and susceptible to chemical attacks. Lignocellulosic biomass is a composite of cellulose fibers in a matrix of hemicellulose and lignin, as shown in Figure 2.1 (left). Biomass generally consists of 38-50%

cellulose, 23-32% hemicellulose and 15-25% lignin [4]. Hemicellulose consists of various sugars, other than glucose, and encase the cellulose fibers. Lignin is a high molecular weight polymer and provides strength to the wood fiber and operates as a glue to hold the hemicellulose in place. Figure 2.2 demonstrates a lignin fragment. Hardwoods in general contain more hemicellulose and less lignin compared to softwoods.

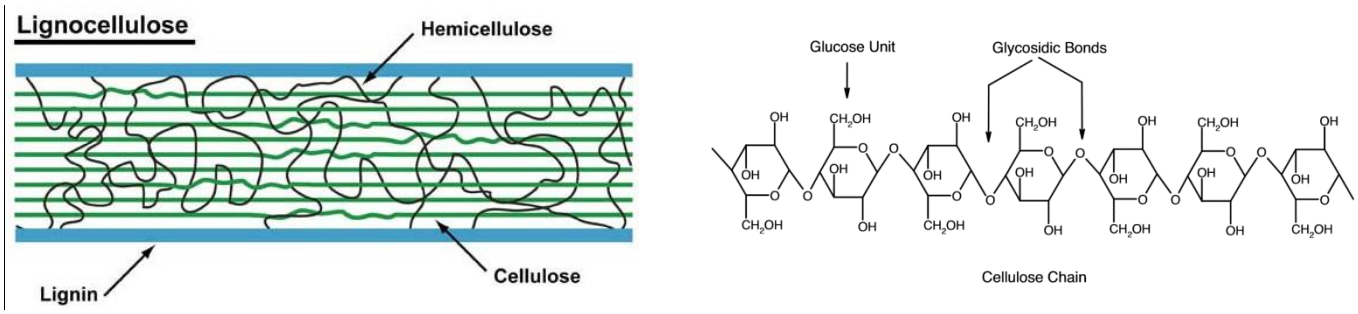

Figure 2.1: Left: Lignocellulose – a matrix of cellulose and hemicellulose held together by lignin [5].

Right: Cellulose consists of a chain of glucose molecules attached by glycosidic bonds. [6].

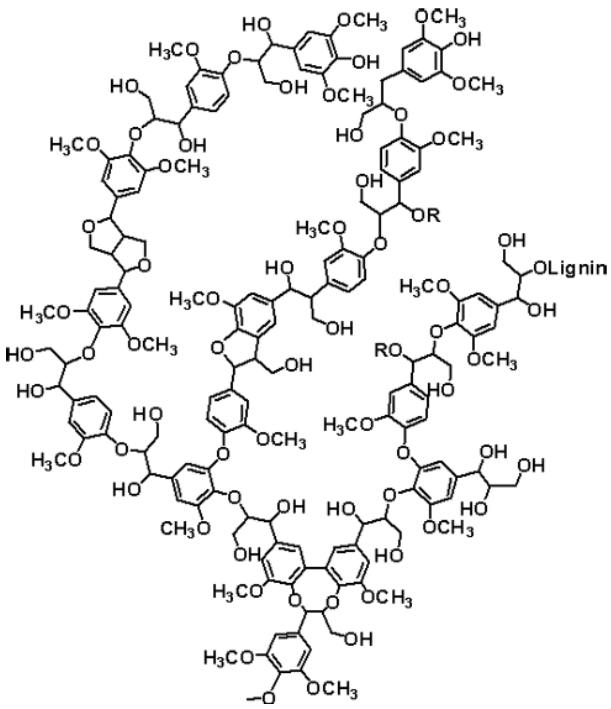

Figure 2.2: Lignin fragment [7].

Biomass has provided a decreasing share of total energy resources since the Industrial Revolution when it was superseded by high energy density fuels such as coal, peat, gas and oil. As concerns about energy security, resource depletion, and global warming grow, biomass is becoming an increasingly important part of the energy portfolio. The same amount of CO_2 absorbed by biomass during its growth, due to the photosynthetic process, is released as it dies and decomposes or is burned. Biomass is in that sense considered CO_2 neutral and a renewable source of energy as long as it is based on sustainable biomass production. Energy derived from biomass is projected to be the largest non-hydroelectric renewable resource of electricity in the U.S between 2000 and 2020. Biomass fuels provided about 5% of the energy used in the United States in 2013. Of the 5%, about 45% was from wood and wood-derived biomass, 44% was from biofuels, and about 11% was from municipal waste [8]. Researchers continue to develop ways to use more biomass for fuel. Table 2.1 summarizes energy sources for any use in residential homes in the U.S. in 2009. Approximately 13 million homes used wood as an energy source for residential use [9].

Table 2.1: Energy sources used for any use in residential homes in the United States in 2009 [9].

Fuels Used for Any Use	**Total Housing Units (millions)**
Electricity	113.6
Natural Gas	69.2
Propane/LPG	48.9
Wood	13.1
Fuel Oil	7.7
Kerosene	1.7
Solar	1.2

2.2 Biomass Combustion

Combustion is an exothermal reaction between fuel and oxygen to form mainly carbon dioxide and water vapor. Although various kinetic models exist for the biomass combustion process, it is generally classified into four steps as demonstrated in Figure 2.3:

1. Heating and drying
2. Solid fuel pyrolysis
3. Gas phase pyrolysis and volatile combustion
4. Char oxidation

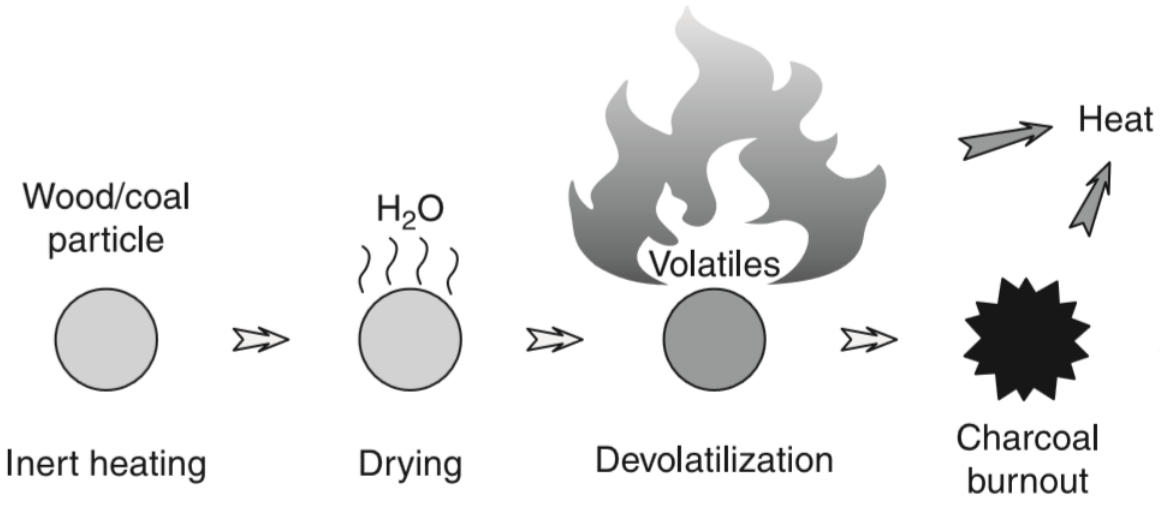

Figure 2.3: Sequential stages of wood combustion Figure from [10].

These steps are sequential for small wood particles but they can occur simultaneously in larger particles and in wood logs. The individual steps are briefly reviewed below.

2.2.1 Heating & Drying

During the combustion process, wood is heated from ambient temperature to the pyrolysis temperature. This is an endothermic process and depends on several heat transfer parameters, including the specific heat of the biomass. An external energy source (e.g. wall radiation or heat of combustion) vaporizes water, decreasing temperature of the combustion process. Biomass moisture can be either free or bound and is a very important variable in fuel composition. Bound moisture is water adsorbed into the wood microstructure while water absorbed by capillary uptake is referred to as free moisture. Moisture increases the energy required to heat wood up to the pyrolysis temperature, limits core temperature of the fuel particle, increases thermal conductivity and heat capacity and reduces flame temperature. Energy required to evaporate water from the wood is the sum of energy required to heat the wood, energy required to heat water and energy required for vaporization of water[11].

2.2.2 Solid Particle Pyrolysis

Pyrolysis, or devolitilization, is the thermal decomposition in the absence of oxygen. Pyrolysis starts when the biomass surface reaches temperature just below 500 K and glycosidic linkages (Figure 2.1) break down. A series of chemical reactions follow which split molecules into gases. The products are heavy hydrocarbons (tars), low molecular weight gases which escape by advection and diffusion. Products such as acetic acid and acetaldehyde are generated and break down to form methane, ethylene, carbon monoxide and carbon dioxide. Gas products from lignin pyrolysis also include CO, CO_2, CH_4 and C_2H_6. Solid state pyrolysis of biomass is experimentally studied in isothermal or steadily heated

environments. Figure 2.4 shows the results of TGA (thermogravimetric analysis) and DTG (derivative thermogravimetric analysis) experiments. Small wood samples (2 mm x 2 mm x 0.2 mm) were suspended on a microbalance and exposed to a heating rate of 10 °K/min, exposing the sample to temperatures between 300 and 773 K. Weight changes were recorded (upper figure) and weight change derivative calculated (lower figure). Initially, drying occurs and devolitilization starts at approximately 200 °C (473 K). Volatiles are driven off faster as the temperature is raised. At 400 °C (673 K), rate of devolitilization decreases and mostly char remains. Two separate regions of weight loss can be identified from the DTG results, drying and devolatilization. The devolatilization contains a plateau at a lower temperature, corresponding to the decomposition of hemicellulose, and a peak representing the degradation of cellulose. The hemicellulose content of hardwoods (acacia, beech white and birch) is greater compared to softwoods (spruce) and therefore the plateau region is less observable for spruce. Weight lost from 673 – 773 K corresponds to the decomposition of lignin. The remaining char can be converted to activated carbon. The amount of char is strongly influenced by the heating rate.

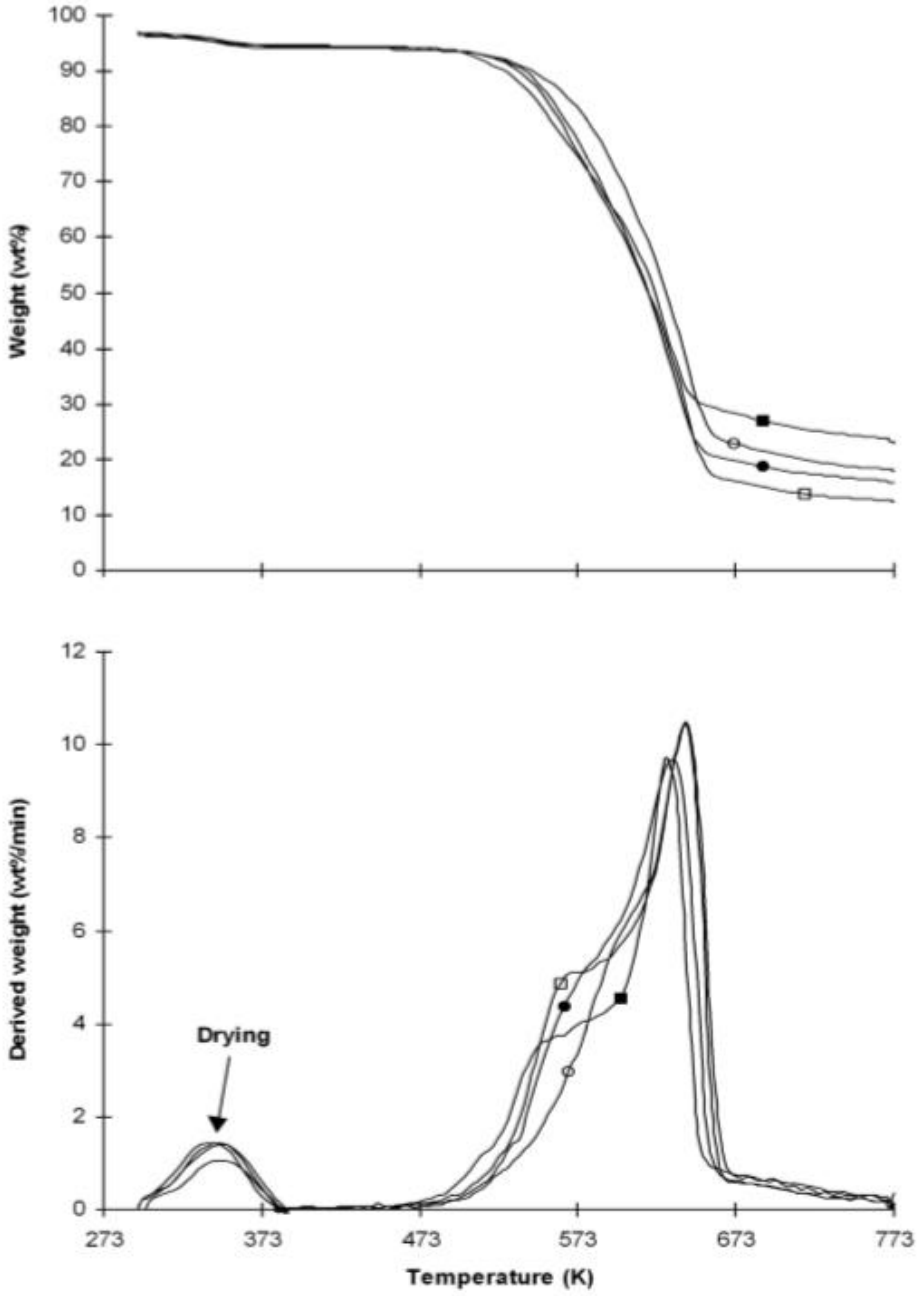

Note: ❍ = spruce, □ = birch, ● = beech white, ■ = acacia. 5mg samples heated at a rate of 10°C/min

Figure 2.4: TGA and DTG results of four wood samples. Figure taken from Van Loo [3].

Figure 2.5 shows TGA (upper) and DTG (lower) results for white oak to be similar to Figure 2.4. The conversion is defined as $X = \frac{W-W_0}{W_0-W_\infty}$ where W is the weight of the sample, W_0 is the original sample mass and W_∞ is the residual sample mass.

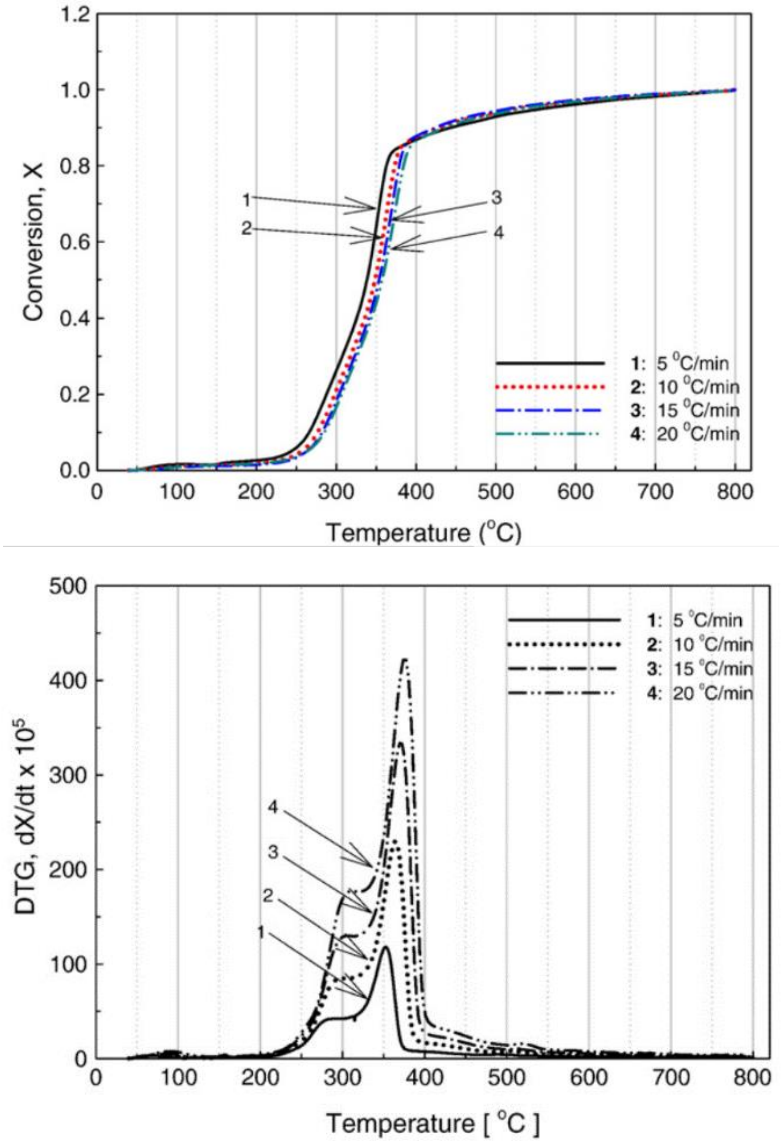

Figure 2.5: TGA and DTG analysis of white oak [12].

2.2.3 Gas Phase Pyrolysis & Volatile Combustion

The gas phase oxidation involves secondary devolitilization of tars to gases and volatile combustion of those gases. Combustible gases released from the wood will burst into an orange-yellow diffusion flame upon mixing with air.

2.2.4 Char oxidation

After volatiles have been driven off the wood particle a layer of porous carbon, char, is left over. The dynamic of char combustion resembles that of burning lump charcoal or briquettes for cooking. Char contains free radical sites for O_2 attacks. Oxygen and carbon dioxide diffuse towards the char particle and interact with the solid carbon according to:

2.1 $$CO_2 + C(s) \longrightarrow 2[CO]_s$$

2.2 $$2[CO]_s \longrightarrow 2CO$$

2.3 $$2CO + O_2 \longrightarrow 2CO_2$$

where $[CO]_s$ is carbon monoxide attached to the solid surface. The reaction rate is determined by the rate of oxygen diffusion to the char surface and the chemistry rate at the surface. The net reaction of char combustion can be expressed as:

2.4 $$C(s) + O_2 \longrightarrow CO_2.$$

As the char oxidation stage dominates, the burn rate will be dramatically reduced as shown in Figure 2.6

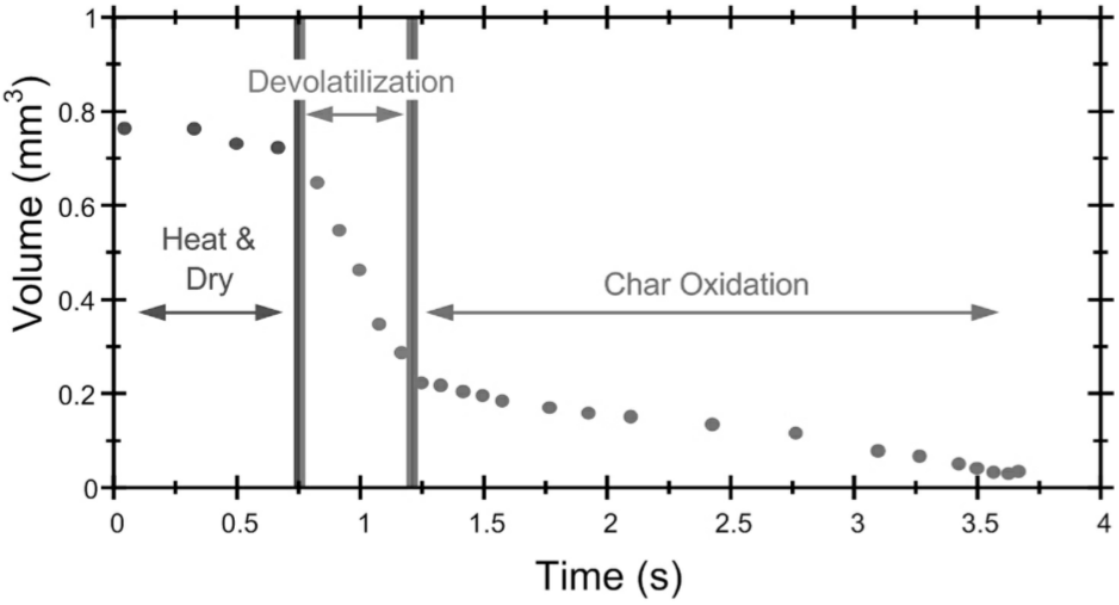

Figure 2.6: Major stages in combustion of a solid biomass particle [3].

2.3 Chemical Kinetics

Complete combustion of a hydrocarbon fuel with excess air can be represented in a global reaction of the form:

$$C_xH_yO_z + w\phi(O_2 + 3.76N_2) \longrightarrow xCO_2 + \frac{y}{2}H_2O + 3.76w\phi N_2 + w(\phi - 1)O_2 \quad 2.5$$

where $w = \frac{1}{2}\left(2x + \frac{y}{2} - z\right)$ and $\phi = \frac{{m_{fuel}}/{m_{ox}}}{\left({m_{fuel}}/{m_{ox}}\right)_{st}}$ is the ratio of the fuel-to-oxidizer ratio to the stoichiometric fuel-to-oxidizer ratio. At stoichiometric conditions, $\phi = 1$, all the carbon is converted to CO_2 and the hydrogen and oxygen form H_2O. A biomass combustion process can be expressed in a simplified manner as a global reaction:

$$C_xH_yO_zN_\alpha S_\beta + w\phi(O_2 + 3.76N_2) \longrightarrow aCO_2 + bH_2O + cO_2 + dN_2 + eCO + fNO + hNO_2 + iC_jH_k + mSO_2 + jN_2O \quad (2.6)$$

The coefficients (a-j) can be found by applying elemental balances and making assumptions about product composition and chemical equilibrium. However, in reality, hundreds of reversible elementary reactions are needed to describe the combustion process in detail and capture the formation of intermediate species and potential pollutants. Chemical kinetics is the study of the elementary reactions, their rates and species concentrations. Methane gas, for example, is a light hydrocarbon and an important intermediate in biomass combustion. A detailed description of methane combustion involving 325 elementary reactions of 53 species is given by GRI-Mech developed by the Gas Research Institute [13]. This is one of the most detailed and accepted description of methane combustion at present and includes an extensive database of rate coefficients and thermochemical data to describe elementary reactions.

The reaction rate of an elementary reaction depends on mixing through the availability of reactants in the flame zone, residence time and temperature through the reaction rate coefficient, k. For a bimolecular reaction of a fuel and oxidizer, the rate coefficient is defined as:

$$\text{Fuel} + \beta\ \text{Oxidizer} \longrightarrow \gamma\ \text{Poducts} \quad (2.7)$$

$$\frac{d(\text{Fuel})}{dt} = -k[\text{Fuel}][\text{Oxidizer}] \quad \text{mole}/(\text{m}^3\,\text{s}) \quad (2.8)$$

$$k(T) = A\exp\left(\frac{-E_A}{R_u T}\right) \quad \text{s}^{-1} \quad (2.9)$$

where A is the pre-exponential factor, E_A is the reaction activation energy, and R_u is the universal gas constant. A theoretical description of the temperature dependent pre-exponential factor, A, involves statistical mechanics, molecular collision theory and is outside the scope of this study. Further details can be found in Turns [14] and Glassman [15]. Equation 2.9 expresses the rate coefficient in Arrhenius form.

Biomass combustion involves solid pyrolysis and combustion of pyrolysis products. Predicting concentrations of species of interest and pollutants such as carbon monoxide, tars and nitrogen oxides requires simulating the combustion process as a multi-step chemical mechanism where the net rate of production of species i is expressed as:

2.10
$$\begin{aligned}\text{net production of species i} &= [\text{sum of all individual rates producing species i}] \\ &- [\text{sum of all individual rates destroying species i}]\end{aligned}$$

2.11
$$\frac{d[X_i]}{dt} = f_i\{\,[X_1](t), [X_2](t), \dots, [X_n](t)\,\} \qquad \text{mole}/(\text{m}^3\,\text{s})$$

where $[X_i](t)$ is the time dependent concentration of species i. An equation of the form 2.11 can be written for each species participating in the mechanism, yielding a system of differential equations which, with initial conditions and appropriate conservation equations for energy, mass and momentum can be solved numerically. Several models have been developed to simulate combustion systems. An extensive review is given by Di Blasi [16] and Prakash et al. [17].

2.4 Chemical Reactor Network Models

Flow fields can reach high levels of complexity in combustion systems. Applying computational methods to solve flow-related processes and chemical reactions simultaneously can be time consuming. A chemical reactor network (CRN) model is capable of simulating chemical processes by using the full chemical mechanism of combustion, offering fast convergence times towards predicting efficiency and pollutant emissions. A CRN is an arrangement of perfectly stirred reactor (PSR) and plug flow reactor (PFR) elements used to model combustion systems. A PSR (Figure 2.7 – left) achieves uniform mixing inside a control volume. Properties and chemical composition within the reactor are everywhere the same. A PFR (Figure 2.7 - right) is a frictionless-flow, steady-state reactor in which chemical composition and flow properties vary along its length.

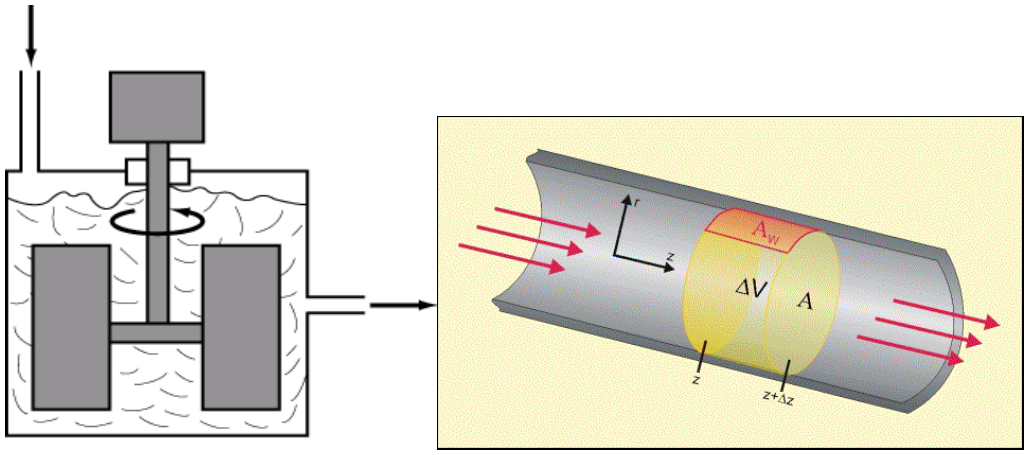

Figure 2.7: Left: PSR is a steady-state, steady-flow, perfectly mixed reactor. Right: PFR is a steady-state, steady-flow reactor and has no axial mixing.

Longitudinal mixing does not occur inside a PFR. Steady state species, mass, momentum and energy conservation equations can be solved for the reactor geometries. A mathematical description for the PSR and PFR reactors can be found in Turns [14] and Glassman [15].

An important parameter for chemical reactors is the residence time, τ, an average time gases spend inside the reactors, defined as

2.12 $$\tau = \frac{\rho V}{\dot{m}} \quad \text{s}$$

Figure 2.8 demonstrates a conceptual model of a gas turbine combustor using two PSR reactors with recycle (recirculation) and a PFR.

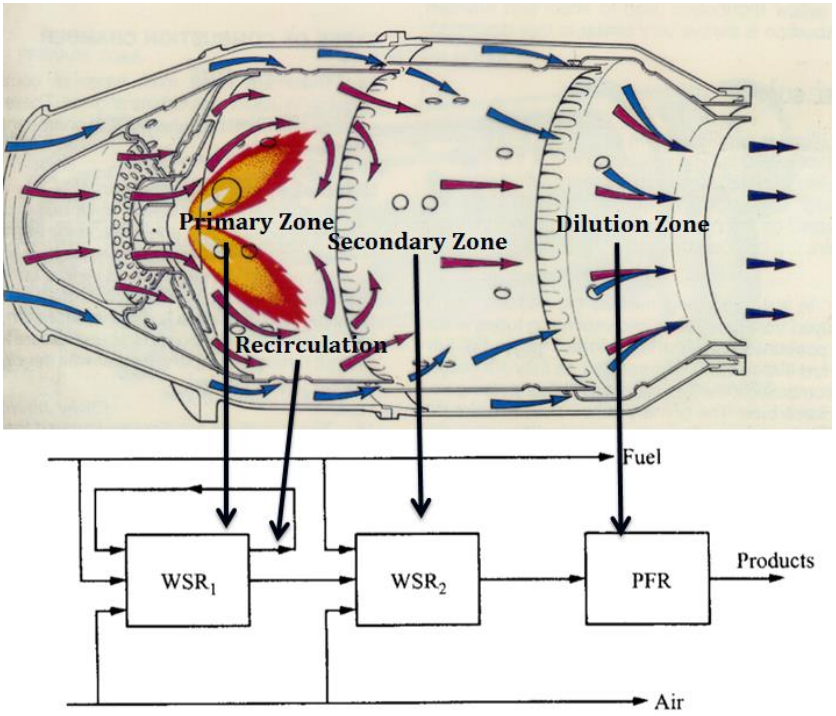

Figure 2.8: Gas turbine combustor modeled with a CRN consisting of two PSR elements and a PFR [14]. WSR stands for well stirred reactor and is practically equivalent to a PSR for the purpose of this figure.

The first PSR represents the primary combustion zone, the second PSR the secondary zone and the dilution zone is simulated with a PFR. Other CRN models have been successfully developed for combustion systems. Novosselov developed several CRNs to model combustion systems, including a gas turbine combustor [18] to generate simplified

mechanism for methane combustion at lean-premixed conditions and a wood burner operated with sawdust and sanderdust to predict pollutant emissions [19].

2.5 Pollutant Formation

Biomass combustion emissions are usually classified into two categories depending on if they are emitted from complete or incomplete combustion. Emissions from the first group include CO_2, NOx, SOx and particulate matter (PM) as inorganic minerals. Emissions from incomplete combustion include CO, unburned hydrocarbons (UHC), dioxins and PM as condensed tars, soot or organic minerals. In this study we are interested in CO and particulate matter. We will briefly review these pollutants of interest.

2.5.1 Carbon Monoxide

Conversion of fuel carbon to carbon dioxide occurs through multiple elementary reactions and pathways. Of the intermediate species formed, CO is one of the most important one and it oxidizes to CO_2 if enough oxygen is available. If the oxidation is incomplete, CO is released. Figure 2.9 shows the CO emission level as a function of excess air ratio for various biomass combustion systems. The CO concentration has a minimum value at a specific excess air ratio. A lot of excess air results in lower combustion temperatures while lower excess air ratios leads to fuel rich pockets and incomplete combustion. Sufficient residence time is also important to ensure low CO emission levels, primarily since CO generally appears late in the combustion process. At high temperatures, CO_2 can disassociate to form CO. Hydrogen and hydroxyl (OH) radicals are important intermediate species in CO oxidation. Dry fuels low in

hydrogen, e.g. charcoal, may lack adequate radical concentration to accomplish proper CO oxidation to CO_2 [3].

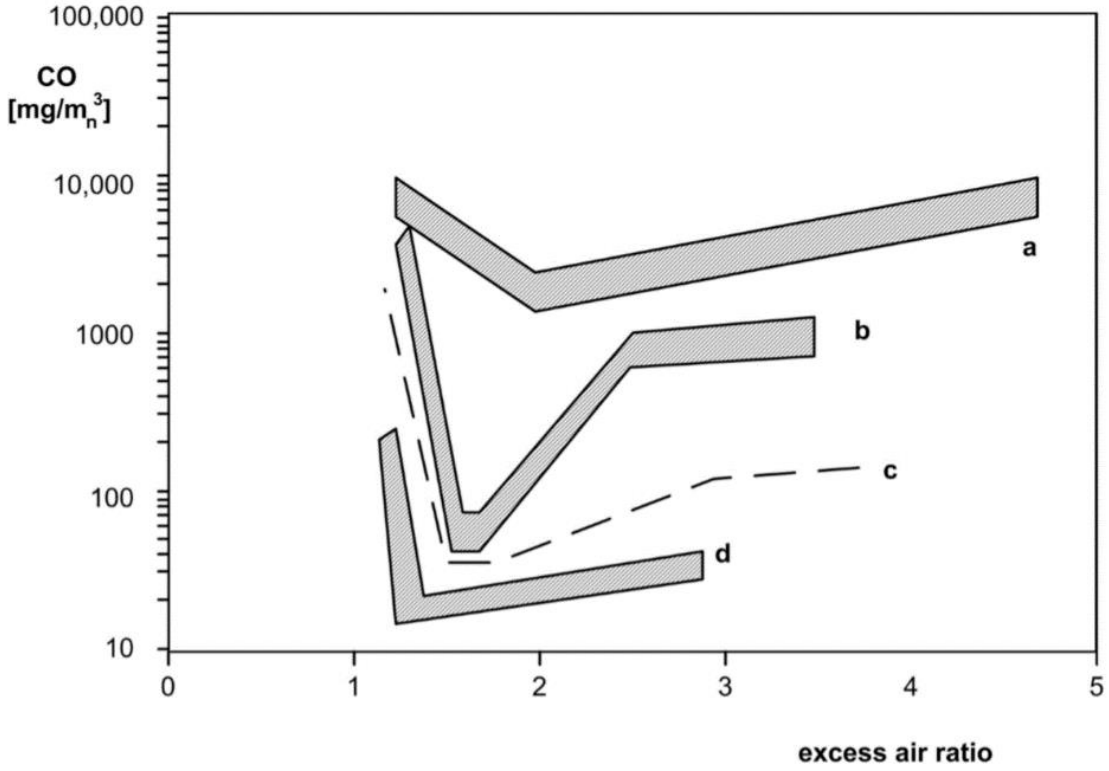

Figure 2.9: CO emissions from a) a simple, manually charged wood boiler b) a down-draught wood log boiler c) an automatic furnace with combustion technology as of 1990; d) an automatic furnace with enhanced combustion technology as of 1995 [20].

2.5.2 Particulate Matter

Particle emissions are generally classified as inorganic aerosols, black carbon (i.e. soot) and brown carbon. The formation of these pollutants and emissions from biomass furnaces are reviewed.

Inorganic aerosols: Consist of coarse fly-ashes (particles with a diameter larger than 1μm) which are ash (Ca, Mg, Si, K, Al) particles entrained in the flue gas. Fine salt particles (particles

with a diameter less than 1μm) are formed from heavy metal vapors (K, Na, S, Cl) during the combustion process by nucleation and condensation.

Soot: Polycyclic aromatic hydrocarbons (PAH) are intermediates in the conversion of fuel carbon to CO_2 and fuel hydrogen to water. PAH are precursors to soot formation, which is caused by agglomeration and coagulation of PAH as demonstrated in Figure 2.10

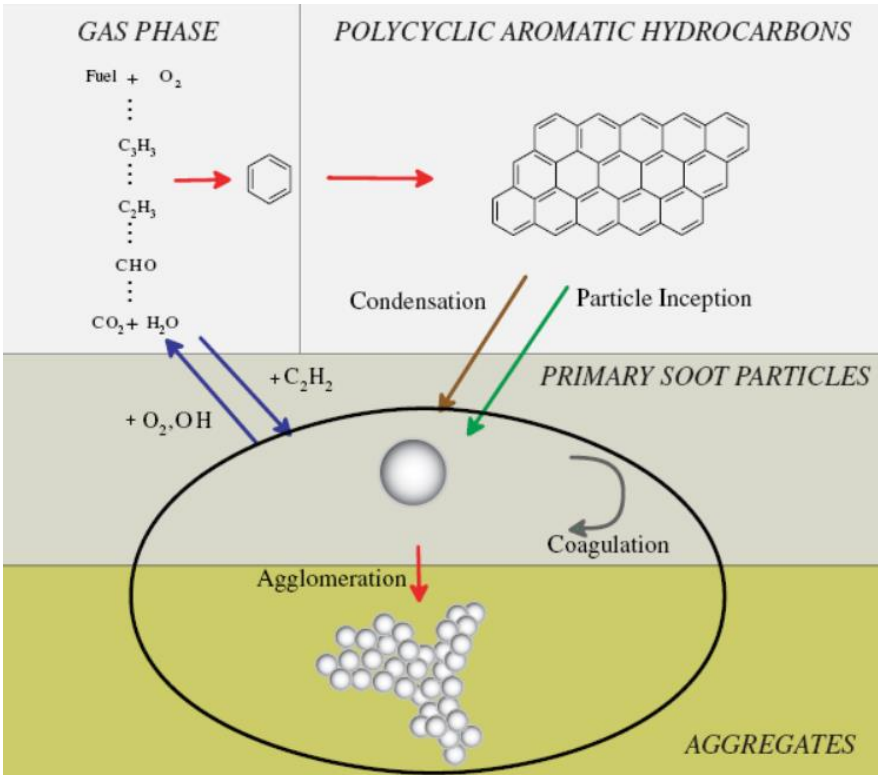

Figure 2.10: Graphical overview of soot formation from fuel species [7].

Soot is mutagenic, carcinogenic and inhaled particles form a serious health risk. During combustion, hydrocarbons undergo pyrolysis and can form aromatics which combine to form PAH (Figure 2.10). PAH and soot are primarily formed at low combustion temperatures, short residence times, in zones lacking oxygen or extinction regions. Figure 2.11 demonstrates CO and PAH concentration versus combustion temperature and shows

the competition between pyrolysis and oxidation rates. At low combustion temperatures, PAH form by pyrolysis and rate of release increases with larger temperatures but oxidation rate increases faster with increasing temperature [21],[21].

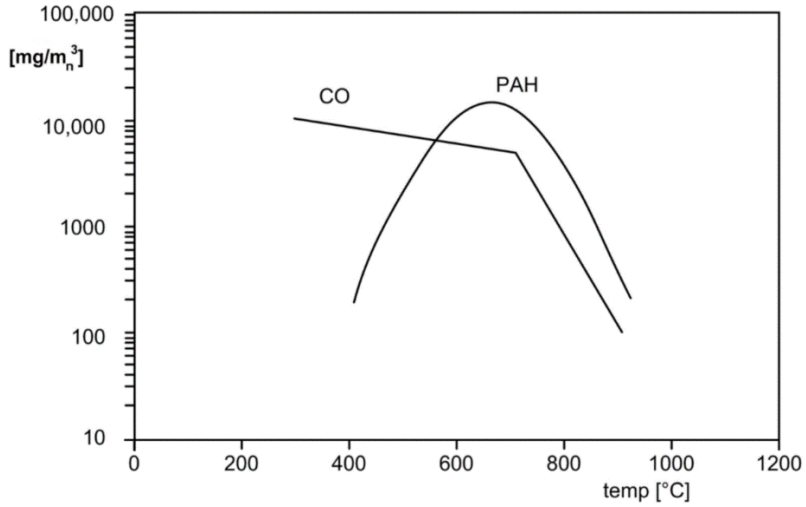

Figure 2.11: Evolution of CO and PAH with combustion temperature [3].

Diffusion flames are highly susceptible to soot formation since fuel and oxygen are separated before entering the combustion zone. Mixing of fuel and air starts in the flame and the range of fuel-air ratios is wide. During charcoal combustion, low density char particles may also get entrained in the flue gas, specifically at high flue gas velocities.

Brown Carbon: Another source of PM is condensed heavy hydrocarbons (tars) which are a product of wood pyrolysis. In zones at low temperature and oxygen, secondary pyrolysis (conversion of tars to gases) can be quenched resulting in formation of PM. If these particles are allowed to escape the white smoke is produced and the combustion efficiency decreases. Condensed heavy hydrocarbons are an important and in some cases the main contributor to

the total particle emission level in small-scale biomass combustion applications such as wood-stoves and fireplaces.

The Technical University of Munich measured emissions from domestic wood applications [22]. Their results are presented in Table 2.2.

Table 2.2: Arithmetic average values of pollutants from various small-scale sources. Emissions are reported at 13 % O_2 [22].

Combustion System	Load [kW]	CO [mg/m³]	Particles [mg/m³]	C_XH_Y [mg/m³]
Wood-Stove	9.33	4986	130	581
Fireplace Inserts	14.07	3326	50	373
Heat-storing stoves	13.31	2756	54	264

Skreiberg and Saanum[23] surveyed emissions from domestic and industrial biomass combustion systems from various IEA countries (Norway, Switzerland, Finland, UK, and Denmark) and reported their results. From wood boilers, tar content was 499 mg/MJ, CO 4975 mg/MJ, UHC (as Methane) 200 mg/MJ and PAH 26 μg/MJ [3].

Johansson et al. [24] did an extensive investigation on emissions from residential wood log and pellet furnaces under varying firing conditions. The reported size distribution of PM, normalized to 10% O_2, is shown in Figure 2.12 and Figure 2.13. Even though particle concentration varies depending on combustion technology, the size distribution remains unchanged. Most of the emitted particles were less than 1 micron in size and the concentration peaks at particle size around 130 nm. The number of particles emitted was reported to increase with emissions of un-oxidized gaseous compounds.

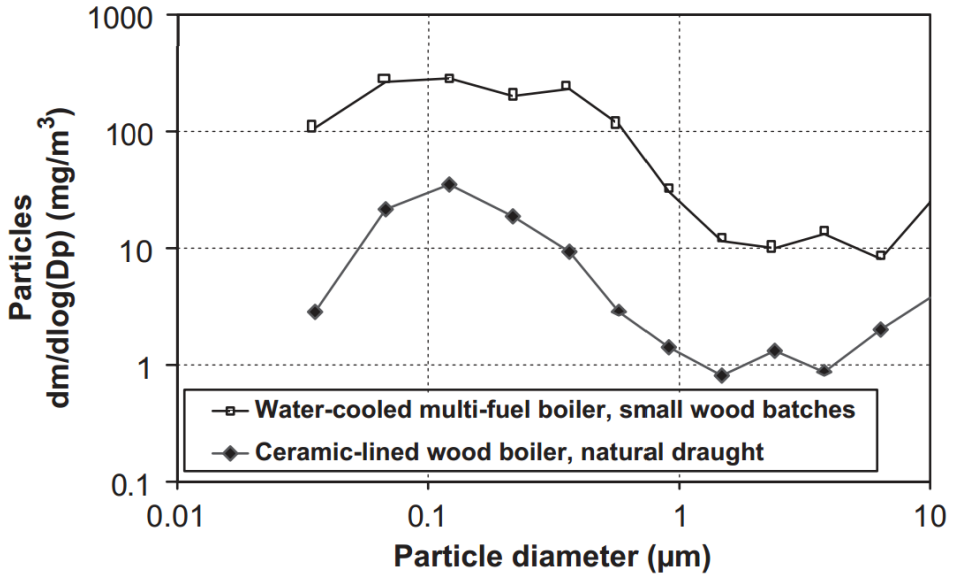

Figure 2.12: Particle size distribution of PM from residential wood furnaces on a mass basis [24] .

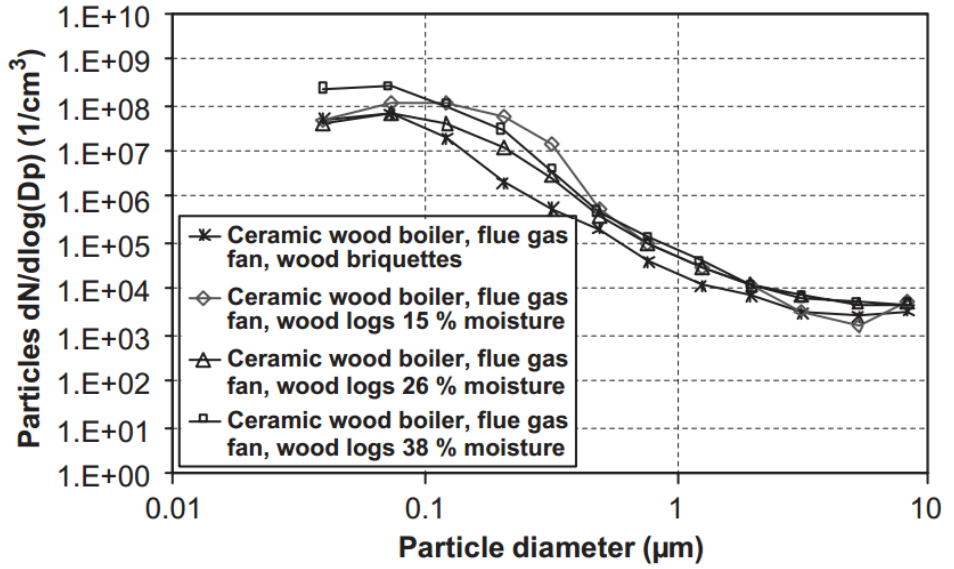

Figure 2.13: Number concentration of particles from residential wood furnaces [24].

Chapter 3
Experimental Data Collection & Results

This chapter describes the biomass furnace used for low-cost sensor evaluation and model development. The combustion of white oak in the biomass furnace was studied. Experimental results for concentration of gas species of interest and particulate matter are presented.

3.1 Furnace Description

The principle of operation of the biomass over-fire wood log furnace used for the experiments is demonstrated in Figure 3.1. This is a commercially available residential wood furnace which uses a fixed bed, forced draft technology and is used to heat water with energy released from biomass combustion.

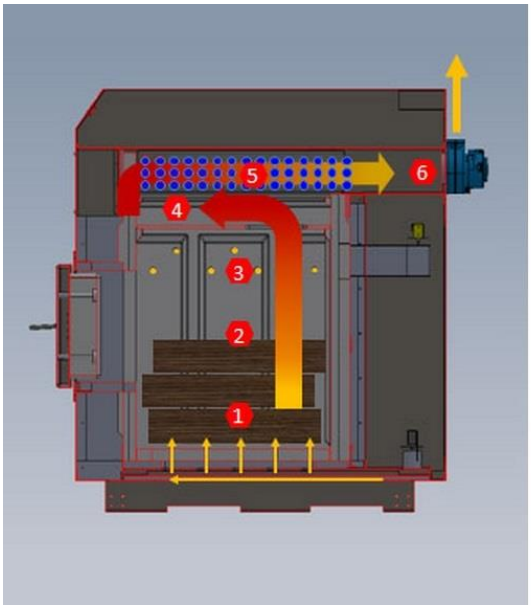

1. UNDER-FIRE ZONE: Under-fire air from the pinhole grate drives the rate of pyrolysis.
2. COMBUSTION ZONE
3. CROSSFIRE ZONE: Over-fire air is added following the separation of gases from the wood pile.
4. BURN-OUT ZONE: Combustion is completed in the burn-out zone
5. HEAT EXCHANGE ZONE: Heat is transferred to the water-tube heat exchanger in an isolated chamber. This is the only area where heat is transferred to water.
6. EXHAUST ZONE: Exhaust gases leave the boiler at temperatures of 250 - 450° F depending on firing rate.

Figure 3.1: Experimental biomass furnace

Dimensional lumber or cord wood is placed on the furnace floor which has an array of small air inlets - the under-fire zone (Figure 3.2). The walls are made of ceramic material and are a source of radiative heat required for biomass pyrolysis. Volatile gases from wood pyrolysis are driven up and mix with under-fire air which oxidizes hydrocarbon gases in the combustion zone. At this point, the fuel gases have ignited and a diffusion flame is established over the fuel. Secondary air in the crossfire zone serves to break up major flame structures and to oxidize residual hydrocarbons and CO in the burn-out zone. The secondary cross-fire air inlets are located on each side-wall. Hot gases from the combustion process are transferred to a heat-exchanger. Combustion products leave the furnace through the exhaust zone. The air flow rates are controlled by a fan which determines the under- and over-fire air flow rates. The air intake by each zone is controlled by an automated solenoid vent. Temperatures are measured at various point in the furnace, our main interest are the firebox and burn-out zone measurements. Figure 3.2 shows white oak being burned in the furnace.

Figure 3.2: White Oak burning in the biomass furnace.

Fixed bed combustion systems are capable of using fuels with high moisture, varying size distribution, high ash and moisture content and large variety of fuel mixtures. Fixed bed systems are also inexpensive compared to fluidized bed and suspension combustion technology. The downside involves drying, pyrolysis and char oxidation processes occurring irregularly on the grate. Volatile formation can be uneven and rich fuel volatile zones can be formed and secondary air may be unable to fully oxidize the volatiles before the flue gases leave the furnace - resulting in pollutant emissions. As a result, large amount of excess air, which decreases efficiency, is necessary to oxidize the volatiles [25], [3]. Large versions of these furnaces are often installed outdoors in rural parts of North America for residential and commercial use.

3.2 Experimental Setup

Figure 3.3 demonstrates the experimental setup for data acquisition of combustion gases and PM concentration. The exhaust stack is sampled at two locations, one for gas species of interest and the other for aerosols. For gas analysis, a Bacharach ECA-450 combustion efficiency and environmental analyzer is employed to measure CO, CO_2, unburned hydrocarbons and O_2. An aerodynamic particle counter (TSI-3321) measures the aerodynamic diameter and concentration of aerosols. A dilution system mixes filtered air with the sample exhaust gas to reduce the aerosol concentration to the operational range of the diagnostics. The dilution ratio is determined by the diameter of capillary sampling tubes and the settings of a pump pulling the exhaust samples. Low cost sensors for PM and carbon monoxide are placed in series and their signal compared to the commercial instruments. The furnace is located on a scale that measures fuel weight and allows for calculation of

devolatilization rates. Further technical information about the dilution system and the low cost sensor can be found in the appendix, sections A.1 through A.4

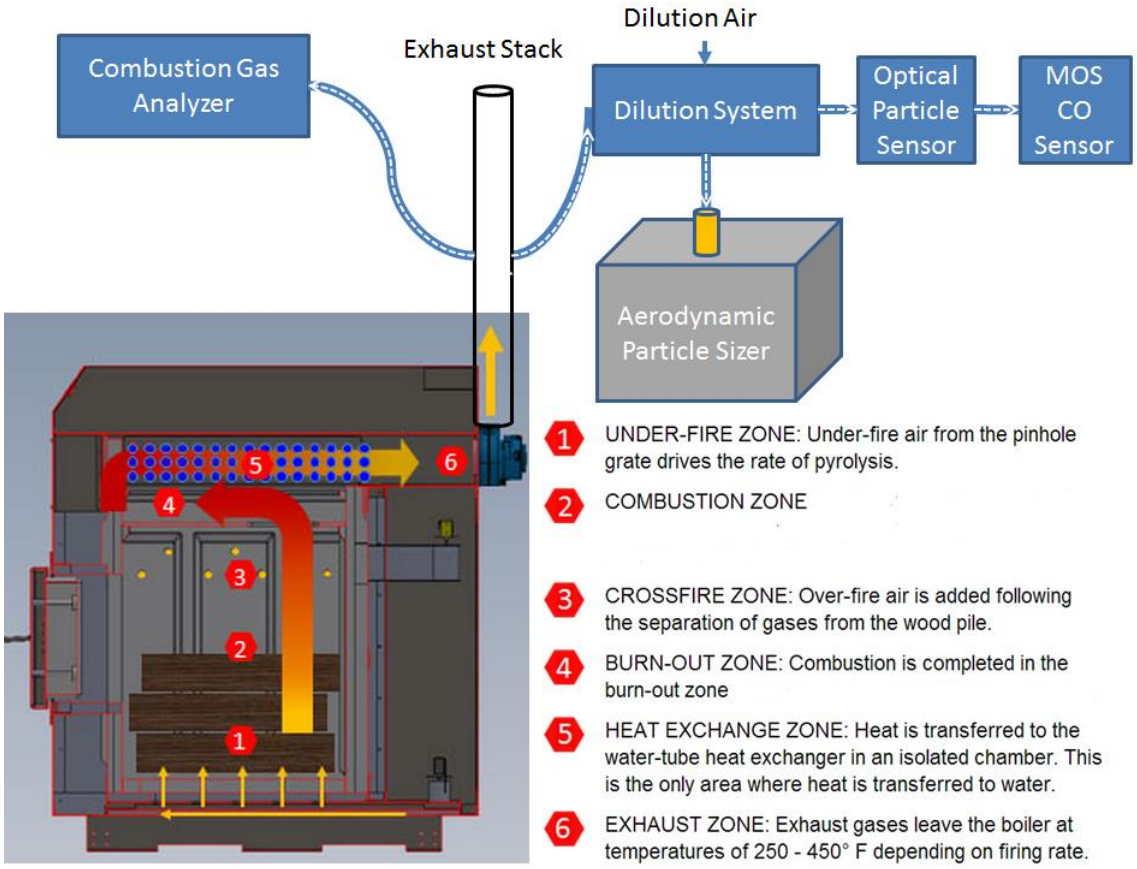

Figure 3.3: Experimental furnace and data acquisition system.

3.3 Experimental Results

3.3.1 Dec. 12th 2013 Burn

Figure 3.4 shows fuel burned in one experiment, 47 lbs. white oak. This experiment was done on Dec. 12th 2013. The fuel consists of 6 pieces of wood stock with dimensions of 4 x 2 x 15 inches, along with 4 pieces with 4 x 4 x 15 inch dimensions. The dimensional lumber is stacked orthogonally in three layers.

The average moisture content of the wood logs is 17 % with standard deviation of 0.02 %. Table 3.1 lists average elementary composition of white oak based on proximate and ultimate analysis results [26]. Ignoring nitrogen and sulfur content yields $C_{4.22}H_{6.10}O_{2.68}$.

Figure 3.4: White oak fuel used in one of the experiments.

Table 3.1: Experimental White Oak composition [26].

CompoundsCompounds	**%**
Volatile Matter	73
Fixed Carbon	8.5
Moisture	18.5
Carbon	50.60
Oxygen	42.90
Hydrogen	6.10
Nitrogen	0.30
Sulfur	0.10
$C_{4.22}H_{6.10}O_{2.68}$	

The biomass furnace was operated using normal air staging as recommended by manufacturer.

Figure 3.5 shows the weight of the white oak fuel in the furnace with time. The figure also shows temperatures in the firebox and burn-out zone. Three distinguishable regimes are noticeable from these results. During the first few minutes, fuel is being heated and drying occurs. When the fuel is placed in the furnace it gets heated by radiation from the hot ceramic walls. Moisture evaporates from the wood surface. Temperature decreases in the burn-out zone. Smoldering occurs and a few local ignition regions may exist on the exposed wood surfaces, resulting in increasing firebox temperature. This is a smoldering regime of the combustion process. Approximately 5 minutes into the experiment, a major ignition event occurs followed by flaming combustion. Rate of fuel weight loss and temperatures increase.

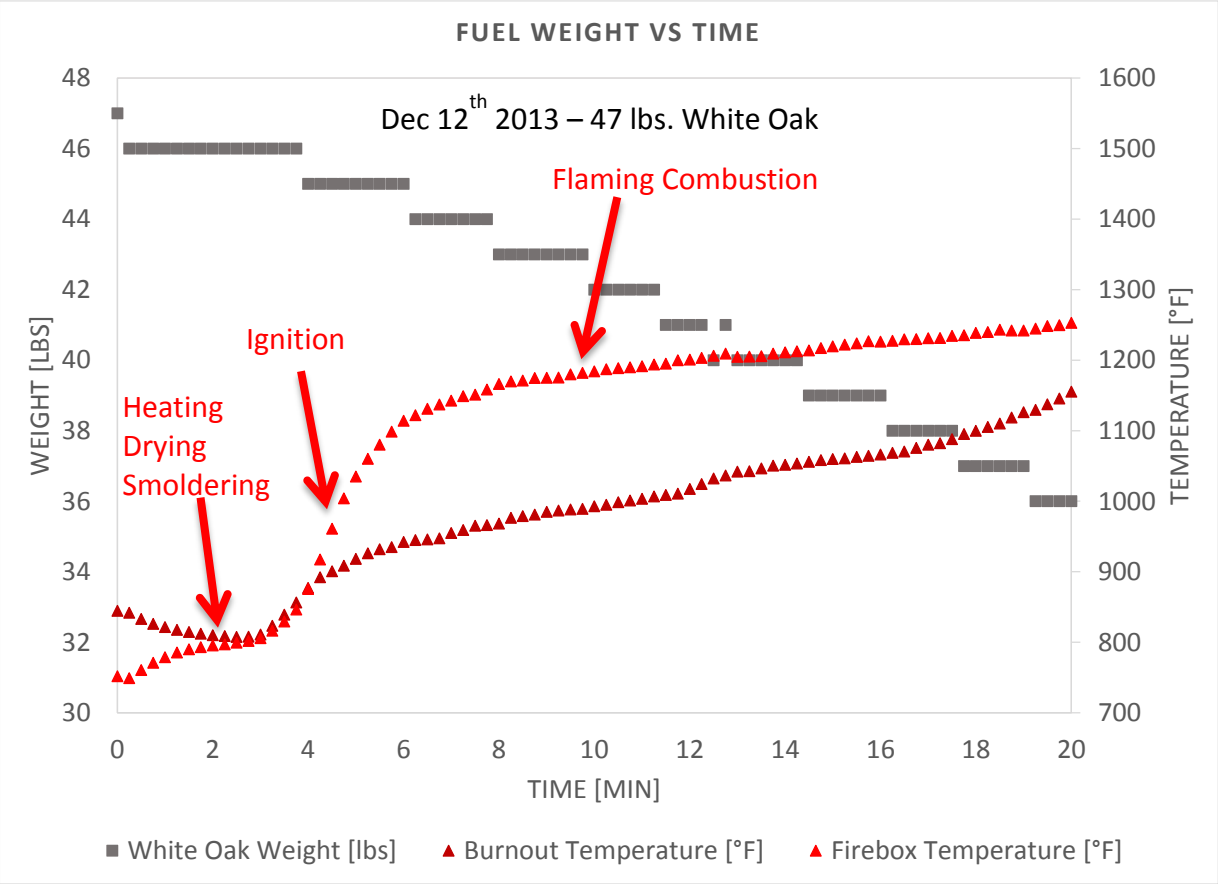

Figure 3.5: Fuel weight and temperatures in the furnace throughout a burn process.

In Figure 3.6, concentrations of CO, CO_2 and O_2 are plotted against time. The same three regimes can be identified. Smoldering occurs initially and CO concentration increases. At ignition, oxygen concentration reduces to 10 % followed by a rise in CO and CO_2. Feedback from the exothermic combustion reactions accelerates drying and pyrolysis of wood logs deeper into the pile; CO and CO_2 continue to rise. Approximately 12 minutes into the burn, the rate of oxidation of CO to CO_2 surpasses CO release from pyrolysis, causing CO concentration to rise.

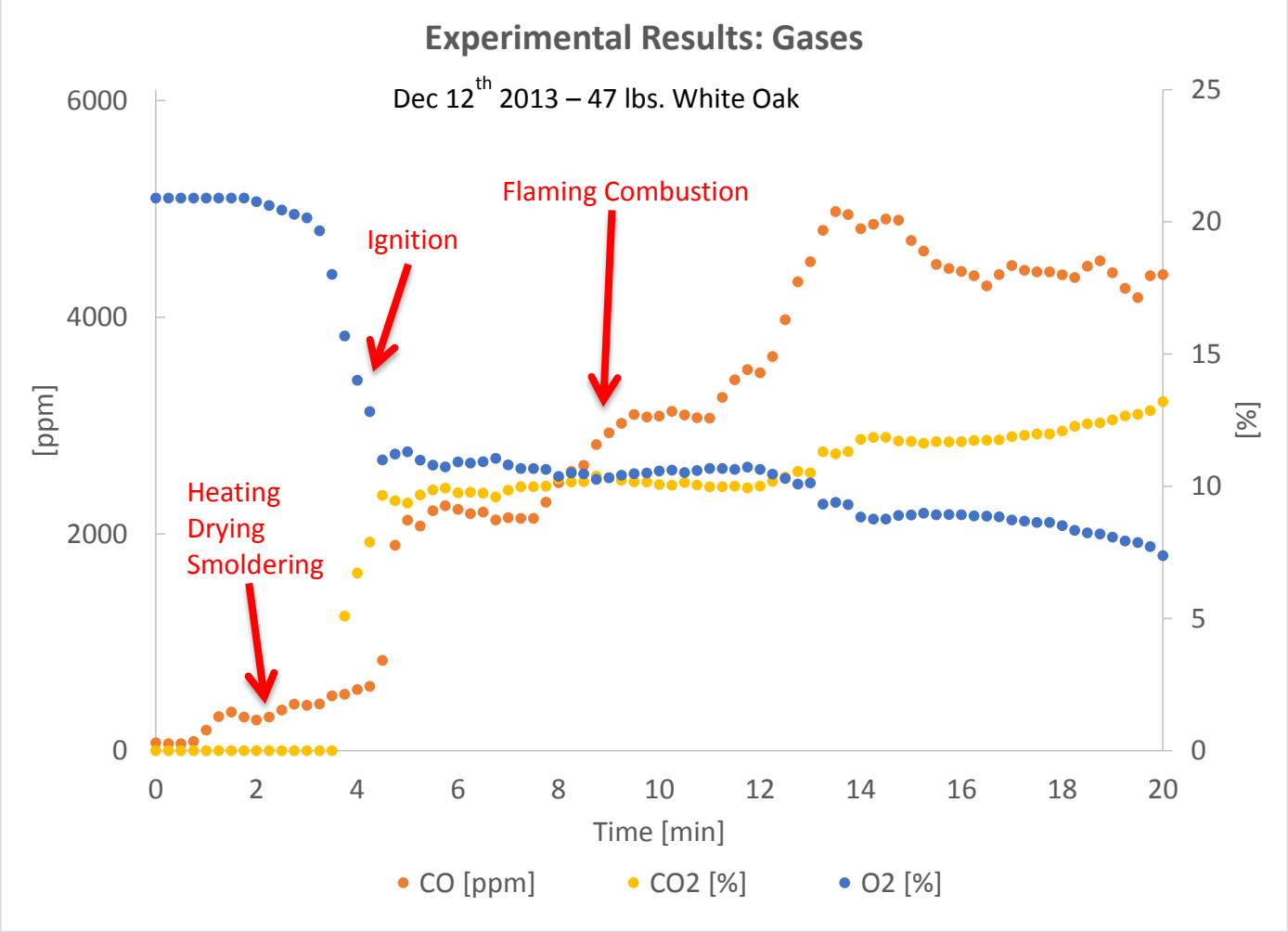

Figure 3.6: CO, CO_2 and oxygen concentrations for the Dec. 12th 2013 white oak experiment.

Figure 3.7 shows the particle concentration during the burn process. The concentration follows that of CO, suggesting the particles consist of condensed hydrocarbons which failed to oxidize. The three regimes are also identifiable in Figure 3.7.

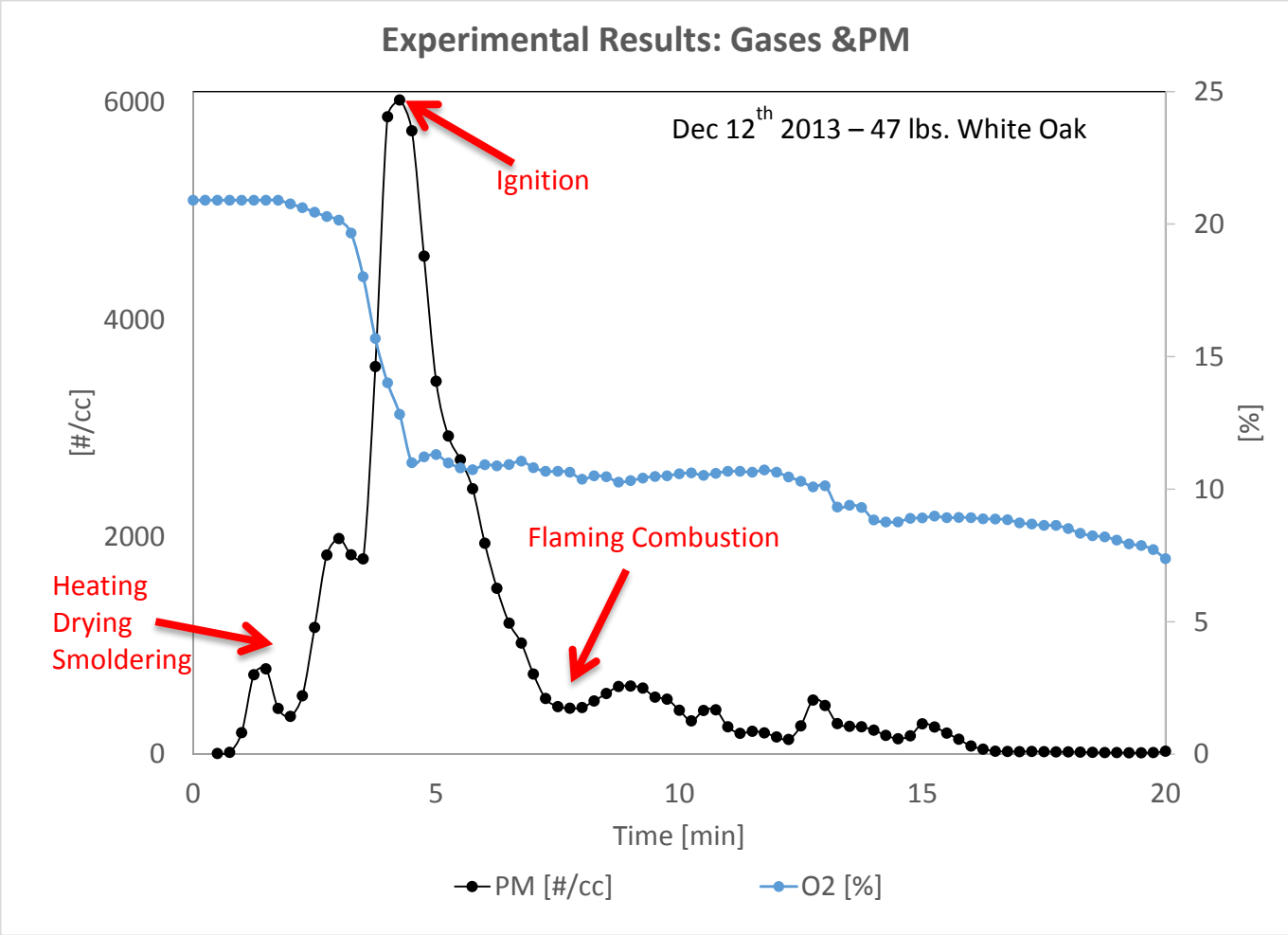

Figure 3.7: Particulate matter (PM) concentration & CO from 47 lbs. white oak combustion experiment.

3.3.2 Air Staging Effects

The effects of furnace air staging on the combustion process and pollutant formation were identified. Figure 3.8 presents results from two separate experiments. One is conducted under normal air staging conditions, where all air inlets are open (Figure 3.1). In the other

experiment, one of the over-fire air inlet is blocked. When one of the secondary air inlet is blocked, the under-fire air flow rate is greater (air diverted from the blocked over fire inlet). The addition of the air to the under-fire zone quenches the initial combustion resulting in the high CO emissions and PM emissions (not shown).

Approximately five minutes into the burn process, the previously closed inlet is unblocked and the combustion process is allowed to establish in the primary zone; the CO concentration returns to previous levels for typical air control scenario. However, it takes approximately 15 minutes for CO to return to previous levels. Even when the air staging is changed back to normal conditions, the flame zone is still hot and volatiles are driven off the wood particles at a rapid rate resulting in high PM emissions. It takes time to re-establish the optimal regime for combustion.

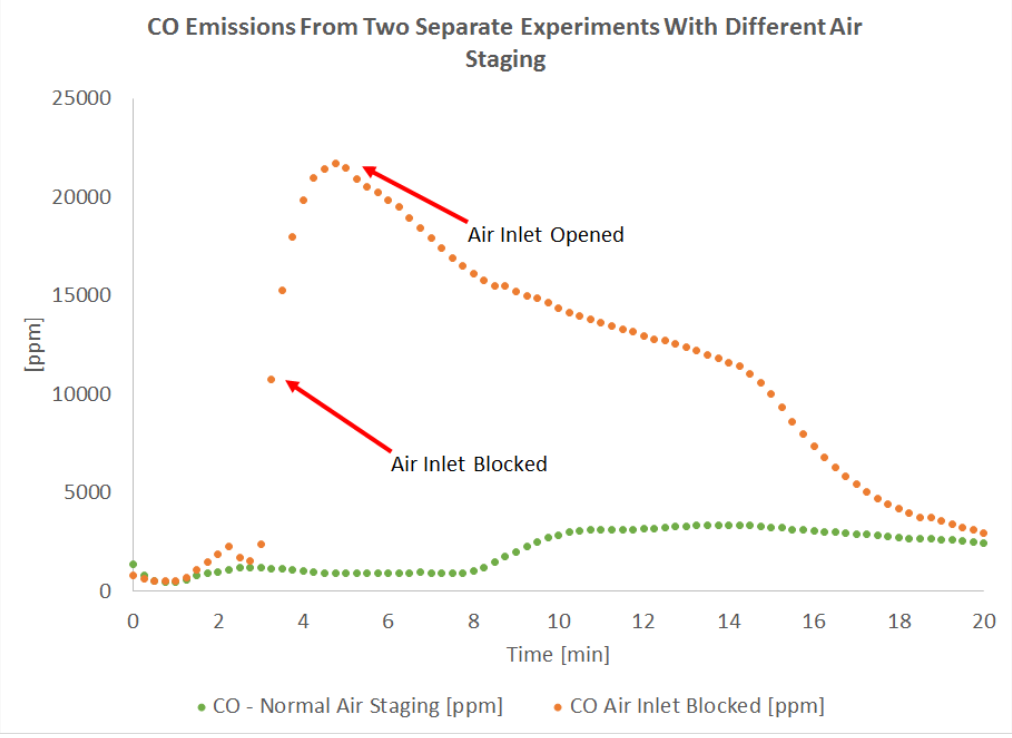

Figure 3.8: Burn experiment conducted with poor air control. One over-fire air inlet is blocked

3.4 Conclusions

Experimental results of three combustion experiments using white oak fuel were described An experiment with the biomass burner operating at normal operating condition with 47 lbs. white oak was described thoroughly (Dec. 12th 2013 Burn). Smoldering, ignition and flaming combustion regimes were identified based on temperature, CO, PM, O_2 and CO_2 measurements.

Effects of air staging on emissions were analyzed and emissions of CO increased dramatically when secondary air inlet was closed, preventing proper mixing of combustible pyrolysis gases with combustion air.

These results are used to compare results from a CRN model of the combustion process. The CRN development and model results are described in the following two sections.

Chapter 4
Chemical Reactor Network Development

The goal of developing a chemical reactor network (CRN) is to simulate thermo-chemical processes in the furnace. The CRN simulates chemical processes by assembling an appropriate configuration of PSR and PFR elements. The inputs to the network are air and fuel flow rates, fuel composition and wood temperature. Fuel flow rates are determined by scale measurements and air flow rates are determined by pressure drop measurements of air inlets to the furnace. The wood temperature is estimated by applying a heat transfer model to the furnace and the wood fuel. This analysis is reported in section A.6

In this chapter, wood composition, chemical pathways and chemical rates of wood to be used in the reactor elements are reviewed. The purpose of each reactor element in the CRN configuration is described

4.1 Chemical Composition of Wood & Kinetics

The composition of the fuel based on final yields is listed in Table 4.1. Figure 4.1 shows the wood decomposition pathway used by the model. The composition is based on chemical yields according to Nunn et al. [28] and Borosen et al. [29] who studies primary and secondary reactions of hardwood pyrolysis. The composition in Table 4.1 has been adjusted to account for the white oak volatile composition as listed in Table 3.1. The pyrolysis mechanism has been integrated into the UW-CRM code (see section A.7 which includes about 150 species and 220 reactions. Rate data were determined by following an alternative expression of equation 2.9:

4.1 $$\frac{dV_i}{dt} = (V_i^* - V_i)\ 10^{A_i}\ exp\left(\frac{-E_A}{RT}\right) \qquad s^{-1}$$

Here V_i is the % weight yield of species i on the basis of the original fuel and V_i^* is the asymptotic yield of the species. The rate constant for each species is expressed as $k = 10^{A_i}\ exp\left(\frac{-E_A}{RT}\right)$. Separating variables and integrating equation 4.1 yields:

4.2 $$V_i = V_i^*\left(1 - exp\left(-10^{A_i} exp\left(\frac{-E_A}{RT}\right)t\right)\right) \qquad [\,]$$

Chemical species C_2H_5O and C_3H_6 participate in the wood pyrolysis but they are not included in the UW-CRM mechanism. These species are substituted by the simpler species CH_2O and C_2H_4. In addition, since we are focusing on devolatilization regimes, the char species have been removed and CO content increased accordingly.

Table 4.1: Model fuel composition. The composition is based on the wood composition reported by Nunn and the elemental composition listed in Table 3.1.

Species	V_i^* [%]	10^{A_i}	$\frac{E_A}{R}$ [K]
Wood → Tar	53.2	$10^{3.60}$	8304
Wood → Tar → CO	28.7	$10^{3.60}$	8304
Wood → Tar → CO_2	5.5	$10^{3.60}$	8304
Wood → Tar → CH_4	8.2	$10^{3.60}$	8304
Wood → Tar → C_2H_4	10.4	$10^{3.60}$	8304
Wood → Tar → H_2	0.2	$10^{3.60}$	8304
Wood → Tar → HCN	0.2	$10^{3.60}$	8304
Wood → H_2O	27.1	$10^{2.39}$	5788
Wood → H_2	0.8	$10^{2.39}$	5788
Wood → OH	0.2	$10^{2.39}$	5788
Wood → CH_2O	1.6	$10^{2.58}$	6492
Wood → C_2H_5O	1.1	$10^{4.87}$	10720
Wood → C_3H_6	0.3	$10^{10.27}$	21540
Wood → CO_2	3.3	$10^{3.60}$	8304
Wood → CO	3.3	$10^{3.60}$	8304

Wood → CH_4	0.3	$10^{3.60}$	8304
Wood → Char	8.5	$10^{3.60}$	8304

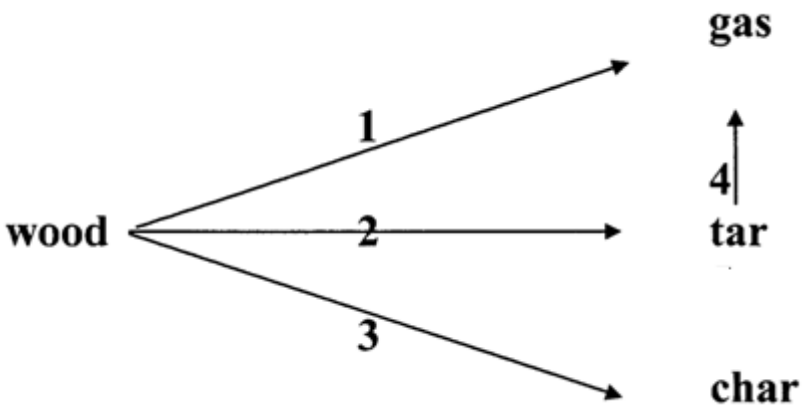

Figure 4.1: Chemical pathways of wood combustion according to proposed model.

4.2 CRN Configuration

Figure 4.2 demonstrates the proposed CRN configuration. The model consists of four reactor elements. Each reactor element is described below.

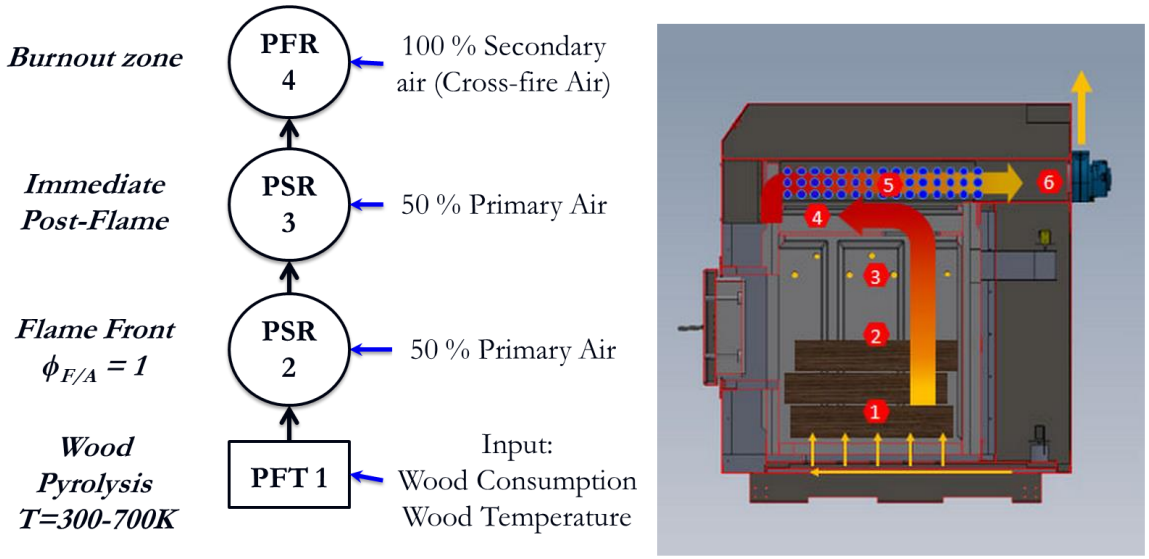

Figure 4.2: Proposed chemical reactor network model (left) and experimental furnace (right).

4.2.1 PFT1

The first element, PFT1, is a plug flow reactor at an assigned temperature. The purpose of this element is to model wood pyrolysis. Air is absent in this reactor since kinetic rates were developed based on TGA result conducted in the absence of air[29], [28]. The fuel mass flow rate is based on scale measurements in the biomass furnace. Figure 4.3 shows model results for wood consumption by pyrolysis as a function of temperature in the PFT1 reactor. According to the PFT1 output, pyrolysis starts close to 500 K, volatiles are rapidly driven off with increasing temperature and most of the wood is consumed at 700 K. These results compare well to the TGA results of Figure 2.4 and Figure 2.5. Figure 4.4 shows how CO and tar yields develop with PFT1 temperature. The figure demonstrates tar formation from wood decomposition and tar conversion to CO as depicted in Figure 4.1. The output of the PFT1 element is a mixtures of volatiles that combine with air in subsequent reactor elements to form a combustible mixture.

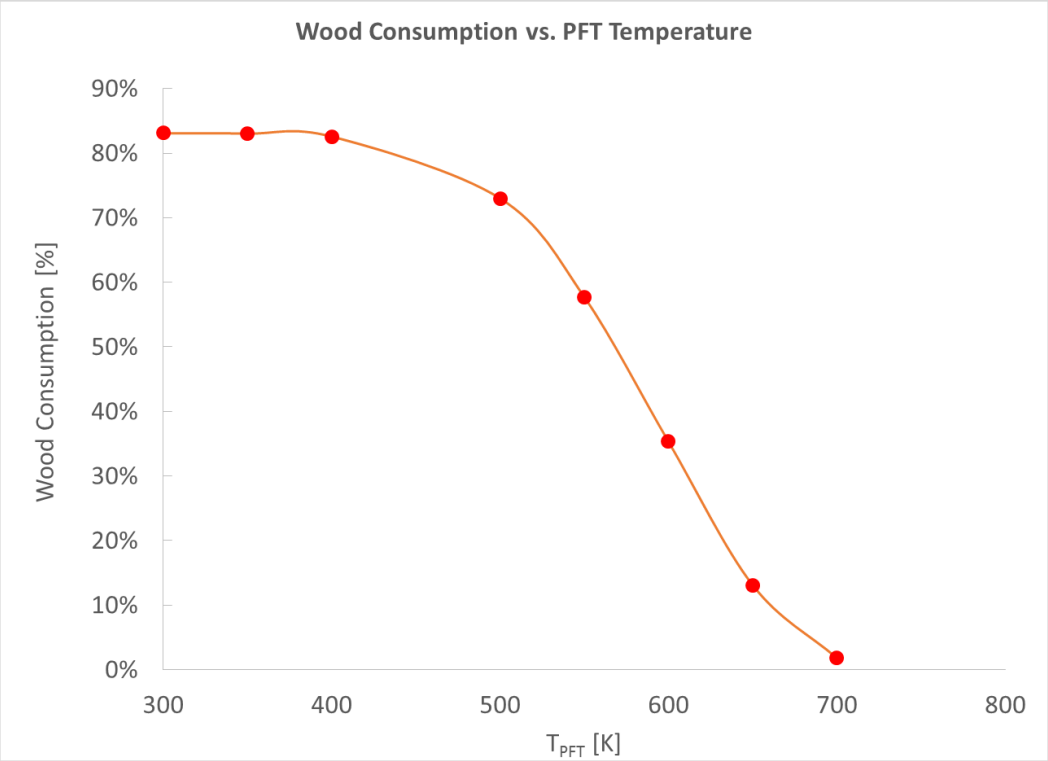

Figure 4.3: Wood consumption in the PFT1 reactor.

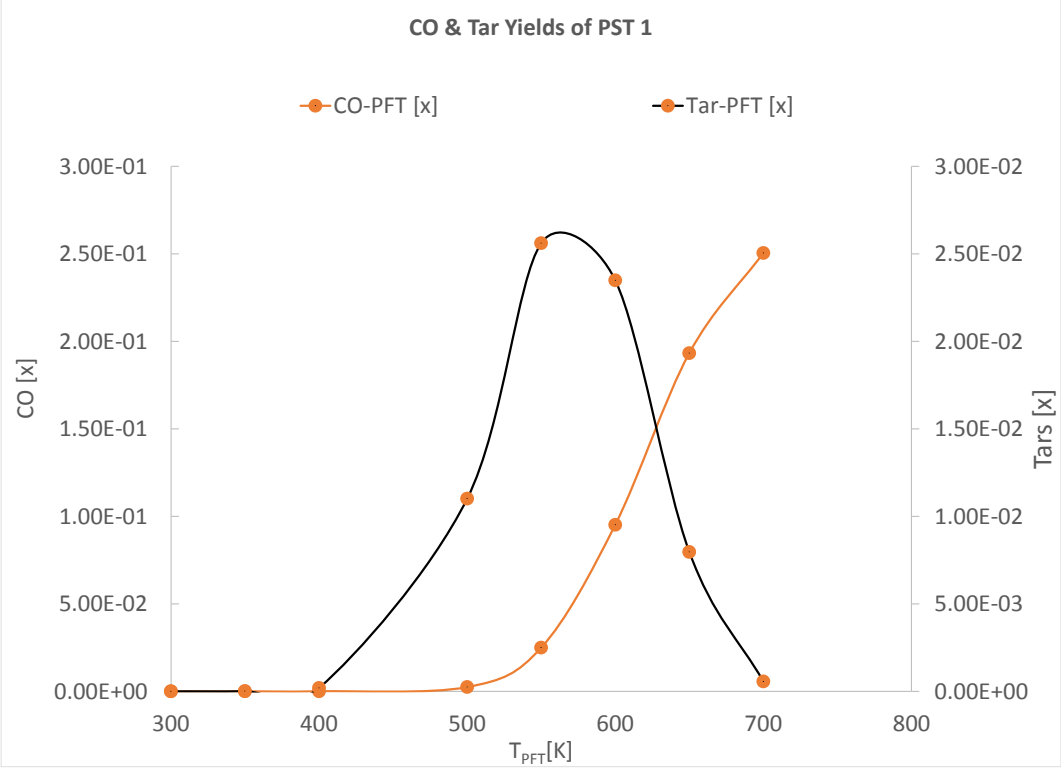

Figure 4.4: CO & Tar yields from PFT1.

4.2.2 PSR2

The second element, PSR2, simulates the stoichiometric diffusion flame front. The flame front is simulated with a PSR due to its fast, uniform mixing. Air input is set to make $\phi_{PSR2} = 1$ in the reactor at ignition to represent the diffusion flame. It turns out that 50 % of the measured under-fire air flow rate is required to achieve this. The flame will increase heat transfer to the wood logs and speed up pyrolysis.

4.2.3 PSR3

The post-flame region is simulated by the third element, PSR3. The other half of the under-fire air enters this element and mixes with a portion of residual volatiles and combustibles which have bypassed the flame. The resulting chemical mixture enters the last element of the model, the plug flow reactor.

4.2.4 PFR4

The furnace burn-out zone, or cross-fire zone, is represented with a plug flow reactor (PFR4) which typically represents dilution zones in gas turbines. The over-fire air enters this reactor and mixes with the fuel mixture output of PSR3. The output from PFT4 simulates the biomass furnace exhaust and is compared to experimental gas exhaust measurements.

4.3 Conclusions

Chemical constituents and chemical kinetic rates are based on TGA experimental results of Nunn and Boroson. Wood is assumed to convert to tars and gases. Tars are assumed to undergo secondary pyrolysis to gases.

The proposed CRN model consists of a plug flow reactor to simulate pyrolysis, perfectly stirred reactors to simulate stoichiometric diffusion flame front and post-combustion zone and a plug flow reactor to simulate the cross-fire dilution zone in the biomass furnace.

The next chapter describes how the CRN is able to simulate smoldering, ignition and flaming combustion as reported by section 3.3.1 and the air staging effect as reported in section 3.3.2

Chapter 5
CRN Model Validation

In this chapter, the CRN model, as described in section 4.2 is evaluated against experimental results. Yields of CO and tars from the model are compared to experimental results for the 47 lbs white oak burn (Dec. 12th 2013) as described in section 3.3.1 (Figure 3.5, Figure 3.6 and Figure 3.7). Air staging effect on CO concentration, reported in section 3.3.2 is also simulated.

The inputs to the CRN are air and fuel flow rates, fuel composition and wood temperature. Fuel flow rates are determined by scale measurements and air flow rates are determined by pressure drop measurements at air inlets to furnace. The wood temperature is estimated by applying a heat transfer model to the furnace and the wood fuel. This analysis is reported in section A.6

5.1 Dec. 12th 2013 Burn

Table 5.1 summarizes the residence times and equivalence ratios in the reactors used to simulate the combustion process in this experiment.

Table 5.1: Residence time and equivalence ratio ranges in the reactors. Smaller residence times correspond to larger fuel flow rates. Total residence time from oxidizing reactors ranges from 21 – 37 ms.

Reactor	τ	ϕ
PSR2	5 ms	0.96 – 1.36
PSR3	0.9 – 1.1 ms	0.49 – 0.70
PFR4	15-31 ms	0.19 – 0.22
Total	(21 – 37) ms	-
PFT1	15 s	-

The calculated average air velocity through the floor grates is 10 m/s. The height of the furnace box, from the wood sample, up to the heat exchanger is approximately 0.5 m. The physical residence time is therefore approximately 50 milliseconds residence time, which is close to the total residence time listed in Table 5.1.

The output from PFT4 is compared to gas exhaust measurements. Figure 5.1 demonstrates CO and tar concentration outputs from PFR4 for different PFT1 temperatures.

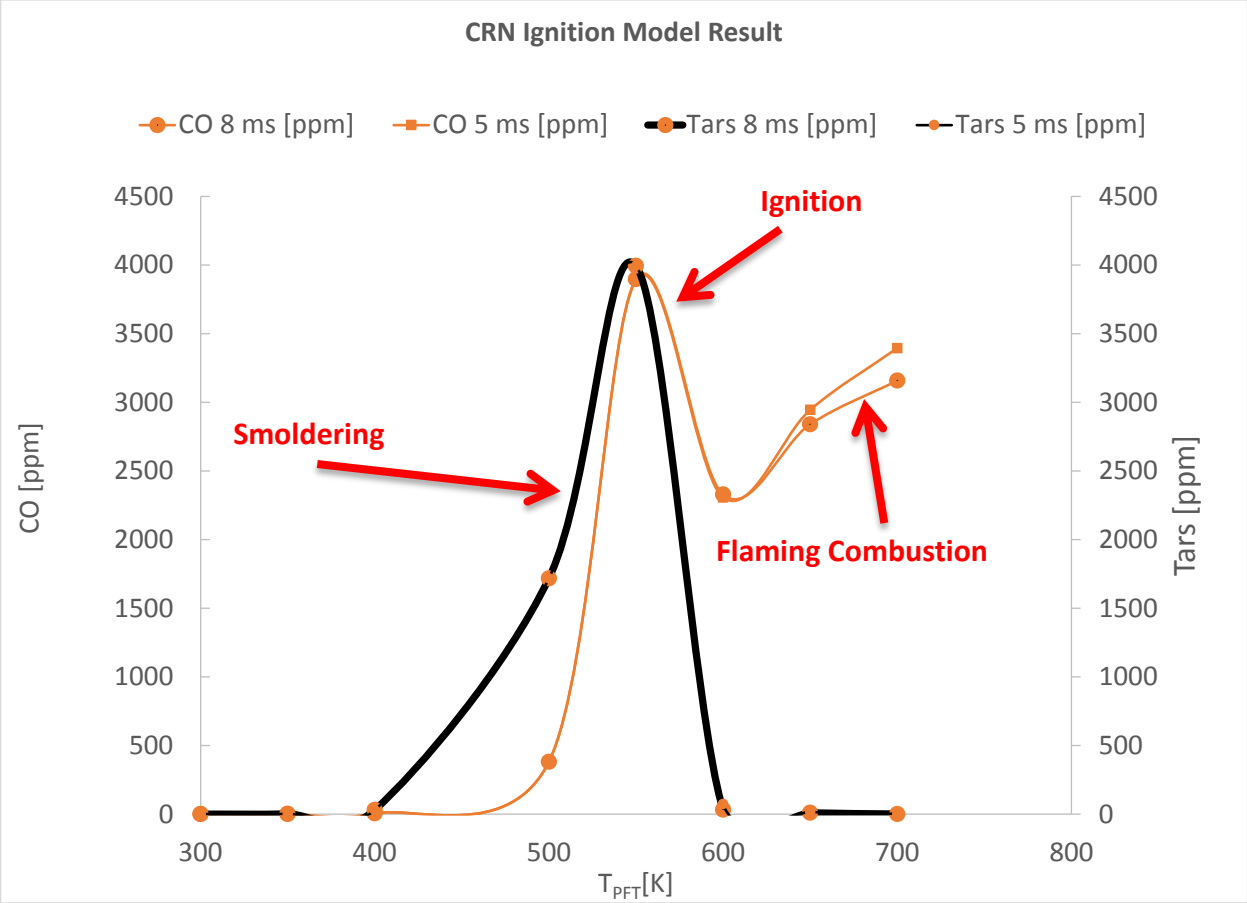

Figure 5.1: CO & Tar yields from the model (PFR4 output) at different temperatures

As temperature increases, wood species convert to tars which are then converted to CO. Wood also converts to CO (Table 4.1) in primary pyrolysis. This is the smoldering regime

(Figure 5.1). Between 550 and 600 K, the volatile mixture released from the wood ignites and the temperature of the PSR2 element reaches beyond 2000 K. This is the ignition regime. For lower PFT1 temperatures, the temperature of the chemical mixture exiting PSR2 is 380 K. As the temperature increases, more of the wood gets converted to CO in the flaming combustion regime. Figure 5.1 shows how decreasing PSR2 residence time limits oxidization of CO. The CRN model is able to simulate the three regimes identified in the experiment; smoldering, ignition and flaming combustion.

Figure 5.2 compares CRN CO concentration to the experimental results taken on Dec. 12th 2013.

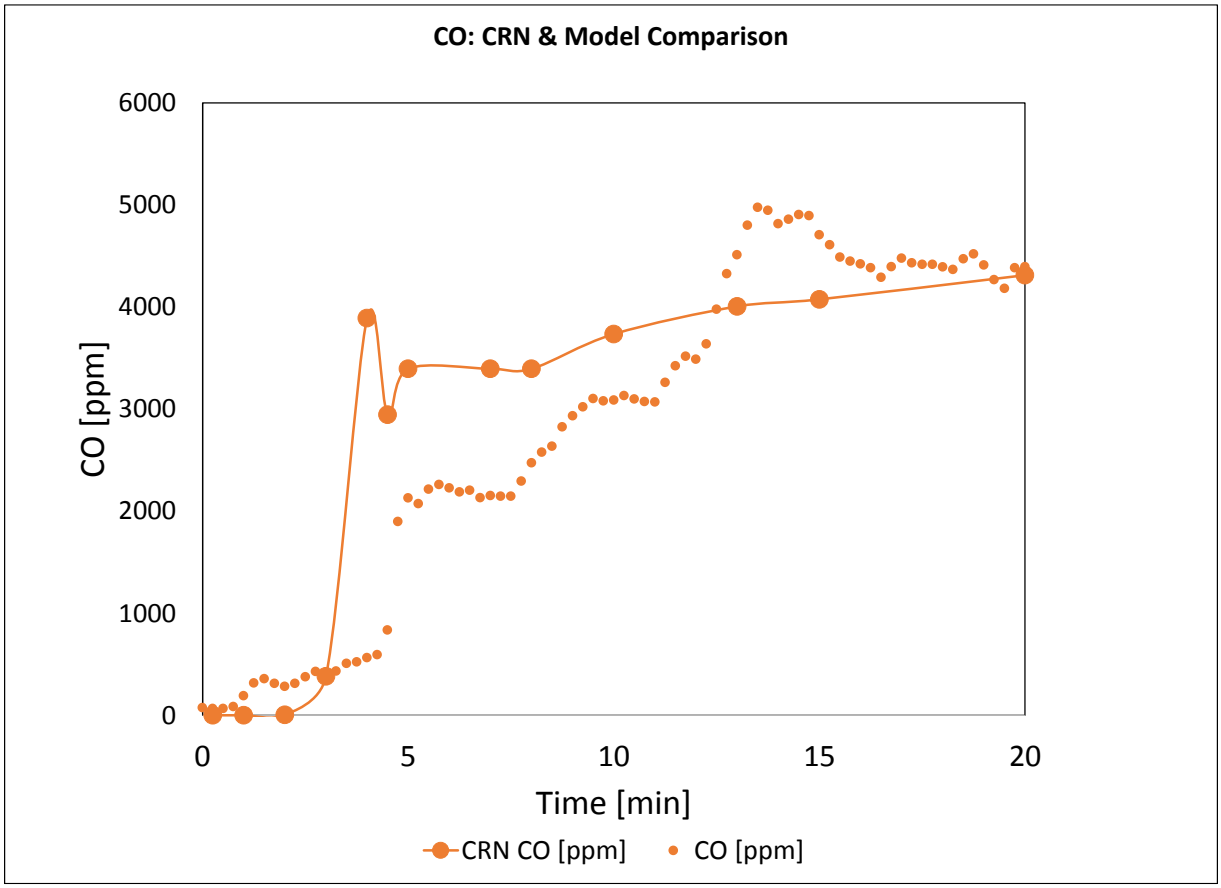

Figure 5.2: CO yields from model compared to experiments.

Model inputs are measured flow rate and wood temperatures from heat transfer model presented in section A6. Using the results from the heat transfer model, wood temperature can be correlated for different times in the experiment. For volatiles to be completely driven off, the wood temperature has to remain at 700 K according to TGA results (Figure 4.3 and Figure 2.5). According to heat transfer calculations, the surface of the wood reaches this temperature in approximately 5 minutes (section A6). Figure 5.3 demonstrates tar yields from the CRN model.

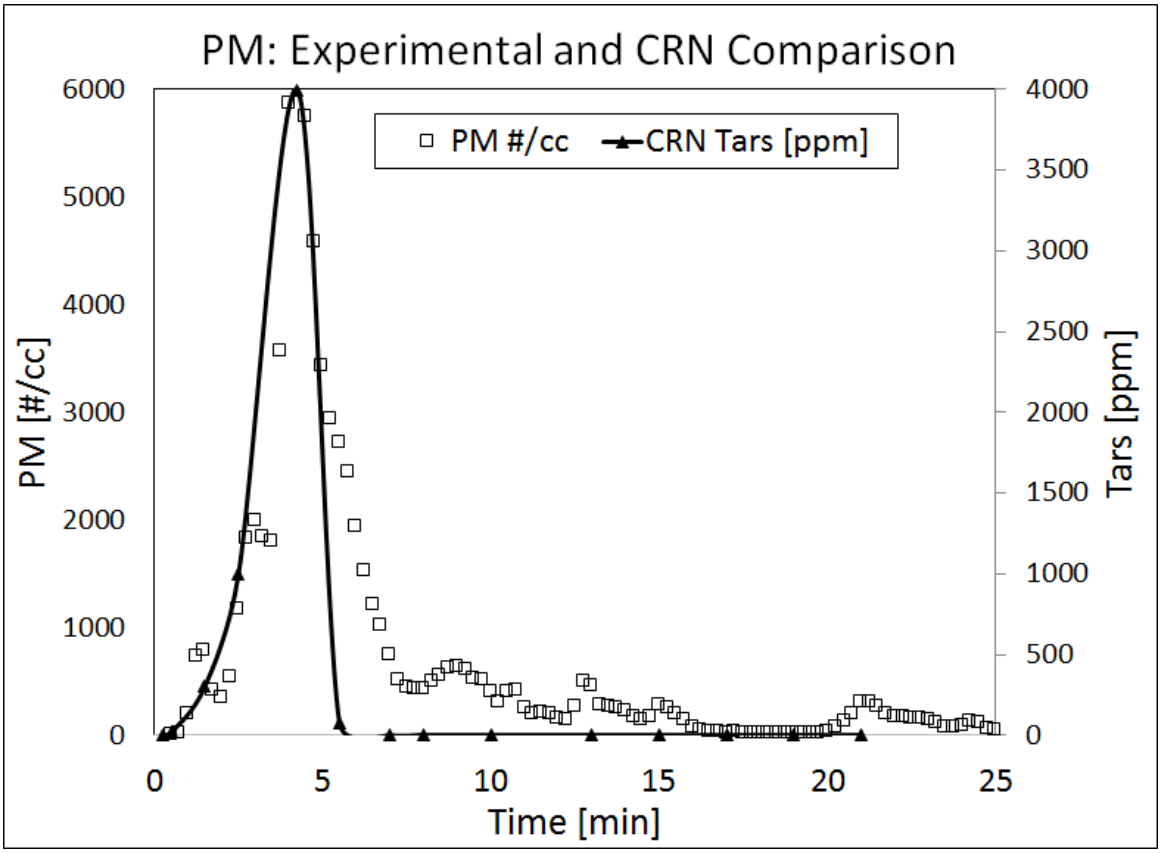

Figure 5.3: Tar yields from model compared to experiments.

The wood batch receives heat from the diffusion flame which increases rate of weight-loss. Table 5.2 lists how the fuel mass flow rate is influenced by the flame in the experiment. The PSR2 element, which represents the flame front, receives more fuel for the same amount of air and becomes fuel richer, increasing CO concentration in the element.

Table 5.2: Fuel flow rate and equivalence ratio in the ignition PSR (PSR2).

t_{burn} [min]	Fuel flow [g/s]	Φ_{PSR2}
1	3.30	0.96
2	3.45	1
3	3.56	1.04
5	3.80	1.11
6	3.88	1.14
8	4.05	1.19
10	4.19	1.25
12	4.32	1.27
14	4.43	1.29
15	4.47	1.31
20	4.64	1.36

5.2 Effects of Air Staging on CO Concentration

To simulate the poor air staging (Figure 3.8) case (section 3.3.2 and Figure 3.8), the furnace air is rerouted as depicted in Figure 5.4. An over-fire air inlet is closed, forcing more under-fire air through the floor grates and the other over-fire inlet. This action resulted in a CO spike in the experimental data and approximately three-fold increase in the CO output in the CRN model. CRN model results and comparison to experimental data is presented in Figure 5.5. Residence times and equivalence ratios for reactor elements are presented in Table 5.3. The CRN model describes cooling of the wood batch and decreasing residence times in some of the reactors, resulting in CO concentration spikes.

Table 5.3: Equivalence ratio and residence times for CRN model of poor air staging experiment.

Reactor	T	ϕ
PSR2	3.33 ms	0.59
PSR3	1 ms	0.31
PFR4	27 ms	0.15
Total	(21 – 37) ms	-
PFT1	15 s	-

The flame front (PSR2 and PRS3) cannot sustain combustion due to the decrease in the fuel-air equivalence ratio and lower zonal temperatures from the cool air added. In the model, the PSR2 reactor reverts from ignition to smoldering and does not ignite unless the temperature increases or the residence time increases to approximately 33 milliseconds. In the associated experiment, combustion reverted into the smoldering regime and produced high emission levels. A corrective measure designed to re-establish combustion was initiated in the model: the primary air was reduced to increase the pyrolysis element temperature to 700 K, which resulted in the return of the CO levels to the previous values. When this corrective action was applied to the physical biomass burner, the combustion also changed from the smoldering to flaming regime as depicted in Figure 3.8; however this did not happen immediately—a delay of 15 minutes was observed before the furnace CO level normalized.

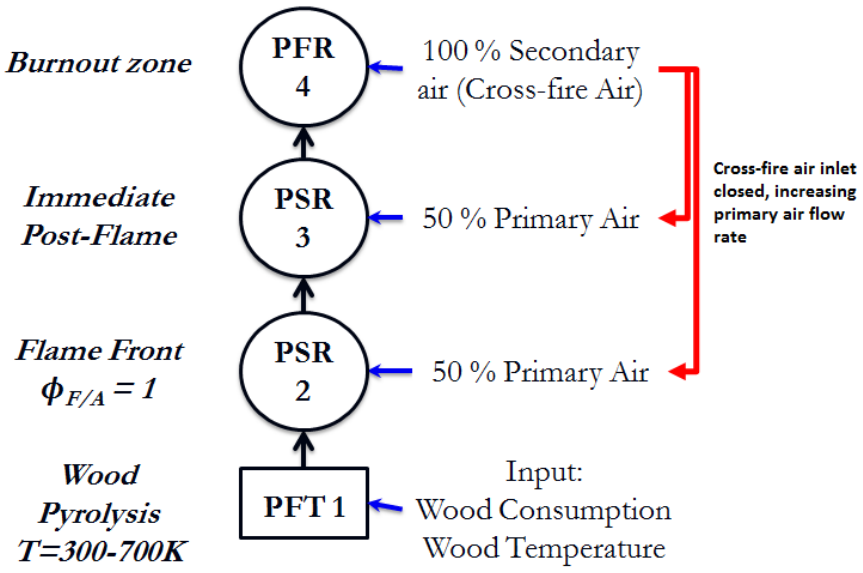

Figure 5.4: Over-fire air is rerouted to enter primary air reactors to simulate burn with poor air staging.

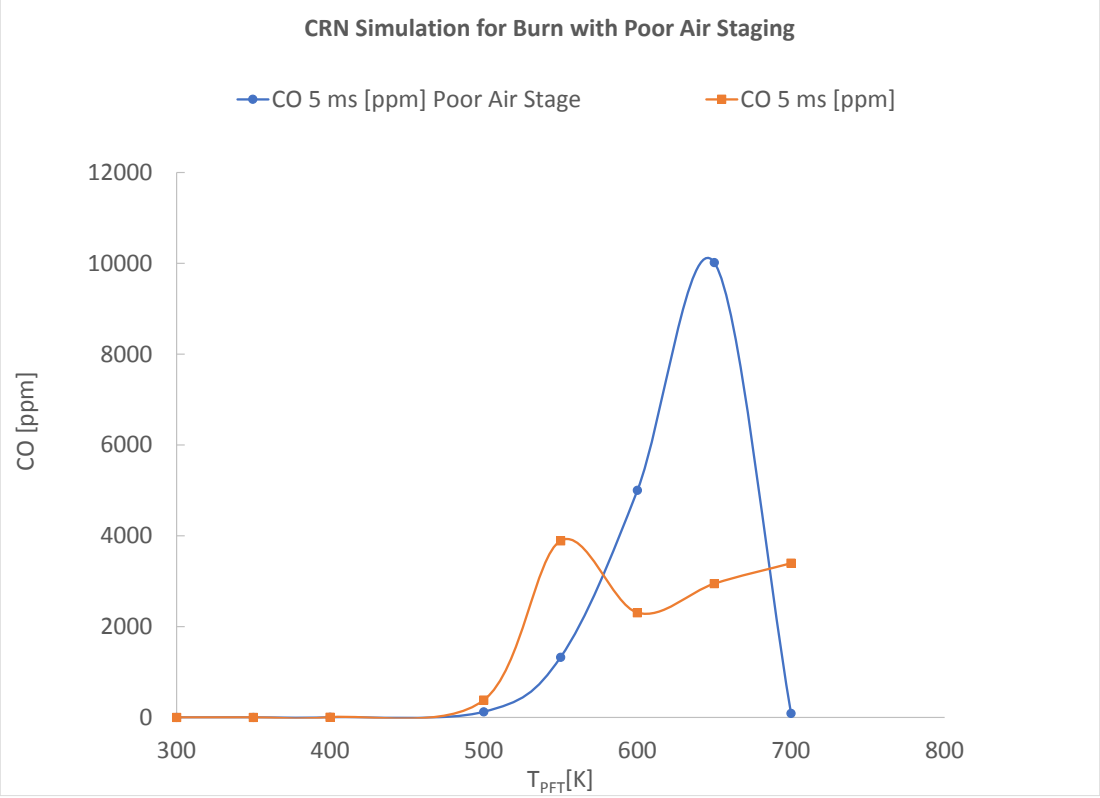

Figure 5.5. Model results for poor air stage burn compared to regular burn.

.

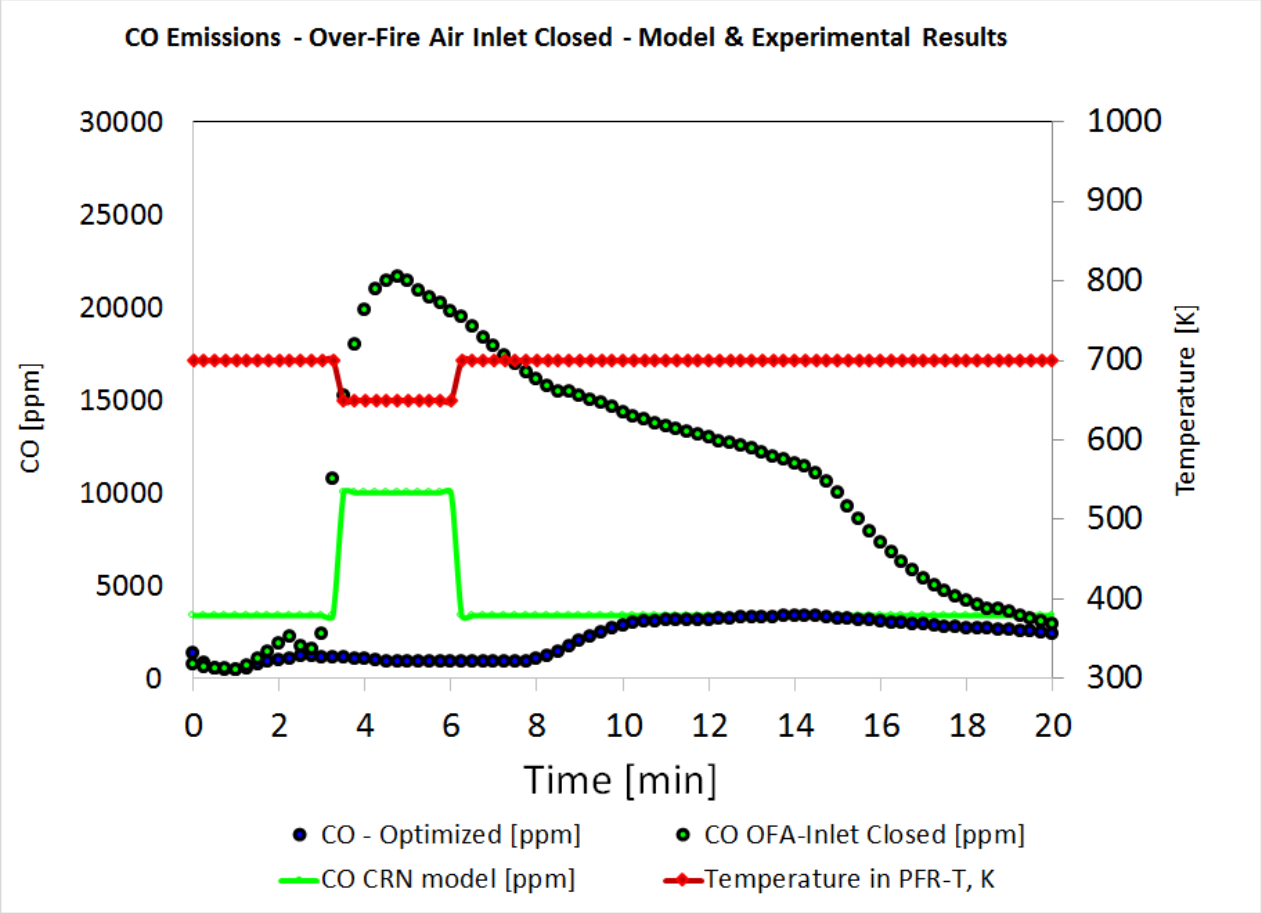

Figure 5.6: CO concentration from model compared to experimental data.

5.3 Conclusions

The developed CRN uses measured fuel and air flow-rates and calculated wood temperature from a heat transfer model and successfully simulates wood smoldering, ignition and flaming combustion and is able to capture effects of poor air staging on pollutant emissions.

Chapter 6
Conclusions

Low cost sensors and a CRN model for an advanced biomass combustion control system have been evaluated.

A CRN model, consisting of PFT-PSR-PSR-PFR, was developed. The model is capable of predicting several key parameters associated with the biomass combustion process, namely smoldering, ignition, flaming combustion and trends of CO and tar concentration at different stages in the biomass burn process. The model also captures effects of poor air staging (one air inlet closed) on pollutant emissions. By rerouting secondary cross-fire air, the model predicts carbon monoxide concentration to increase three-fold.

The optical sensor response to PM concentration was compared with an APS that was placed in series with the optical sensor. The optical PM sensor response was nearly identical to the reference instrument (Figure A.10). This and similar data show that the chosen optical PM sensor and data acquisition hardware are appropriate for detection of varying PM concentrations in a biomass furnace.

The MOS gas sensors were also tested in an experimental furnace and compared to a Bacharach ECA-450 combustion gas analysis system. The readings from the sensor array were recorded similarly to the PM measurement and interpreted using a custom algorithm. The MOS sensors were able to detect varying concentrations of CO from the experimental furnace. The sensor was able to capture low levels of CO before ignition event, the rise in CO concentration during the typical biomass combustion process and the CO spike associated

with inefficient combustion due to improper air-staging in the furnace. These data shows the feasibility of using low-cost CO sensors for monitoring exhaust gas from biomass combustor.

Chapter 7
Future Work

The proposed CRN has been shown to successfully simulate major combustion events in the experimental furnace. The ultimate goal of the CRN is to provide a fast, near-real-time means of determining the influence of combustor parameters on emissions and it can be improved in a few ways to advance towards that goal. Applying a computational fluid dynamic (CFD) simulation on the experimental furnace can facilitate development of a more complete CRN arrangement. In addition, more chemical species and recent rate coefficients can also be adopted to the thermochemical database for more accurate emission predictions.

7.1 CRN Based on CFD Simulations

Computational fluid dynamics (CFD) has been applied extensively for evaluation of fuel performance in bench, pilot and full scale furnaces. CFD uses numerical methods and algorithms to analyze flow-related processes occurring during thermochemical conversion of solid biomass. CFD modelling allows computation of reactive flows including species, temperature and residence time distributions in biomass furnaces and provides a powerful, fast, less risky and reliable analysis of combustion technologies. Continuously improving computing performance allows integration of reaction kinetics and equilibrium modelling into CFD simulations, generating a spatially resolved three-dimensional model and visualization of the highly complex biomass combustion process.

The overall approach to utilize CFD results towards development of a more complete CRN involves developing a CFD model of the furnace and using the resulting flow field,

temperature field, and reaction rates to develop the CRN arrangement. The furnace will be subdivided into zones based on the characteristic chemical process prevailing in those regions, such as: fuel rich zone, flame zone, recirculation zone, over-fire air zone and burnout zone. Figure 7.1 demonstrates how CFD results can be used to define major flame zones in a round jet diffusion flame for CRN development. Figure 7.2 shows how CFD can be used to develop improvements to furnace design by adjusting air systems.

Due to high complexity of the reaction and transport processes inside the biomass, a coupled pyrolysis and flame model should not be attempted. Rather, experimental weight loss data can be used to treat the wood surface as a boundary that releases gas-phase volatiles. Based on the results of the CFD study, further improvements on the CRN can be applied, .e.g. by incorporating wall-quenching and recirculation zones.

zone	zone limits	reactor criteria
upstream zone (USZ)	$z < 0$ m	n/a
fuel-rich zone (FRZ)	$z > 0$ m, $0.9 < f < 1.0$	$\Delta f = 0.01$, $\Delta z = 0.01$ m
low-temperature flame zone (LFZ)	$z > 0$ m, $0.1 < f < 0.9$, $T < 1400$ K	$\Delta T = 100$ K
high-temperature flame zone (HFZ)	$z > 0$ m, $0.1 < f < 0.9$, $T > 1400$ K	$\Delta T = 100$ K ($T < 1800$ K), $\Delta T = 50$ K (1800 K $< T < 2000$ K), $\Delta T = 2$ K ($T > 2000$ K)
jet expansion zone (JEZ)	$z > 0$ m, $0.01 < f < 0.1$	$\Delta T = 100$ K
co-flow zone (CFZ)	$z > 0$ m, $0 < f < 0.01$	$\Delta z = 0.2$ m

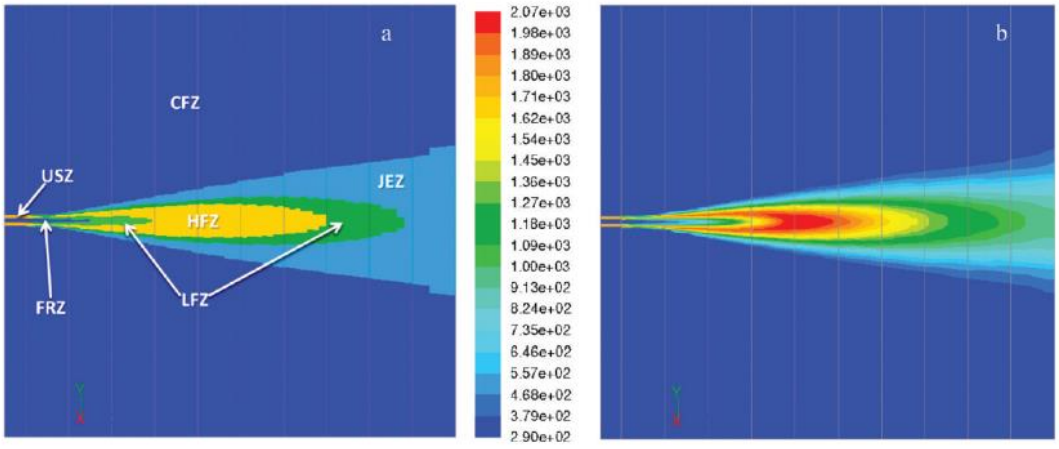

Figure 7.1: CFD temperature field of a methane/air round jet diffusion flame. Different zones and reactor criteria are defined to be used as reactor element inputs. Figure taken from Monoghan et al. [31].

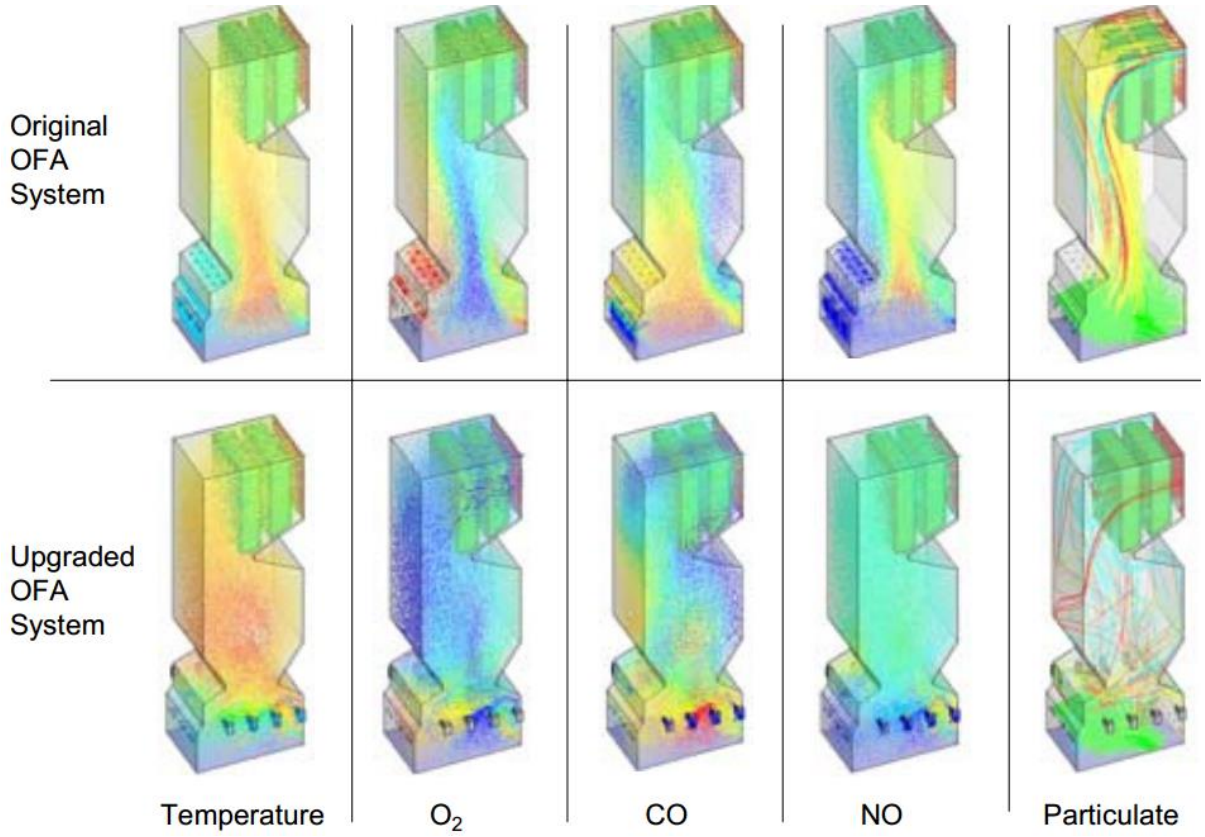

Figure 7.2: Simulations of improved over-fire air system in a waste fuel boiler. The model results suggest the new system improves mixing, efficiency, emissions and burning capacity. Figure from Jansen Combustion & Boiler Technologies [32][32].

7.2 Chemical Species and Reaction Rates

Existing reaction mechanism codes and databases are continuously improving. Commercial reaction kinetic models, software (e.g. CHEMKIN) and thermodynamic equilibrium models are also being developed. The improvement of these models advances our understanding of the combustion processes with respect to emissions and efficiencies. Existing databases contain information on the properties of almost all chemical species. Available

thermochemical information and continuing research in biomass pyrolysis and combustion promotes adding chemical species and recent kinetic rates to the proposed model.

Typically biomass combustion processes are modeled by defining solid pyrolysis (primary and secondary devolitilization) models using existing literature information or by performing new experiments. The combustion of volatile gases released is then modeled with existing gas kinetic models. The primary research interest and efforts in biomass combustion is therefore related to pyrolysis or the rate of release and composition of combustible volatiles from the solid biomass.

The current model divides the wood to 12 volatile species which are released in 16 kinetic steps with associated rate coefficients. Recent biomass pyrolysis modeling efforts (e.g. Ranzi et al. [33] and later Gauthier et al. [34]) treat the biomass as consisting of three main components (cellulose, hemicellulose and lignin). The thermochemical decomposition pathways for the three components are modeled individually and assumed to be independent (recent results by Hosoya et al. [35] contradicts this assumption), releasing approximately 25 volatile species (e.g. levoglucosan, xylofuranose, phenols and methoxy-guaiacol) using simplified lumped kinetic models with reaction rate parameters derived mainly from TG experiments and semidetailed kinetic scheme [33]. The current model can hopefully be improved by adding the additional species with associated thermochemical information and adopting the recent modeling methodology.The current model divides the wood to 12 volatile species which are released in 16 kinetic steps with associated rate coefficients. Recent biomass pyrolysis modeling efforts (e.g. Ranzi et al [33] and later Gauthier et al. [34]) treat the biomass as consisting of three main components (cellulose,

hemicellulose and lignin). The thermochemical decomposition pathways for the three components are modeled individually and assumed to be independent (recent results by Hosoya et al. [35] contradicts this assumption), releasing approximately 25 volatile species (e.g. levoglucosan, xylofuranose, phenols and methoxy-guaiacol) using simplified lumped kinetic models with reaction rate parameters derived mainly from TG experiments and semidetailed kinetic scheme [33]. The current model can hopefully be improved by adding the additional species with associated thermochemical information and adopting the recent modeling methodology.

7.3 Model Temperature Input

The CRN model requires a temperature input. This temperature is calculated by applying a heat transfer model to the wood batch inside the furnace. If the control system is to operate independently of fuel source, it is not feasible to calculate wood temperature by applying a heat transfer model for every fuel used. The control system has to operate with real-time temperature measurement of wood temperature.

Appendix A
Low-Cost Sensors, Heat Transfer Model & CRN Info.

This appendix includes technical information on low cost sensors which are capable to measure concentration of UHC, CO and PM. An optical particle sensor detects a scattered light signal from a particle sample and a metal oxide semiconductor sensor responds to reducing gases, e.g. CO and methane. The response from the low cost sensors is compared to commercially available diagnostics for combustion gases and aerosols. This information is included in sections A.1 through A4.

Section A5 includes properties of white oak.

Heat transfer analysis used to calculate wood temperature is presented in section A6.

The appendix also includes further information about the CRN. Sample input and output files are presented in sections A7 and A8.

A.1 Optical Particle Sensor

Performance tests of a low cost optical Sharp dust sensor of type GP2Y1010AU0F, models 10-F-25 and 10-F-01 [36], have been carried out to investigate the feasibility of employing an inexpensive sensor to detect PM emissions in combustion systems. In the sensor, an infrared light source and a phototransistor are arranged diagonally to detect scattered light from a particle sample. The output voltage from the phototransistor is proportional to the intensity of the scattered light.

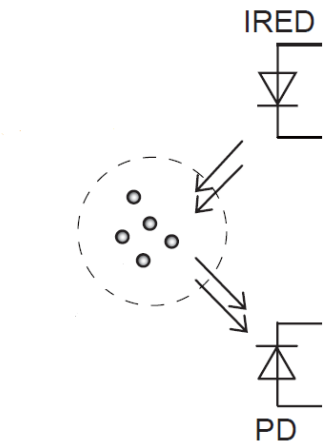

Figure A.1: Optical particle sensor. Infrared light is emitted from the IRED LED, scattered off the sample and detected by the phototransistor [36].

Scattering is a physical process by which a particle in the path of an electromagnetic wave continuously abstracts energy from the incident wave and reradiates that energy in all directions. Scattering by particles whose diameter is much smaller than the incident radiation wavelength is described by Rayleigh scattering. If the particle size is of the same order of magnitude as the wavelength, the appropriate scattering description is given by Mie theory. The mathematical description of Mie theory is attained by solving Maxwell's equations of electromagnetism for a spherical geometry. The derivation is outside the scope of this work; a detailed description is given in Hulst [37]. The following are the relevant results for the far field solution.

The intensity of a scattered light from a single particle is given by:

A.1 $$\mathrm{I}(\mathrm{a}, \lambda, m, \theta) = I_0 \frac{i_1 + i_2}{2k^2 r^2} \quad \mathrm{W/m^2}$$

where I_0 is the incident light intensity, θ is the scattering angle, r is the scattering distance, a represents the radius of the particle and m is the index of refraction. The parameters i_1 and i_2 are the (dimensionless) intensity functions,

$$i_1 = |S_1|^2 \qquad i_2 = |S_2|^2$$

$$\mathrm{S}_1 = \sum_{n=1}^{\infty} \frac{2n+1}{n(n+1)} \left\{ a_n \pi_n(\cos\theta) + b_n \tau_n(\cos\theta) \right\}$$

$$\mathrm{S}_2 = \sum_{n=1}^{\infty} \frac{2n+1}{n(n+1)} \left\{ b_n \pi_n(\cos\theta) + a_n \tau_n(\cos\theta) \right\}$$

$$a_n = \frac{\psi'_n(y)\psi_n(x) - m\psi_n(y)\psi'_n(x)}{\psi'_n(y)\zeta_n(x) - m\psi_n(y)\zeta'_n(x)}$$

$$b_n = \frac{m\psi'_n(y)\psi_n(x) - \psi_n(y)\psi'_n(x)}{m\psi'_n(y)\zeta_n(x) - \psi_n(y)\zeta'_n(x)}$$

$$\pi_n(\cos\theta) = \frac{1}{\sin\theta} P_n^1(\cos\theta) \qquad \tau_n(\cos\theta) = \frac{d}{d\theta} P_n^1(\cos\theta)$$

$$x = ka = \frac{2\pi a}{\lambda}, \qquad y = \frac{2\pi m a}{\lambda}$$

The functions ψ_n, ζ_n are the Riccati-Bessel functions, their derivatives are denoted by ψ'_n, ζ'_n and P_n^1 are the Legendre polynomial. The refractive index m is a complex number $m = m_r + im_i$. The real component determines wave speed in a medium compared to the speed of light and the complex component determines the absorption of the incident wave by the medium.

The scattering intensity and the optical sensor output are determined by the refractive index, particle size, scattering angle and the LED wavelength.

A.1.1 Experiments & Results

Optical responses of aerosolized particles of various sizes and combustion generated smoke were measured, see Figure A.3

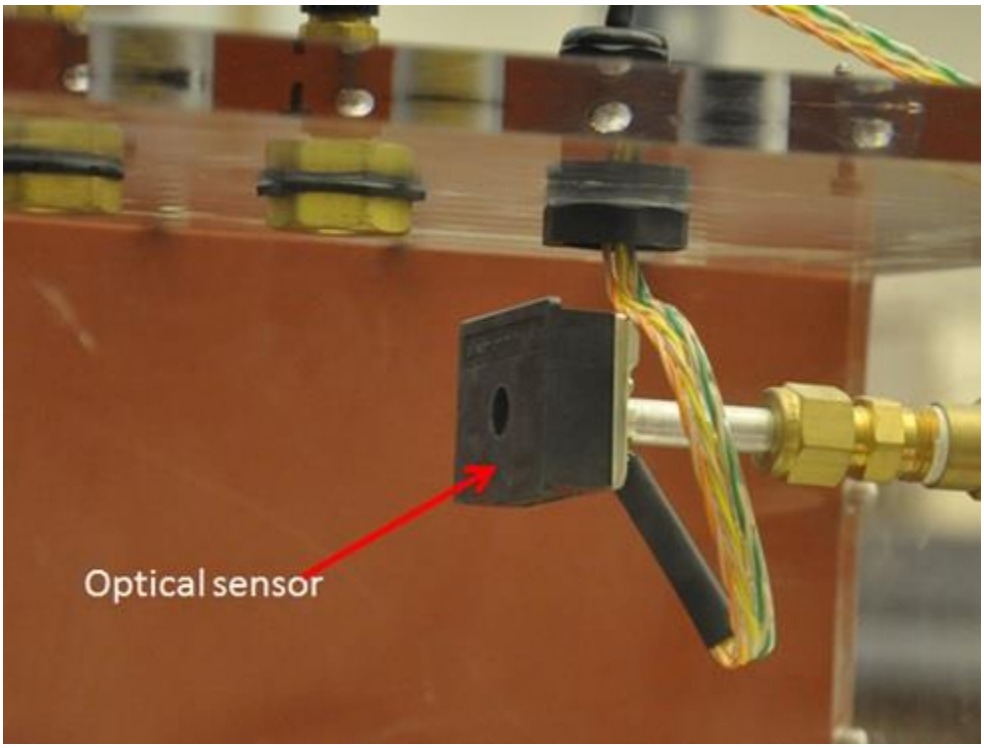

Figure A.2: Low cost optical dust sensor.

The experiments were performed in a specially designed aerosol chamber. Table A.1 summarizes physical and optical properties of the aerosolized particles.

Table A.1: Optical particle sensor. Infrared light is emitted from the IRED LED, scattered off the sample and detected by the phototransistor (Sharp, 2013).

Average Diameter	**Material**	**Density [g/cc]**	$m_r\,(\lambda = 1\mu m)$	$m_i\,(\lambda = 1\mu m)$	$\frac{(i_1 + i_2)}{2}$	**Average Diameter**
0.95 μm	Red Fe-Ox	1.2	2.7	0	2.3	0.95 μm
2.3 μm	Silica	1.8	1.45	0	13	2.3 μm
3.9 μm	Silica	1.8	1.45	0	26	3.9 μm

Table A.1 summarizes physical and optical properties of the aerosolized particles. A TSI Aerodynamic Particle Counter (model 3321) measured particle size and concentration. The intensity parameters are computed using the LightLab far field Mie scattering code [38]. The values listed are averages over the range of particles in the sample.

Figure A.3 shows the sensor response is greater for larger particles on a number-density basis. For large number densities, the curves diverge from each other, indicating breakdown of the independent scattering assumption and the influence of multiple scattering on the sensor response.

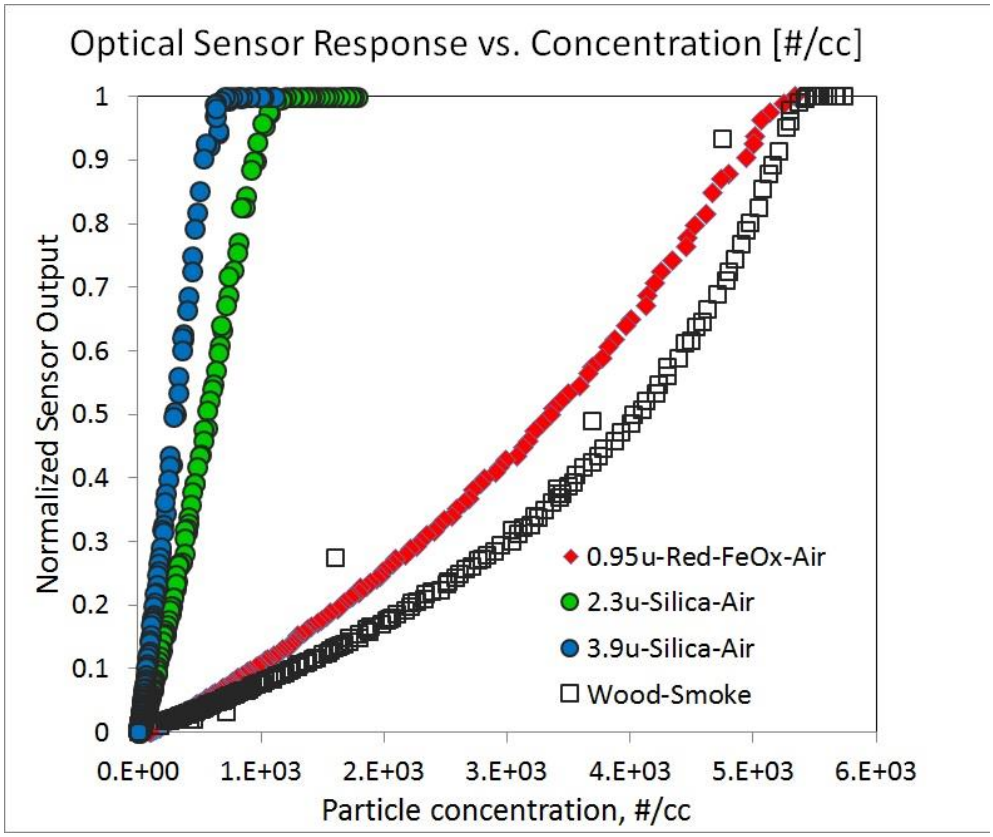

Figure A.3: Normalized optical sensor output. In general, as the particle size gets smaller, more particles are required to give the same sensor output.

Assuming independent scattering, i.e. each particle scatters light in exactly the same way as if all other particles did not exist, the data collapses on a single curve by plotting the product of total concentration and the average of the intensity functions.

A2 $$I_t \approx N_t I_0 \frac{i_1 + i_2}{2k^2 r^2} \propto N_t \frac{i_1 + i_2}{2}$$ $\mathrm{W/m^2}$

After applying a Mie scattering correction based on the surface area and optical properties of the particles, the sensor response was found to be linearly related to the normalized surface areas, as Figure A.3 indicates.

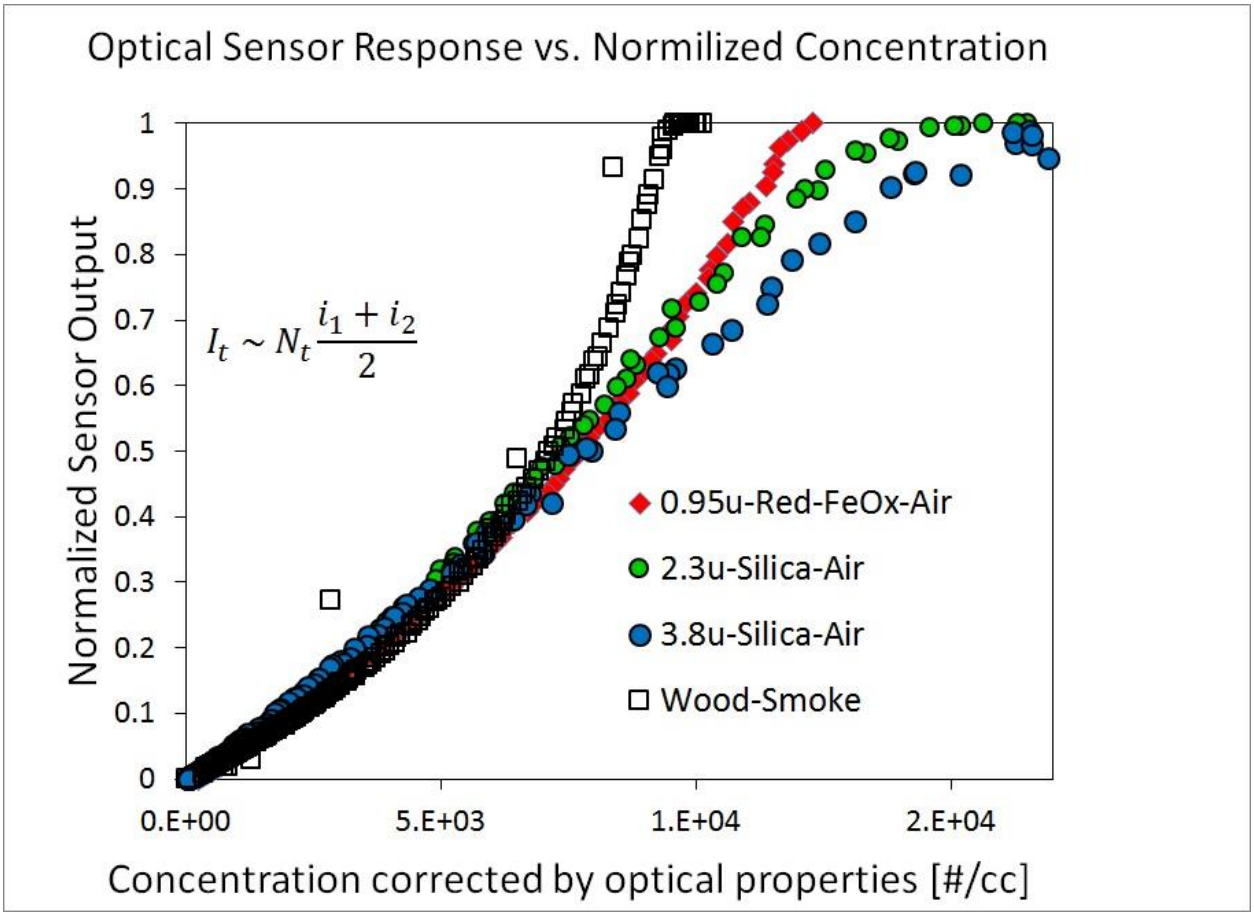

Figure A.4: Calibration of low-cost PM sensor demonstrates linearity when Mie scattering is accounted for.

This analysis shows that the low-cost optical particle sensor can be used reliably for measurements of combustion generated aerosols. The low-cost particle sensor not only captures the particle emission trends but also can be used for estimating total particle concentration.

A.2 Metal Oxide Semiconductor Carbon Monoxide & Hydrocarbon Sensor

A sensing unit consisting of a pair of Metal Oxide Semiconductor (MOS) MICS-5521[39] CO and HC sensors and an additional sensing unit that monitors relative humidity and temperature was built to evaluate feasibility of its integration for measuring concentration of gases in combustion exhaust. A microcontroller and a MOS sensor evaluation board are also present to control operating conditions of the sensors. Figure A.5 demonstrates the sensor module.

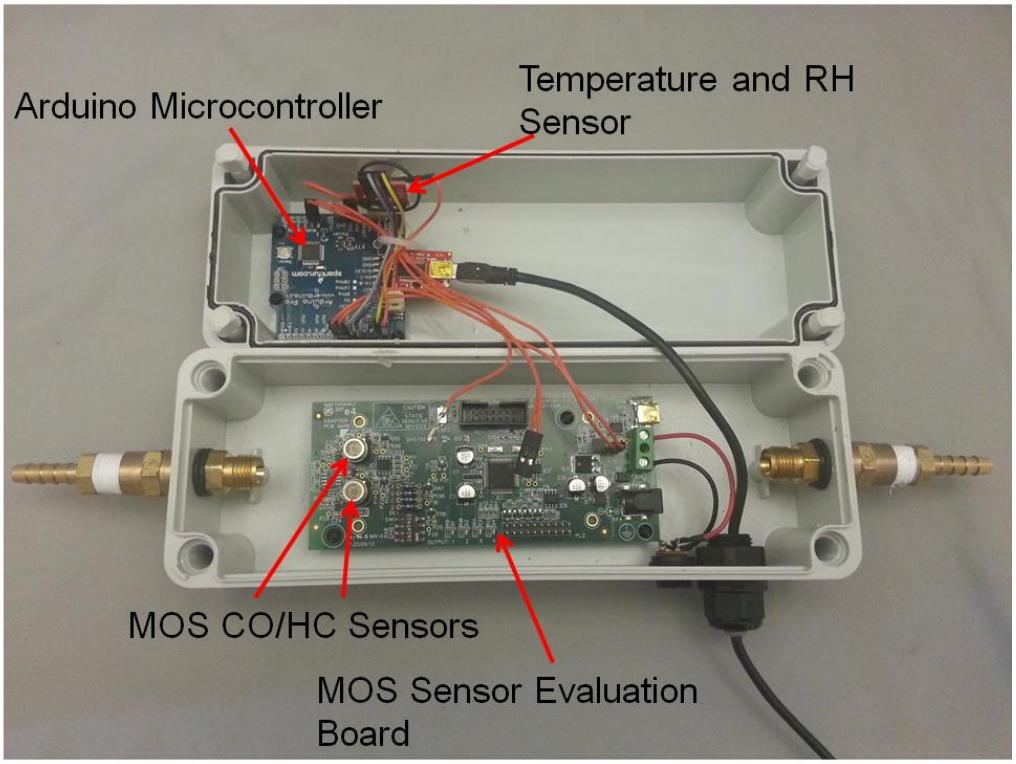

Figure A.5: A sensor module for detection of carbon monoxide and HC gases, relative humidity and temperature

The MOS sensors consist of a diaphragm with an embedded heating resistor and a sensing layer on top. The evaluation board controls the supplied power to the heaters. The sensors can be operated in static and pulsed mode. In static mode, a constant DC voltage is supplied

to the heating resistor. Pulsed modes consists of powering the heaters with pulses and utilizing the dynamic behavior of the sensing resistance. In addition, the high voltage increases the temperature of the sensing layer at which point water vapor and interfering gases are removed from the sensing layer. Figure A.8 demonstrates the dynamic behavior of a MOS sensor operated in pulsed mode when exposed to CO.

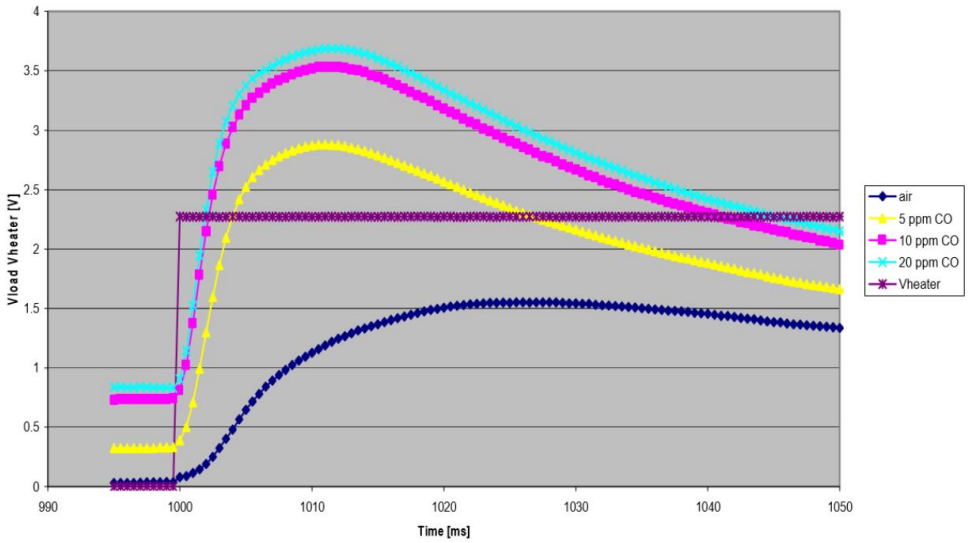

Figure A.6: Dynamic behavior of MOS sensors operating in pulsed mode.

The MOS sensor operates by decreasing the resistivity of the semiconductor layer when exposed to reducing gases. The reducing gases react with the oxygen surface ions, thereby freeing electrons that migrate to the conduction band to increase the conductivity and decrease resistivity of the MOS. Monitoring resistance over time provides information about variable CO and HC concentrations. The magnitude depends on morphology, geometrical characteristics, composition and doping of the base material, as well as temperature [40].

The MOS sensor was calibrated for CO and hydrocarbon (CH4). The CO calibration was carried out using diluted CO (750 ppm) and make-up air in order to further reduce the CO

concentration. One of the CO sensors was operated in static mode, and the other in pulsed mode to compare the accuracy and dynamic response of both approaches. The pulse length and the analysis algorithm were varied to determine the most reliable technique. Figure A.8 shows CO calibration curve for pulsed sensor operation. Two-second-long sensor membrane heating pulses were initiated by the evaluation board. The signal was analyzed using a custom algorithm implemented in MATLAB. Several techniques for analyzing the sensor output were evaluated, including initial-slope analysis and fixed-time-interval analysis. The sensor peak-to-equilibrium voltage ratio was selected since it produced reliable measurements in all experiments and was easy to implement.

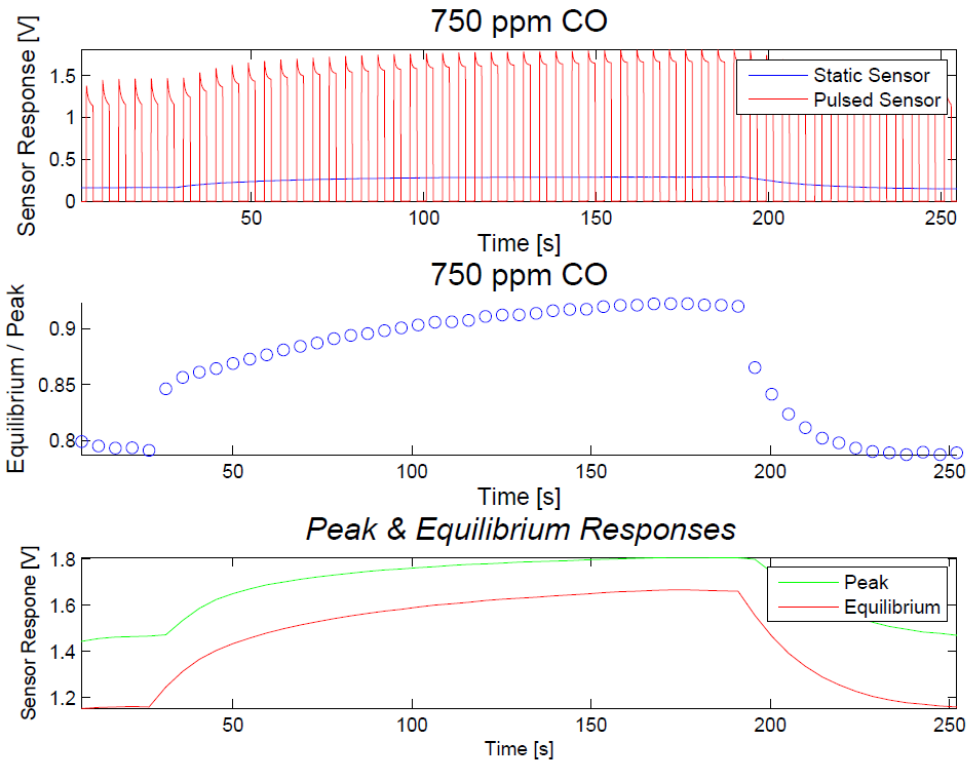

Figure A.7: Sensor response to 750 ppm CO.

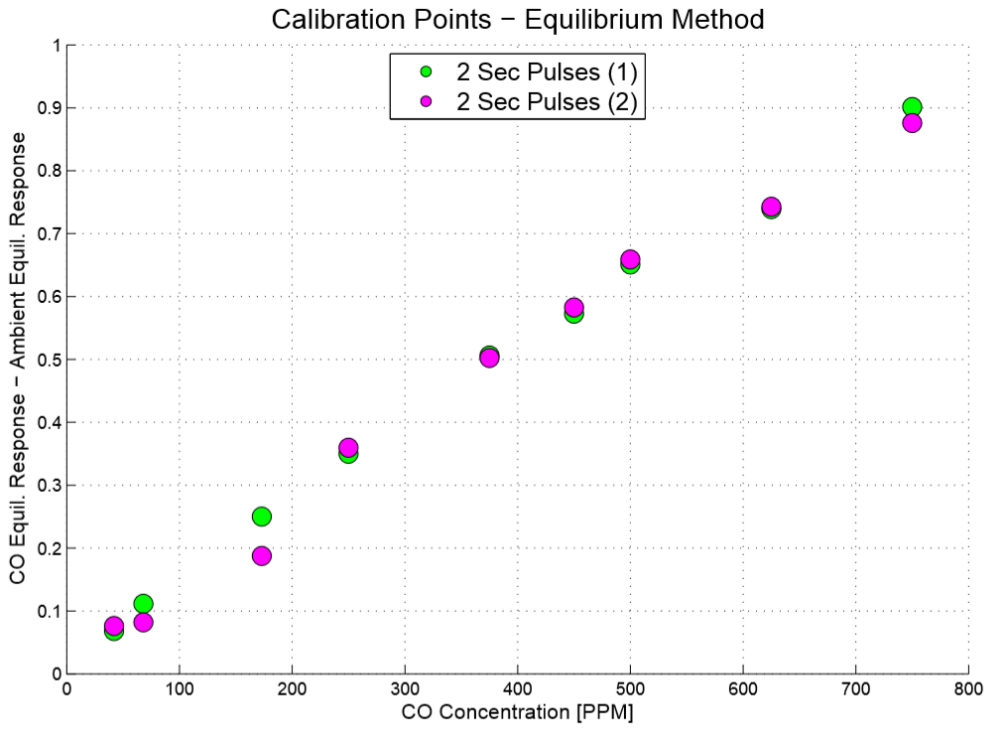

Figure A.8: Normalized sensor response for various CO concentration

Sensor responses to hydrocarbons were also measured. Methane-air mixtures were prepared in a custom mixing chamber at the UW combustion lab. The sensor module was plumbed to the chamber, which was evacuated at a flow rate of 4 LPM. The sensors were unable to detect methane for concentrations smaller than 10,000 ppm. Since the selectivity of the sensing layer to CO is much greater compared to hydrocarbons, the response of the sensors is much weaker when exposed to methane. These results indicate the sensor to be applicable to CO measurements in combustion gas exhaust but limiting for detection of hydrocarbons.

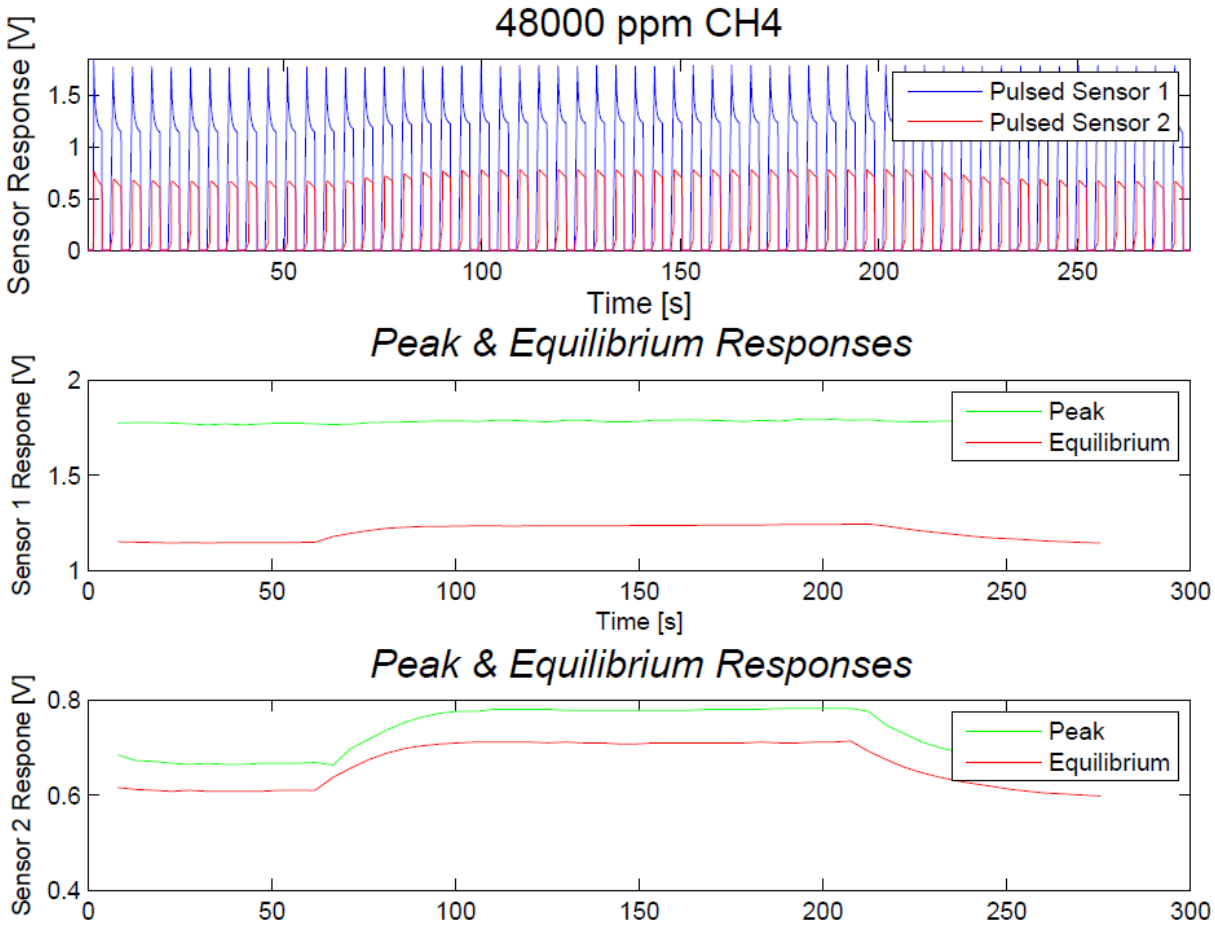

Figure A.9: Response from two sensor operated in pulsed mode to 48,000 ppm of methane.

A.3 Low Cost Sensor Measurements of Biomass Combustion Exhaust

A prototype of the sensing array was built for testing in a biomass furnace environment. The sensing system included the low-cost particle sensor, two MOS sensors for CO and hydrocarbon (HC) measurement, and relative humidity and temperature sensors.

The optical sensor response to the PM concentration was compared with an aerodynamic particle counter (TSI model 3321) which was placed in series with the optical particle sensor. Figure A.11 shows a comparison of the responses of the optical PM sensor and the APS. The

figure shows the initial spike in PM associated with tar release from the wood during pyrolysis and then significant reduction in PM emission at the onset of the flaming combustion regime. The optical PM sensor response is nearly identical to the reference instrument. This and similar data show that the chosen optical PM sensor and data acquisition hardware are appropriate for detection of varying PM concentrations in a biomass furnace.

The MOS sensors were also tested in a biomass furnace and compared to a Bacharach ECA-450 combustion gas analysis system. The Bacharach is capable of detecting CO, hydrocarbons, oxygen, NOx and other combustion gas species of interest. The signal from the sensor array were recorded similarly to the PM measurement and interpreted using a custom algorithm based on the laboratory sensor calibration discussed previously. The MOS sensors are able to detect varying concentrations of CO from the biomass furnace. Figure A.11 compares the inexpensive MOS CO sensor response with the combustion analyzer data. The sensor is able to capture low levels of CO before the ignition event and the rise in CO concentration during the typical biomass combustion process. These data shows the feasibility of using low-cost CO sensors for monitoring exhaust gas from biomass combustor.

The combination of PM, CO and temperature measurements demonstrated in these results show that it is feasible to monitor combustion exhaust gases using low-cost sensors; this information can be used to optimize the combustion process by maximizing efficiency and minimizing pollution levels from biomass combustion.

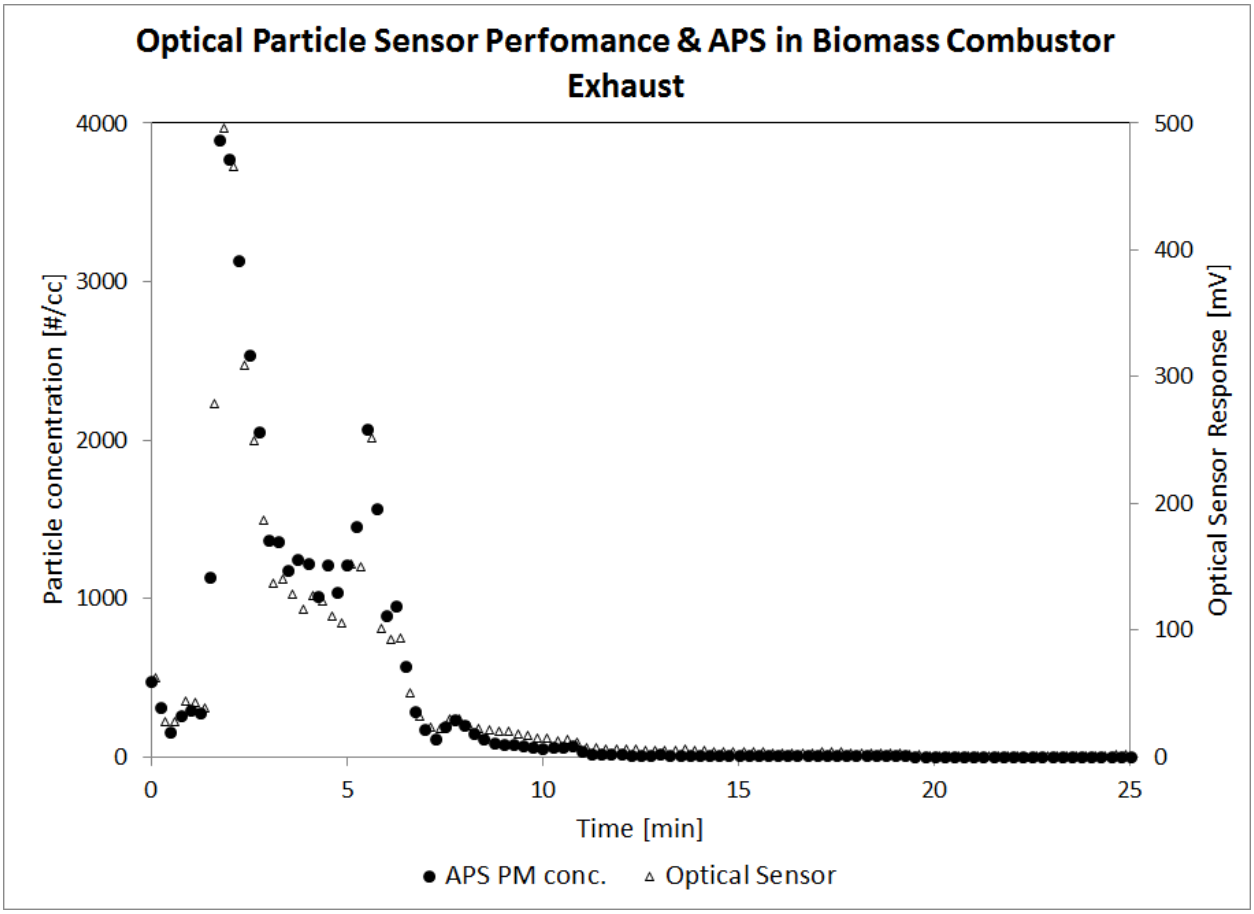

Figure A.10: Optical particle counter and APS comparison.

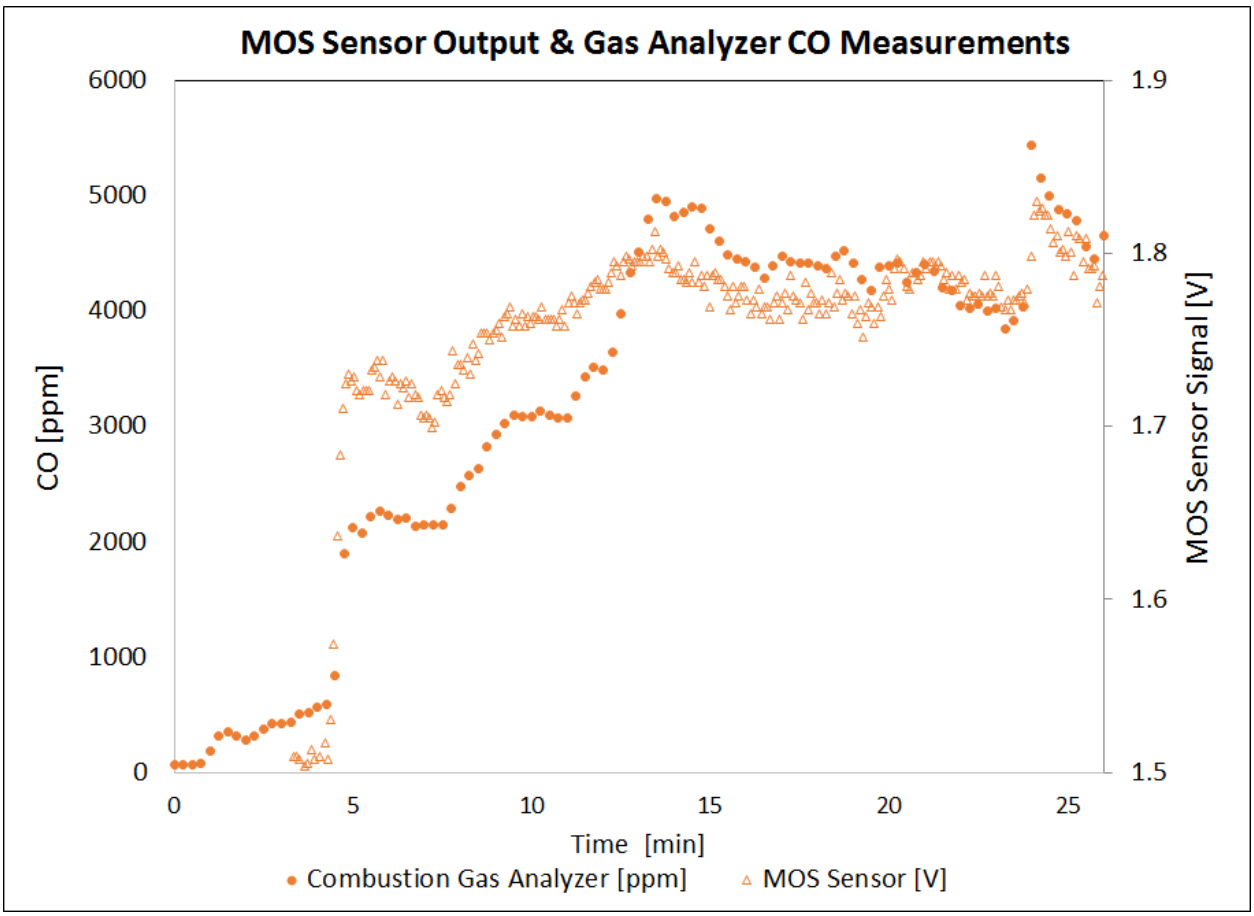

Figure A.11: MOS CO sensor compared to CO concentration from a commercial gas analyzer

A.4 Dilution System

Sampling particulate matter and aerosols often requires concentrations to be reduced by dilution. Diluting an aerosol sample can bring the concentration to within range of measuring instruments, quench chemical reactions and prevent particle coagulation and diffusion losses. Multiple diluters with a wide variety of applications have been described in the literature. These systems usually function by extracting a sample by generating a suction with flowing dilution air or with an external vacuum pump [41].

Uncertainty in the dilution rate (DR) is strongly influenced by which flow is measured. The dilution rate (DR) is defined as:

A3
$$DR = \frac{Q_t}{Q_s} = \frac{Q_d + Q_s}{Q_s} = \frac{Q_t}{Q_t - Q_d}$$

Where Q_t is the total flow, Q_s is the sample flow and $Q_d$is the dilution flow.

Table A.2: Uncertainties in dilution rate – depending on measured flow.

Flow Measured	Δ(DR)
Q_s & Q_t	$\sqrt{\Delta(Q_s)^2 + \Delta(Q_t)^2}$
Q_s & Q_d	$\left(1 - \frac{1}{DR}\right)\sqrt{\Delta(Q_s)^2 + \Delta(Q_d)^2}$
Q_d & Q_t	$(DR - 1)\sqrt{\Delta(Q_t)^2 + \Delta(Q_d)^2}$

Table A.2 shows the influence of measured flow on the dilution rate uncertainty. If the sample flow is measured, the uncertainty in the dilution rate calculation is similar to the uncertainties of the flow measurements. If the total and dilution flows are measured, the uncertainty in the dilution rate can be much greater than the uncertainties in the flow measurements for large dilution rates [42]. It is therefore desirable to measure the sample flow. The diluter used in this study is based on systems reported by Brockmann et al. [41] and TSI [43]. The system is demonstrated in Figure A.12. The sample is extracted through a 1 ft.-long stainless steel capillary tube with an inner diameter of 0.3175 mm (0.012″) [44]. The choice of a capillary tube is made for a few reasons. Particle loss by Brownian diffusion in laminar flow tubes can be calculated from equations described by Gormley and Kennedy. The relationship between pressure drop and volumetric flow rate is well known for a developing laminar flow in cylindrical tubes [41]. In addition, for a given downstream

vacuum level, the long, narrow capillary resists flow, permitting small sample flow and wider range of dilution rates.

Figure A.12 demonstrates the two dilution systems employed for the experiments in this study. The measuring instruments require different concentration ranges for reliable outputs, necessitating two dilution systems. The principal operation of the systems is the same. An external vacuum source extracts a combustion gas sample from the exhaust through the narrow capillary tube. Compressed dilution air is filtered before mixing with the sample flow before the mixture is sampled by the TSI or the low cost sensors.

The TSI sample was 75 cc/min, the TSI continuously samples at 5 LPM and the dilution rate is 67. The custom, inexpensive sensor sample flow was 180 cc/min, the dilution flow 3.8 LPM and the dilution rate 22. A water filter was placed upstream of the sample lines to extract dry samples.

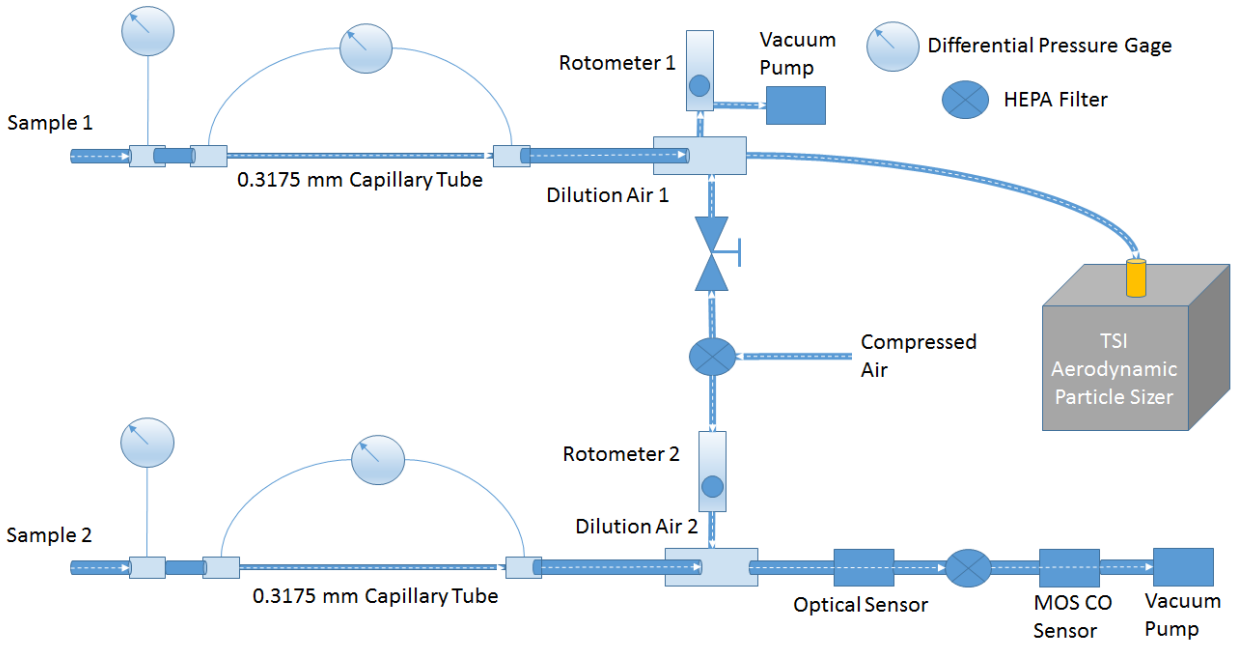

Figure A.12 Dilution System used for the experiments.

A.5 Properties of Experimental White Oak

Table A.3: Properties of experimental white oak.

Variable		Unit
ϵ [45]	0.87	
c [46]	1900	W
V	0.0177	m^3
ρ [45]	770	kg/m^3
A_s	0,3980	m^2
HHV [47]	6406	Btu/lbs.

A.6 Heat Transfer Analysis To Calculate Wood Temperature

The PFT1 element in the CRN requires inputs for fuel and air flow rates and wood temperature. Wood temperature was not measured during the experiments and has to be calculated by applying a heat transfer analysis to the wood batch in the furnace. The goal of the model is to calculate the surface temperature of the wood as a function of time and predict the onset of ignition. The wood batch is modeled as a continuous material. Figure A.13 demonstrates the problem setup.

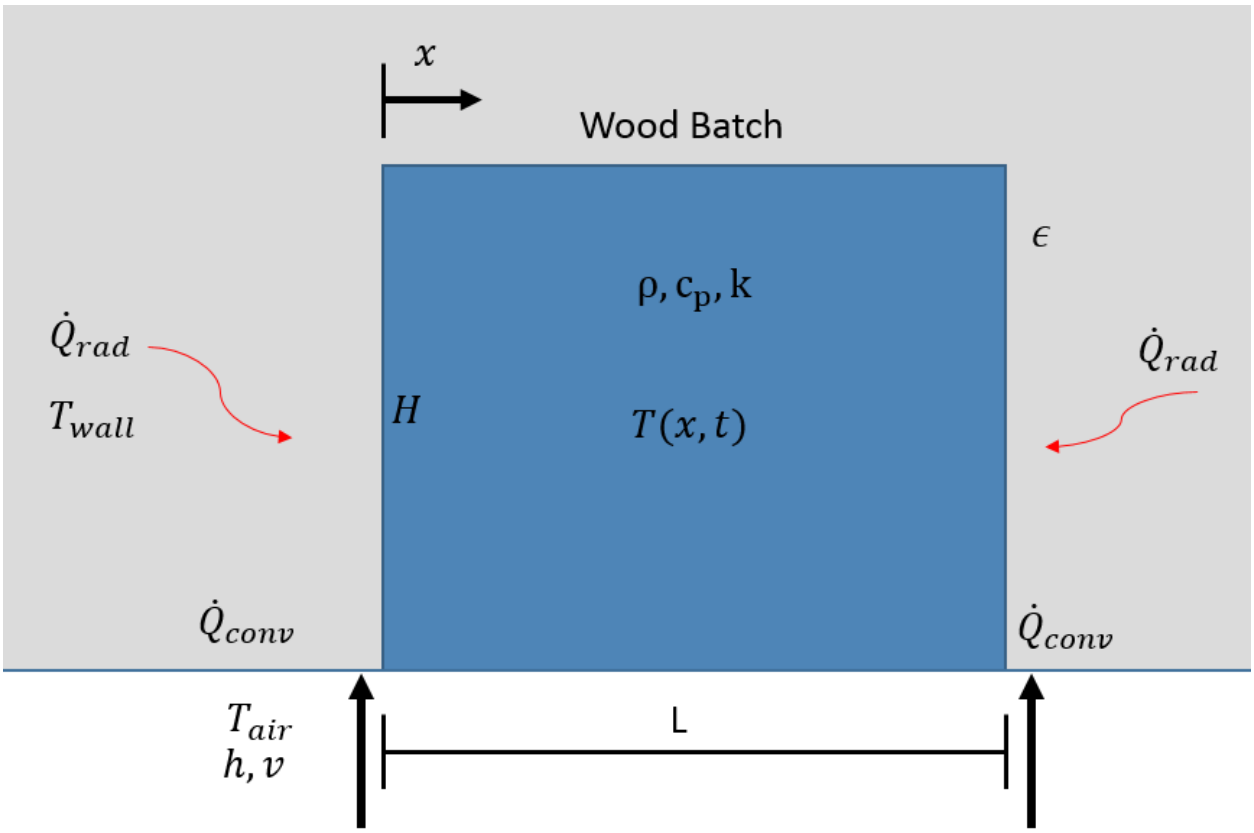

Figure A.13 Control surface for heat transfer model. Heat transfer mechanisms are radiative from the furnace walls and convective from the under-fire air inlet.

The wood receives energy by radiation ($\dot{Q}_{rad}$) and convection ($\dot{Q}_{conv}$) to the sides. Modeling temperature gradients from the top face into the wood is not attempted, i.e. the problem is

limited to one spatial dimension. Energy penetration to the wood is limited by thermal conduction – the thermal conductivity of wood is 0.2 W/(mK). Table A.4 lists dimensional and physical properties of the wood. Applying conservation of energy to the wood yields the following differential equation, initial and boundary conditions.

A4 $$\frac{\partial^2 T(x,t)}{\partial x^2} = \frac{1}{\alpha}\frac{\partial T(x,t)}{\partial t}$$ K/m²

A5 $$T(x,0) = 300\ K$$ K

A6 $$-k\frac{\partial T(0,t)}{\partial x} = h\big(T_\infty - T(0,t)\big) + \varepsilon\sigma\big(T_{wall}^4 - T^4(0,t)\big)$$ W/m²

A7 $$-k\frac{\partial T(L,t)}{\partial x} = h\big(T_\infty - T(L,t)\big) + \varepsilon\sigma\big(T_{wall}^4 - T^4(L,t)\big)$$ W/m²

Table A.4: Properties of white oak.

Variable		Unit
ϵ [45]	0.87	
c_p [46]	1900	W
ρ [45]	770	kg/m³
k [48]	0.2	W/(mK)
L	400	mm
H	400	mm

Using measured temperature values for T_{wall} = 800 K , T_{air}= 320 K and $T_\infty = \frac{T_{air}+T_{wall}}{2}$ = 560 K. The convective heat transfer coefficient, h, is calculated based on Nusselt number correlations for a flow past a flat plate.

A8 $$\mathrm{h} = \frac{Nu\ k}{H}$$ W/(K·m²)

A9 $$\mathrm{Nu} = 0.664\, Re^{0.5} Pr^{0.33}$$ $\mathrm{W/(K \cdot m^2)}$

which is the Nusselt number correlation for laminar flow (Re < 500,000) past a flat plate. Based on measured flow rate and geometry of the furnace, the calculated velocity through the small holes on the floor grates is 64 m/s, indicating the air enters through the holes as jets. Accounting for jet entrainment[49], the average velocity used in the analysis is $v =$ 10 m/s, yielding $\mathrm{Re_L}$ = 242,000, Nu = 282 and h = 19 $\mathrm{W/(m^2K)}$. Figure A.14 demonstrates model results for temperature profiles inside the wood for the first five minutes. The temperature profiles are calculated by solving equations A4-A7 numerically. The temperature reaches approximately 675 K in 5 minutes, close to the temperature (700 K) required to drive off all the volatiles according to Figure 2.4.

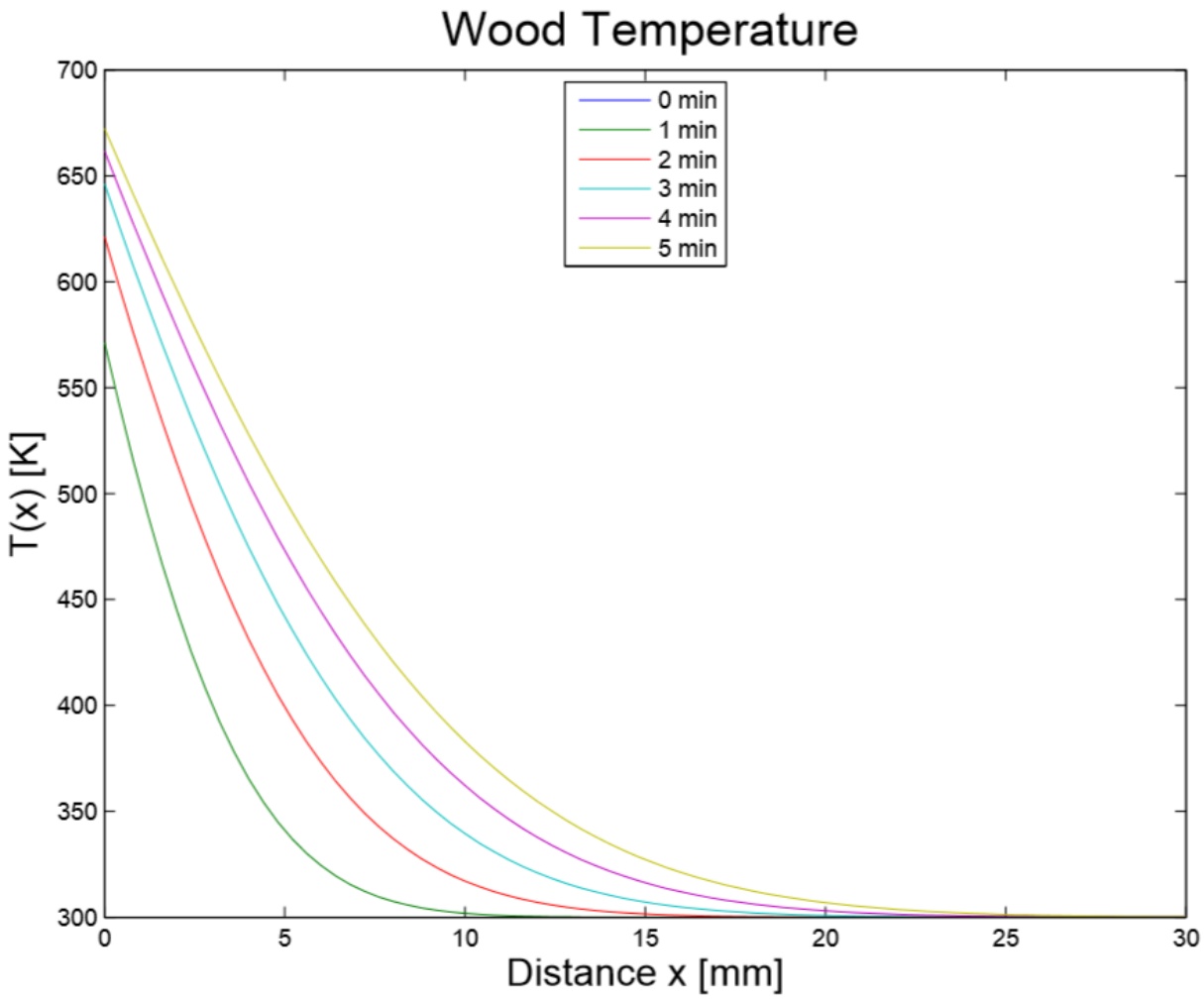

Figure A.14 Calculated temperature profiles inside the wood for the first five minutes. The wood surface reaches approximately 700 K in 5 minutes.

The following Matlab code is used to generate Figure A.14.

```
function PDEHT
m = 0;

k = 0.2; %thermal conductivity of white oak
rho = 770; %kg/m3 for white oak
c = 1900; %Heat capacity of white oak
alpha = k/(rho*c); %thermal diffusivity of white oak
e = 0.87;
sigma = 5.67E-08; %Stefan Boltzman constant
h = 20; %heat transfer coefficient
```

```
Ti = 300; %initial temperature = 320 K
Tinf = (320+800)/2;
%Ts = 100;
Twall = 800; %Furnace wall temperature

xmesh = linspace(0,0.4,1000);
tspan = [0, 60, 120, 180, 240,300];

sol = pdepe(m,@pdefun,@icfun,@bcfun,xmesh,tspan);
u = sol(:,:,1);

figure
plot(xmesh*10^3,u(:,:))
title('Wood Temperature','FontSize',20);
xlabel('Distance x [mm]','FontSize',16);
ylabel('T(x) [K]','FontSize',16);
legend('0 min','1 min','2 min','3 min','4 min','5
min','location','North');
xlim([0,30]);

set(gcf, 'Position', [100 100 150 150]);
saveas(gcf, 'OneEnd.pdf');

figure
plot(xmesh*10^3,u(:,:))
title('Wood Temperature','FontSize',20);
xlabel('Distance x [mm]','FontSize',16);
ylabel('T(x) [K]','FontSize',16);
legend('0 min','1 min','2 min','3 min','4 min','5
min','location','North');

set(gcf, 'Position', [100 100 150 150]);
saveas(gcf, 'Total.pdf');


    function [c,f,s] = pdefun(x,t,u,DuDx);
        c = 1/alpha;
        f = DuDx;
        s=0;
    end
    function u0 = icfun(x)
        u0 = Ti;
    end
    function [pl,ql,pr,qr] = bcfun(xl,ul,xr,ur,t)
        pl = h*(Tinf-ul) + e*sigma*(Twall^4 - ul^4);
        ql =  k;
        pr = h*(Tinf-ur) + e*sigma*(Twall^4 - ur^4);
        qr = -k;
    end

end
```

A.7 CRN – General Information

The basis of the model is the University of Washington Chemical Reactor Model (UW-CRM) which is a general purpose computer program used to predict and understand chemical processes. The code has mainly been used to predict NOx and CO from turbine engines and sawdust and sanderdust fired wood burners [19]. The code contains three sub-models: thermodynamic, kinetic and zonal. The code includes thermo-chemical data for all gas phase species and pure condensed species of interest (e.g. H2O(l) and C(s)). Malte et al. expanded the thermo-chemical library to include information for wood, tars and char and data for wood kinetics and oxidation. The zonal sub-model consists of arranging PFR, PSR and MIX elements to simulate combustion zones such as initial flame, flame region, recirculation and burnout-zone. Several variations of the ideal reactors can be used as listed in Novosselov [19] and repeated here:

- PSR – adiabatic perfectly stirred reactor with residence time based on the input of the mass flows, volume, and temperature.
- PSB - adiabatic perfectly stirred reactor operated just below blowout conditions.
- PSX – adiabatic perfectly stirred reactor with the input of the mass flows and with the assigned residence time
- PST – non-adiabatic perfectly stirred reactor with the input of the mass flows and volume and with the assigned temperature.
- PSZ - non-adiabatic perfectly stirred reactor with the input of the mass flows and with the assigned temperature and residence time.

- PFR – adiabatic plug flow reactor with residence time based on the input of the mass flows and volume, and calculated temperature.
- PFX – adiabatic plug flow reactor with the input of the mass flows and with the assigned residence time.
- PFT – non-adiabatic plug flow reactor with the input of the mass flows and volume and with the assigned temperature.
- PFZ - non-adiabatic plug flow reactor with the input of the mass flows and with the assigned temperature and residence time.

The code solves the system of non-linear partial differential according to equations 2.11 and conservation expressions for momentum and energy. The code solves the system of equations at stationary time steps, and uses the convergence of Jacobi-Newton (diagonalized Newton-Raphson) or a predictor-corrector scheme if the Newton-Raphson method fails to converge. The initial guess values for the first iteration are calculated for adiabatic equilibrium for the given conditions. Further details about applied numerical algorithm to solve the reaction kinetics and conservation equations of the reactors can be found in Nicol [27]. Information about code networking capabilities and instructions can be found in Novosselov [19]. In this study, several nitric oxide mechanisms have been removed from the code to improve convergence time.

A.8 CRN Input File & Result Sample

The following section includes an input and output file for the CRM to simulate the Dec 12th burn of 47 lbs. white oak.

A.8.1 Input File

```
!
C        12.01115  4.0
H        1.00797   1.0
O        15.9994   -2.0
N        14.0067   0.0

THERMO
C                 121086C   1               G   300.     5000.
1
 0.02602087E 02-0.01787081E-02 0.09087041E-06-0.11499333E-10 0.03310844E-
14    2
 0.08542154E 06 0.04195177E 02 0.02498584E 02 0.08085776E-03-0.02697697E-
05    3
 0.03040729E-08-0.11066518E-12 0.08545878E 06 0.04753459E 02
4
CH                121286C   1H   1          G   300.000  5000.000
1
 0.02196223E 02 0.02340381E-01-0.07058201E-05 0.09007582E-09-0.03855040E-
13    2
 0.07086723E 06 0.09178373E 02 0.03200202E 02 0.02072875E-01-0.05134431E-
04    3
 0.05733890E-07-0.01955533E-10 0.07045259E 06 0.03331587E 02
4
CH2               120186C   1H   2          G   250.000  4000.000
1
 0.03636407E 02 0.01933056E-01-0.01687016E-05-0.10098994E-09 0.01808255E-
12    2
 0.04534134E 06 0.02156560E 02 0.03762237E 02 0.11598191E-02 0.02489585E-
05    3
 0.08800836E-08-0.07332435E-11 0.04536790E 06 0.01712577E 02
4
CH2CO             121686C   2H   2O   1     G   300.     5000.
1
 0.06038817E 02 0.05804840E-01-0.01920953E-04 0.02794484E-08-0.14588676E-
13    2
-0.08583402E 05-0.07657581E 02 0.02974970E 02 0.12118712E-01-0.02345045E-
04    3
-0.06466685E-07 0.03905649E-10-0.07632636E 05 0.08673553E 02
4
CH2O              121286C   1H   2O   1     G   300.000  5000.000
1
```

```
 0.02995606E 02 0.06681321E-01-0.02628954E-04 0.04737153E-08-0.03212517E-
12    2
-0.15320369E 05 0.06912572E 02 0.16527311E 01 0.12631439E-01-0.01888168E-
03    3
 0.02050031E-06-0.08413237E-10-0.14865404E 05 0.13784820E 02
4
CH2OH             120186H   3C   1O   1     G   250.     4000.
1
 0.06327520E 02 0.03608270E-01-0.03201547E-05-0.01938750E-08 0.03509704E-
12    2
-0.04474509E 05-0.08329365E 02 0.02862628E 02 0.10015273E-01-0.05285435E-
05    3
-0.05138539E-07 0.02246041E-10-0.03349678E 05 0.10397938E 02
4
CH2(S)             31287C   1H   2          G   300.000  4000.000
1
 0.03552888E 02 0.02066788E-01-0.01914116E-05-0.11046733E-09 0.02021349E-
12    2
 0.04984975E 06 0.01686570E 02 0.03971265E 02 0.01699088E-02 0.10253689E-
05    3
 0.02492550E-07-0.01981266E-10 0.04989367E 06 0.05753207E 00
4
CH3               121286C   1H   3          G   300.000  5000.000
1
 0.02844051E 02 0.06137974E-01-0.02230345E-04 0.03785161E-08-0.02452159E-
12    2
 0.16437809E 05 0.05452697E 02 0.02430442E 02 0.11124099E-01-0.01680220E-
03    3
 0.16218288E-07-0.05864952E-10 0.16423781E 05 0.06789794E 02
4
CH3O              121686C   1H   3O   1     G   300.000  3000.000
1
 0.03770799E 02 0.07871497E-01-0.02656384E-04 0.03944431E-08-0.02112616E-
12    2
 0.12783252E 03 0.02929575E 02 0.02106204E 02 0.07216595E-01 0.05338472E-
04    3
-0.07377636E-07 0.02075610E-10 0.09786011E 04 0.13152177E 02
4
CH4               121286C   1H   4          G   300.000  5000.000
1
 0.01683478E 02 0.10237236E-01-0.03875128E-04 0.06785585E-08-0.04503423E-
12    2
-0.10080787E 05 0.09623395E 02 0.07787415E 01 0.01747668E 00-0.02783409E-
03    3
 0.03049708E-06-0.12239307E-10-0.09825229E 05 0.13722195E 02
4
CN                121286C   1N   1          G   300.000  5000.000
1
 0.03720119E 02 0.15183506E-03 0.01987381E-05-0.03798371E-09 0.13282296E-
14    2
 0.05111626E 06 0.02888597E 02 0.03663204E 02-0.11565290E-02 0.02163409E-
04    3
```

```
 0.01854208E-08-0.08214695E-11 0.05128118E 06 0.03739015E 02
4
CO               121286C   1O   1          G   300.000  5000.000
1
 0.03025078E 02 0.14426885E-02-0.05630827E-05 0.10185813E-09-0.06910951E-
13    2
-0.14268350E 05 0.06108217E 02 0.03262451E 02 0.15119409E-02-0.03881755E-
04    3
 0.05581944E-07-0.02474951E-10-0.14310539E 05 0.04848897E 02
4
CO2              121286C   1O   2          G   300.000  5000.000
1
 0.04453623E 02 0.03140168E-01-0.12784105E-05 0.02393996E-08-0.16690333E-
13    2
-0.04896696E 06-0.09553959E 01 0.02275724E 02 0.09922072E-01-0.10409113E-
04    3
 0.06866686E-07-0.02117280E-10-0.04837314E 06 0.10188488E 02
4
C2H               20387C   2H   1          G   300.     5000.
1
 0.04427688E 02 0.02216268E-01-0.06048952E-05 0.09882517E-09-0.07351179E-
13    2
 0.06590415E 06-0.11994418E 01 0.03050667E 02 0.06051674E-01-0.04956634E-
04    3
 0.02804159E-07-0.08193332E-11 0.06630011E 06 0.05954361E 02
4
C2H2             121386C   2H   2          G   300.000  5000.000
1
 0.04436770E 02 0.05376039E-01-0.01912816E-04 0.03286379E-08-0.02156709E-
12    2
 0.02566766E 06-0.02800338E 02 0.02013562E 02 0.15190446E-01-0.16163189E-
04    3
 0.09078992E-07-0.01912746E-10 0.02612444E 06 0.08805378E 02
4
C2H3              12787C   2H   3          G   300.     5000.
1
 0.05933468E 0.04017745E-01-0.03966739E-05-0.14412666E-09 0.02378643E-12
2
 0.03185434E0.08530313E 0.02459276E 0.07371476E-01 0.02109872E-04    3
-0.13216421E-08-0.11847838E-11 0.03335225E 0.11556202E                   4
C2H4             121286C   2H   4          G   300.000  5000.000
1
 0.03528418E 02 0.11485185E-01-0.04418385E-04 0.07844600E-08-0.05266848E-
12    2
 0.04428288E 05 0.02230389E 02-0.08614880E 01 0.02796162E 00-0.03388677E-
03    3
 0.02785152E-06-0.09737879E-10 0.05573046E 05 0.02421148E 03
4
C2H5              12387C   2H   5          G   300.     5000.
1
 0.07190480E 02 0.06484077E-01-0.06428064E-05-0.02347879E-08 0.03880877E-
12    2
```

```
 0.10674549E 05-0.14780892E 02 0.02690701E 02 0.08719133E-01 0.04419838E-
04    3
 0.09338703E-08-0.03927773E-10 0.12870404E 05 0.12138195E 02
4
C2H6              121686C   2H   6          G   300.     4000.
1
 0.04825938E 02 0.13840429E-01-0.04557258E-04 0.06724967E-08-0.03598161E-
12    2
-0.12717793E 05-0.05239506E 02 0.14625387E 01 0.15494667E-01 0.05780507E-
04    3
-0.12578319E-07 0.04586267E-10-0.11239176E 05 0.14432295E 02
4
C2N2              121286C   2N   2          G   300.     5000.
1
 0.06548002E 02 0.03984707E-01-0.16342164E-05 0.03038596E-08-0.02111069E-
12    2
 0.03490716E 06-0.09735790E 02 0.04265459E 02 0.11922569E-01-0.13420142E-
04    3
 0.09192297E-07-0.02778941E-10 0.03547887E 06 0.01713212E 02
4
C3H2              121686C   3H   2          G   300.     5000.
1
 0.06530853E 02 0.05870316E-01-0.01720776E-04 0.02127498E-08-0.08291910E-
13    2
 0.05115213E 06-0.11227278E 02 0.02691077E 02 0.14803664E-01-0.03250551E-
04    3
-0.08644363E-07 0.05284877E-10 0.05219072E 06 0.08757391E 02
4
C3H3              U12/77C   3H   3          G   300.     3000.
1
 0.80916252E 01 0.37372850E-02 0.13886647E-05-0.12298604E-08 0.20681585E-
12    2
 0.35437793E 05-0.18204468E 02 0.25097322E 01 0.17103866E-01-0.45710858E-
05    3
-0.82841574E-08 0.54362287E-11 0.37040680E 05 0.11011264E 02
4
C4H2              121686C   4H   2          G   300.     5000.
1
 0.09031407E 02 0.06047252E-01-0.01948788E-04 0.02754863E-08-0.13856080E-
13    2
 0.05294735E 06-0.02385067E 03 0.04005191E 02 0.01981000E 00 0.09865877E-
04    3
-0.06635158E-07 0.06077413E-10 0.05424065E 06 0.01845736E 02
4
C4H3              U06/78C   4H   3          G   300.     5000.
1
 0.84874201E 01 0.86908937E-02-0.28544437E-05 0.41200798E-09-0.21301093E-
13    2
 0.47970555E 05-0.19018509E 02 0.35539713E 01 0.19461986E-01-0.48102484E-
05    3
-0.97301225E-08 0.62390535E-11 0.49453863E 05 0.70829868E 01
4
```

```
H                120186H   1               G   300.000  5000.000
1
 0.02500000E 0.00000000E 00 0.00000000E 00 0.00000000E 00 0.00000000E 00
2
 0.02547162E0.04601176E 0.02500002E 0.00000000E 00 0.00000000E 00    3
 0.00000000E 00 0.00000000E 00 0.02547162E0.04601176E                   4
HCCO              32387H   1C   2O   1     G   300.     4000.
1
 0.06758073E 02 0.02000400E-01-0.02027607E-05-0.10411318E-09 0.01965164E-
12    2
 0.01901513E 06-0.09071262E 02 0.05047965E 02 0.04453478E-01 0.02268282E-
05    3
-0.14820945E-08 0.02250741E-11 0.01965891E 06 0.04818439E 01
4
HCCOH             32387H   2C   2O   1     G   300.     4000.
1
 0.07328324E 02 0.03336416E-01-0.03024705E-05-0.01781106E-08 0.03245168E-
12    2
 0.07598258E 05-0.14012140E 02 0.03899465E 02 0.09701075E-01-0.03119309E-
05    3
-0.05537732E-07 0.02465732E-10 0.08701190E 05 0.04491874E 02
4
HCN               121286C   1H   1N   1     G   300.000  5000.000
1
 0.03650077E 02 0.03460998E-01-0.12742788E-05 0.02217655E-08-0.14771774E-
13    2
 0.14983916E 05 0.02393220E 02 0.02490462E 02 0.08611280E-01-0.10310342E-
04    3
 0.07481498E-07-0.02229109E-10 0.15208344E 05 0.07904981E 02
4
HCNO              120186H   1C   1N   1O   1G   250.00   4000.0
1
 0.06692412E 02 0.02368360E-01-0.02371510E-05-0.12755033E-09 0.02407137E-
12    2
 0.01694736E 06-0.12454345E 02 0.03184858E 02 0.09752316E-01-0.12802028E-
05    3
-0.06163104E-07 0.03226275E-10 0.01797907E 06 0.06123843E 02
4
HCO               121286C   1H   1O   1     G   300.000  5000.000
1
 0.03557271E 02 0.03345572E-01-0.13350060E-05 0.02470572E-08-0.01713850E-
12    2
 0.03916324E 05 0.05552299E 02 0.02898329E 02 0.06199146E-01-0.09623084E-
04    3
 0.10898249E-07-0.04574885E-10 0.04159922E 05 0.08983614E 02
4
HNCO              31287H   1N   1C   1O   1G   300.     4000.
1
 0.06211867E 02 0.02297137E-01-0.02216128E-05-0.12220438E-09 0.02272406E-
12    2
-0.14770725E 05-0.08016633E 02 0.03694059E 02 0.06657236E-01-0.05054468E-
06    3
```

```
-0.03473411E-07 0.13605694E-11-0.13919758E 05 0.05712742E 02
4
HNO               121286H   1N   1O   1     G   300.000  5000.000
1
 0.03615144E 02 0.03212485E-01-0.12603370E-05 0.02267297E-08-0.15362358E-
13    2
 0.10661911E 05 0.04810263E 02 0.02784402E 02 0.06609646E-01-0.09300223E-
04    3
 0.09437980E-07-0.03753146E-10 0.10918779E 05 0.09035629E 02
4
HOCN              120186H   1O   1C   1N   1G   250.00   4000.0
1
 0.05645607E 02 0.02298206E-01-0.02162629E-05-0.12148014E-09 0.02238636E-
12    2
-0.03178109E 05-0.03590263E 02 0.03628292E 02 0.05664184E-01-0.11702056E-
06    3
-0.02348638E-07 0.08016402E-11-0.02475925E 05 0.07476825E 02
4
HO2                20387H   1O   2          G   300.000  5000.000
1
 0.04072191E 02 0.02131296E-01-0.05308145E-05 0.06112269E-09-0.02841164E-
13    2
-0.15797270E 03 0.03476029E 02 0.02979963E 02 0.04996697E-01-0.03790997E-
04    3
 0.02354192E-07-0.08089024E-11 0.01762273E 04 0.09222724E 02
4
H2                121286H   2               G   300.000  5000.000
1
 0.02991423E 02 0.07000644E-02-0.05633828E-06-0.09231578E-10 0.15827519E-
14    2
-0.08350340E 04-0.13551101E 01 0.03298124E 02 0.08249441E-02-0.08143015E-
05    3
-0.09475434E-09 0.04134872E-11-0.10125209E 04-0.03294094E 02
4
H2CN               41687H   2C   1N   1     G   300.     4000.
1
 0.05209703E 02 0.02969291E-01-0.02855589E-05-0.16355504E-09 0.03043259E-
12    2
 0.02767711E 06-0.04444478E 02 0.02851661E 02 0.05695233E-01 0.10711403E-
05    3
-0.16226120E-08-0.02351108E-11 0.02863782E 06 0.08992751E 02
4
H2O                20387H   2O   1          G   300.000  5000.000
1
 0.02672145E 02 0.03056293E-01-0.08730260E-05 0.12009964E-09-0.06391618E-
13    2
-0.02989921E 06 0.06862817E 02 0.03386842E 02 0.03474982E-01-0.06354696E-
04    3
 0.06968581E-07-0.02506588E-10-0.03020811E 06 0.02590232E 02
4
H2O2              120186H   2O   2          G   300.000  5000.000
1
```

```
 0.45731667E 01 0.43361363E-02-0.14746888E-05 0.23489037E-09-0.14316536E-
13    2
-0.18006961E 05 0.50113696E 00 0.33887536E 01 0.65692260E-02-0.14850126E-
06    3
-0.46258055E-08 0.24715147E-11-0.17663147E 05 0.67853631E 01
4
N                 120186N   1              G   300.000  5000.000
1
 0.02450268E 02 0.10661458E-03-0.07465337E-06 0.01879652E-09-0.10259839E-
14    2
 0.05611604E 06 0.04448758E 02 0.02503071E 02-0.02180018E-03 0.05405297E-
06    3
-0.05647560E-09 0.02099904E-12 0.05609890E 06 0.04167566E 02
4
NCO               121286N   1C   1O   1     G   300.000  5000.000
1
 0.05012045E 02 0.02626773E-01-0.11082433E-05 0.02093860E-08-0.14603470E-
13    2
 0.01737185E 06-0.01830075E 02 0.02830320E 02 0.08871490E-01-0.08945636E-
04    3
 0.05876918E-07-0.01907734E-10 0.01800543E 06 0.09498831E 02
4
NH                 31387N   1H   1          G   300.000  5000.000
1
 0.02760249E 02 0.13753463E-02-0.04451914E-05 0.07692791E-09-0.05017592E-
13    2
 0.04207828E 06 0.05857199E 02 0.03339758E 02 0.12530086E-02-0.03491645E-
04    3
 0.04218812E-07-0.15576179E-11 0.04185047E 06 0.02507180E 02
4
NH2               121686N   1H   2          G   300.     5000.
1
 0.02961311E 02 0.02932699E-01-0.09063600E-05 0.16172575E-09-0.12042003E-
13    2
 0.02191976E 06 0.05777878E 02 0.03432493E 02 0.03299540E-01-0.06613600E-
04    3
 0.08590947E-07-0.03572046E-10 0.02177227E 06 0.03090110E 02
4
NH3               121386N   1H   3          G   300.     5000.
1
 0.02461904E 02 0.06059166E-01-0.02004976E-04 0.03136003E-08-0.01938317E-
12    2
-0.06493269E 05 0.07472097E 02 0.02204351E 02 0.10114765E-01-0.14652648E-
04    3
 0.14472350E-07-0.05328509E-10-0.06525488E 05 0.08127138E 02
4
NNH               120186N   2H   1          G   250.     4000.
1
 0.04415342E 02 0.16143879E-02-0.16328943E-06-0.08559846E-09 0.16147909E-
13    2
 0.02788029E 06 0.09042888E 01 0.03501344E 02 0.02053586E-01 0.07170409E-
05    3
```

```
 0.04921348E-08-0.09671170E-11 0.02833347E 06 0.06391837E 02
4
NO                121286N   1O   1          G   300.000  5000.000
1
 0.03245435E 02 0.12691383E-02-0.05015890E-05 0.09169283E-09-0.06275419E-
13    2
 0.09800840E 05 0.06417293E 02 0.03376541E 02 0.12530634E-02-0.03302750E-
04    3
 0.05217810E-07-0.02446262E-10 0.09817961E 05 0.05829590E 02
4
NO2               121286N   1O   2          G   300.000  5000.000
1
 0.04682859E 02 0.02462429E-01-0.10422585E-05 0.01976902E-08-0.13917168E-
13    2
 0.02261292E 05 0.09885985E 01 0.02670600E 02 0.07838500E-01-0.08063864E-
04    3
 0.06161714E-07-0.02320150E-10 0.02896290E 05 0.11612071E 02
4
N2                121286N   2              G   300.000  5000.000
1
 0.02926640E 02 0.14879768E-02-0.05684760E-05 0.10097038E-09-0.06753351E-
13    2
-0.09227977E 04 0.05980528E 02 0.03298677E 02 0.14082404E-02-0.03963222E-
04    3
 0.05641515E-07-0.02444854E-10-0.10208999E 04 0.03950372E 02
4
N2O               121286N   2O   1          G   300.000  5000.000
1
 0.04718977E 02 0.02873713E-01-0.11974958E-05 0.02250551E-08-0.15753370E-
13    2
 0.08165811E 05-0.16572504E 01 0.02543057E 02 0.09492193E-01-0.09792775E-
04    3
 0.06263844E-07-0.01901825E-10 0.08765100E 05 0.09511222E 02
4
O                 120186O   1              G   300.000  5000.000
1
 0.02542059E0.02755061E-03-0.03102803E-07 0.04551067E-10-0.04368051E-14
2
 0.02923080E 0.04920308E 0.02946428E0.16381665E-02 0.02421031E-04    3
-0.16028431E-08 0.03890696E-11 0.02914764E 0.02963995E                   4
OH                121286O   1H   1          G   300.000  5000.000
1
 0.02882730E 0.10139743E-02-0.02276877E-05 0.02174683E-09-0.05126305E-14
2
 0.03886888E 0.05595712E 0.03637266E 0.01850910E-02-0.16761646E-05    3
 0.02387202E-07-0.08431442E-11 0.03606781E 0.13588605E                   4
O2                121386O   2              G   300.000  5000.000
1
 0.03697578E 02 0.06135197E-02-0.12588420E-06 0.01775281E-09-0.11364354E-
14    2
-0.12339301E 04 0.03189165E 02 0.03212936E 02 0.11274864E-02-0.05756150E-
05    3
```

```
 0.13138773E-08-0.08768554E-11-0.10052490E 04 0.06034737E 02
4
WH2O              121286H   2O   1          G   300.000  5000.000
1
 4.02344809E 4.48774008E-03-1.80554503E-06 3.48537591E-10-2.48544011E-14
2
-1.26194690E2.23224075E1.81052842E 1.93900495E-02-1.52088863E-05    3
 5.78420715E-09-1.12551171E-12-1.14346021E 7.02276992E                   4
WH2               121286H   2              G   300.000  5000.000
1
 4.47049788E-01 4.98637787E-04-2.00616115E-07 3.87263990E-11-2.76160013E-
15    2
-1.40216322E2.48026750E2.01169825E-01 2.15444994E-03-1.68987626E-06    3
 6.42689683E-10-1.25056857E-13-1.27051135E 7.80307769E-01
4
WOH               121286O   1H   1          G   300.000  5000.000
1
 3.79992320E 4.23842119E-03-1.70523697E-06 3.29174391E-10-2.34736011E-14
2
-1.19183874E2.10822738E1.70994351E 1.83128245E-02-1.43639482E-05    3
 5.46286231E-09-1.06298328E-12-1.07993465E 6.63261603E                   4
WA1               121286C   1H   2O   1     G   300.000  5000.000
1
 6.70574682E 7.47956680E-03-3.00924172E-06 5.80895985E-10-4.14240019E-14
2
-2.10324483E3.72040125E3.01754737E 3.23167491E-02-2.53481438E-05    3
 9.64034524E-09-1.87585285E-12-1.90576702E 1.17046165E                   4
WA2               121286C   1H   2O   1     G   300.000  5000.000
1
 6.70574682E 7.47956680E-03-3.00924172E-06 5.80895985E-10-4.14240019E-14
2
-2.10324483E3.72040125E3.01754737E 3.23167491E-02-2.53481438E-05    3
 9.64034524E-09-1.87585285E-12-1.90576702E 1.17046165E                   4
WC1               121286C   1H   4          G   300.000  5000.000
1
 3.57639831E 3.98910229E-03-1.60492892E-06 3.09811192E-10-2.20928010E-14
2
-1.12173058E1.98421400E1.60935860E 1.72355995E-02-1.35190100E-05    3
 5.14151746E-09-1.00045485E-12-1.01640908E 6.24246215E                   4
WC2               121286C   2H   4          G   300.000  5000.000
1
 6.25869703E 6.98092902E-03-2.80862561E-06 5.42169586E-10-3.86624018E-14
2
-1.96302851E3.47237450E2.81637755E 3.01622992E-02-2.36582676E-05    3
 8.99765556E-09-1.75079599E-12-1.77871589E 1.09243088E                   4
WC3               121286C   2H   4          G   300.000  5000.000
1
 6.25869703E 6.98092902E-03-2.80862561E-06 5.42169586E-10-3.86624018E-14
2
-1.96302851E3.47237450E2.81637755E 3.01622992E-02-2.36582676E-05    3
 8.99765556E-09-1.75079599E-12-1.77871589E 1.09243088E                   4
WCO               121286C   1O   1          G   300.000  5000.000
1
```

```
 6.25869703E 6.98092902E-03-2.80862561E-06 5.42169586E-10-3.86624018E-14
2
-1.96302851E3.47237450E2.81637755E 3.01622992E-02-2.36582676E-05    3
 8.99765556E-09-1.75079599E-12-1.77871589E 1.09243088E                   4
WCO2              121286C   1O   2          G   300.000  5000.000
1
 9.83509534E 1.09700313E-02-4.41355452E-06 8.51980777E-10-6.07552028E-14
2
-3.08475909E5.45658850E4.42573614E 4.73978987E-02-3.71772776E-05    3
 1.41391730E-08-2.75125085E-12-2.79512496E 1.71667709E                   4
WCR1              121286C   1               G   300.000  5000.000
1
 2.68229873E 2.99182672E-03-1.20369669E-06 2.32358394E-10-1.65696008E-14
2
-8.41297934E1.48816050E1.20701895E 1.29266997E-02-1.01392575E-05    3
 3.85613810E-09-7.50341140E-13-7.62306808E 4.68184661E                   4
WCR2              121286C   1               G   300.000  5000.000
1
 2.68229873E 2.99182672E-03-1.20369669E-06 2.32358394E-10-1.65696008E-14
2
-8.41297934E1.48816050E1.20701895E 1.29266997E-02-1.01392575E-05    3
 3.85613810E-09-7.50341140E-13-7.62306808E 4.68184661E                   4
WCR3              121286C   1               G   300.000  5000.000
1
 2.68229873E 2.99182672E-03-1.20369669E-06 2.32358394E-10-1.65696008E-14
2
-8.41297934E1.48816050E1.20701895E 1.29266997E-02-1.01392575E-05    3
 3.85613810E-09-7.50341140E-13-7.62306808E 4.68184661E                   4
WCR4              121286C   1               G   300.000  5000.000
1
 2.68229873E 2.99182672E-03-1.20369669E-06 2.32358394E-10-1.65696008E-14
2
-8.41297934E1.48816050E1.20701895E 1.29266997E-02-1.01392575E-05    3
 3.85613810E-09-7.50341140E-13-7.62306808E 4.68184661E                   4
WCR5              121286C   1               G   300.000  5000.000
1
 2.68229873E 2.99182672E-03-1.20369669E-06 2.32358394E-10-1.65696008E-14
2
-8.41297934E1.48816050E1.20701895E 1.29266997E-02-1.01392575E-05    3
 3.85613810E-09-7.50341140E-13-7.62306808E 4.68184661E                   4
WCR6              121286C   1               G   300.000  5000.000
1
 2.68229873E 2.99182672E-03-1.20369669E-06 2.32358394E-10-1.65696008E-14
2
-8.41297934E1.48816050E1.20701895E 1.29266997E-02-1.01392575E-05    3
 3.85613810E-09-7.50341140E-13-7.62306808E 4.68184661E                   4
WCR7              121286C   1               G   300.000  5000.000
1
 2.68229873E 2.99182672E-03-1.20369669E-06 2.32358394E-10-1.65696008E-14
2
-8.41297934E1.48816050E1.20701895E 1.29266997E-02-1.01392575E-05    3
 3.85613810E-09-7.50341140E-13-7.62306808E 4.68184661E                   4
```

```
WTCD              121286C   1O   2          G   300.000  5000.000
1
 9.83509534E 1.09700313E-02-4.41355452E-06 8.51980777E-10-6.07552028E-14
2
-3.08475909E5.45658850E4.42573614E 4.73978987E-02-3.71772776E-05    3
 1.41391730E-08-2.75125085E-12-2.79512496E 1.71667709E                   4
WTCO              121286C   1O   1          G   300.000  5000.000
1
 6.25869703E 6.98092902E-03-2.80862561E-06 5.42169586E-10-3.86624018E-14
2
-1.96302851E3.47237450E2.81637755E 3.01622992E-02-2.36582676E-05    3
 8.99765556E-09-1.75079599E-12-1.77871589E 1.09243088E                   4
WTC1              121286C   1H   4          G   300.000  5000.000
1
 3.57639831E 3.98910229E-03-1.60492892E-06 3.09811192E-10-2.20928010E-14
2
-1.12173058E1.98421400E1.60935860E 1.72355995E-02-1.35190100E-05    3
 5.14151746E-09-1.00045485E-12-1.01640908E 6.24246215E                   4
WTC2              121286C   2H   4          G   300.000  5000.000
1
 6.25869703E 6.98092902E-03-2.80862561E-06 5.42169586E-10-3.86624018E-14
2
-1.96302851E3.47237450E2.81637755E 3.01622992E-02-2.36582676E-05    3
 8.99765556E-09-1.75079599E-12-1.77871589E 1.09243088E                   4
WTH2              121286H   2          G   300.000  5000.000
1
 4.47049788E-01 4.98637787E-04-2.00616115E-07 3.87263990E-11-2.76160013E-
15    2
-1.40216322E2.48026750E2.01169825E-01 2.15444994E-03-1.68987626E-06    3
 6.42689683E-10-1.25056857E-13-1.27051135E 7.80307769E-01
4
WTHCN             121286C   1H   1N   1     G   300.000  5000.000
1
 6.03517214E 6.73161012E-03-2.70831755E-06 5.22806386E-10-3.72816017E-14
2
-1.89292035E3.34836113E2.71579263E 2.90850742E-02-2.28133294E-05    3
 8.67631072E-09-1.68826757E-12-1.71519032E 1.05341549E                   4
TCO               121286C   1O   1          G   300.000  5000.000
1
 6.25869703E 6.98092902E-03-2.80862561E-06 5.42169586E-10-3.86624018E-14
2
-1.96302851E3.47237450E2.81637755E 3.01622992E-02-2.36582676E-05    3
 8.99765556E-09-1.75079599E-12-1.77871589E 1.09243088E                   4
TCO2              121286C   1O   2          G   300.000  5000.000
1
 9.83509534E 1.09700313E-02-4.41355452E-06 8.51980777E-10-6.07552028E-14
2
-3.08475909E5.45658850E4.42573614E 4.73978987E-02-3.71772776E-05    3
 1.41391730E-08-2.75125085E-12-2.79512496E 1.71667709E                   4
TC1               121286C   1H   4          G   300.000  5000.000
1
 3.57639831E 3.98910229E-03-1.60492892E-06 3.09811192E-10-2.20928010E-14
2
```

```
-1.12173058E1.98421400E1.60935860E 1.72355995E-02-1.35190100E-05    3
 5.14151746E-09-1.00045485E-12-1.01640908E 6.24246215E                   4
TC2               121286C   2H   4          G   300.000  5000.000
1
 6.25869703E 6.98092902E-03-2.80862561E-06 5.42169586E-10-3.86624018E-14
2
-1.96302851E3.47237450E2.81637755E 3.01622992E-02-2.36582676E-05    3
 8.99765556E-09-1.75079599E-12-1.77871589E 1.09243088E                   4
TH2               121286H   2              G   300.000  5000.000
1
 4.47049788E-01 4.98637787E-04-2.00616115E-07 3.87263990E-11-2.76160013E-
15    2
-1.40216322E2.48026750E2.01169825E-01 2.15444994E-03-1.68987626E-06    3
 6.42689683E-10-1.25056857E-13-1.27051135E 7.80307769E-01
4
THCN              121286C   1H   1N   1     G   300.000  5000.000
1
 6.03517214E 6.73161012E-03-2.70831755E-06 5.22806386E-10-3.72816017E-14
2
-1.89292035E3.34836113E2.71579263E 2.90850742E-02-2.28133294E-05    3
 8.67631072E-09-1.68826757E-12-1.71519032E 1.05341549E                   4
RH2O              121286H   2O   1          G   300.000  5000.000
1
 4.02344809E 4.48774008E-03-1.80554503E-06 3.48537591E-10-2.48544011E-14
2
-1.26194690E2.23224075E1.81052842E 1.93900495E-02-1.52088863E-05    3
 5.78420715E-09-1.12551171E-12-1.14346021E 7.02276992E                   4
RA1               121286C   1H   2O   1     G   300.000  5000.000
1
 6.70574682E 7.47956680E-03-3.00924172E-06 5.80895985E-10-4.14240019E-14
2
-2.10324483E3.72040125E3.01754737E 3.23167491E-02-2.53481438E-05    3
 9.64034524E-09-1.87585285E-12-1.90576702E 1.17046165E                   4
RHCN              121286C   1H   1N   1     G   300.000  5000.000
1
 6.03517214E 6.73161012E-03-2.70831755E-06 5.22806386E-10-3.72816017E-14
2
-1.89292035E3.34836113E2.71579263E 2.90850742E-02-2.28133294E-05    3
 8.67631072E-09-1.68826757E-12-1.71519032E 1.05341549E                   4
CHR1              121286C   1              G  0300.00   5000.00
1
 0.01490166E 0.01662126E-01-0.06687204E-05 0.01290880E-08-0.09205334E-13
2
-0.07074019E0.08717785E0.06705661E 0.07181500E-01-0.05632921E-04    3
 0.02142299E-07-0.04168562E-11-0.07339498E 0.02601596E                   4
CHR2              121286C   1              G  0300.00   5000.00
1
 0.01490166E 0.01662126E-01-0.06687204E-05 0.01290880E-08-0.09205334E-13
2
-0.07074019E0.08717785E0.06705661E 0.07181500E-01-0.05632921E-04    3
 0.02142299E-07-0.04168562E-11-0.07339498E 0.02601596E                   4
CHR3              121286C   1              G  0300.00   5000.00
1
```

```
 0.01490166E 0.01662126E-01-0.06687204E-05 0.01290880E-08-0.09205334E-13
2
-0.07074019E0.08717785E0.06705661E 0.07181500E-01-0.05632921E-04    3
 0.02142299E-07-0.04168562E-11-0.07339498E 0.02601596E                  4
CHR4              121286C   1               G  0300.00   5000.00
1
 0.01490166E 0.01662126E-01-0.06687204E-05 0.01290880E-08-0.09205334E-13
2
-0.07074019E0.08717785E0.06705661E 0.07181500E-01-0.05632921E-04    3
 0.02142299E-07-0.04168562E-11-0.07339498E 0.02601596E                  4
CHR5              121286C   1               G  0300.00   5000.00
1
 0.01490166E 0.01662126E-01-0.06687204E-05 0.01290880E-08-0.09205334E-13
2
-0.07074019E0.08717785E0.06705661E 0.07181500E-01-0.05632921E-04    3
 0.02142299E-07-0.04168562E-11-0.07339498E 0.02601596E                  4
CHR6              121286C   1               G  0300.00   5000.00
1
 0.01490166E 0.01662126E-01-0.06687204E-05 0.01290880E-08-0.09205334E-13
2
-0.07074019E0.08717785E0.06705661E 0.07181500E-01-0.05632921E-04    3
 0.02142299E-07-0.04168562E-11-0.07339498E 0.02601596E                  4
CHR7              121286C   1               G  0300.00   5000.00
1
 0.01490166E 0.01662126E-01-0.06687204E-05 0.01290880E-08-0.09205334E-13
2
-0.07074019E0.08717785E0.06705661E 0.07181500E-01-0.05632921E-04    3
 0.02142299E-07-0.04168562E-11-0.07339498E 0.02601596E                  4

MECHANISM
CH3     CH3     M       C2H6            M       16.956  -1.18    0.654
CGS
TROECGS 0.641   6927.00 132.000 0.000           41.502  -7.0     2.762
PRES
H2O 5.0 CO2 3.0 H2  2.0 CO  2.0
3BOD
CH3     H       M       CH4             M       16.778  -1.0       0.0
CGS
SRI CGS 0.4500  797.000 979.000 0.000           26.903  -3.0       0.0
PRES
H2O 5.0 CO2 3.0 H2  2.0 CO  2.0
3BOD
CH4     O2              CH3     HO2             13.898  0.00      56.0
CGS
CH4     H               CH3     H2               4.342  3.00      8.75
CGS
CH4     OH              CH3     H2O              6.204  2.10    2.4600
CGS
CH4     O               CH3     OH               9.009  1.5       8.604
CGS
CH4     HO2             CH3     H2O2            11.255  0.00      18.7
CGS
```

```
CH3     HO2             CH3O    OH              13.301  0.00       0.0
CGS
CH3     O2              CH3O    O               18.312  -1.57    29.229
CGS
CH3     O               CH2O    H               13.903  0.00       0.0
CGS
CH2OH   H               CH3     OH              14.000  0.00       0.0
CGS
CH3O    H               CH3     OH              14.000  0.00       0.0
CGS
CH3     OH              CH2     H2O              6.875  2.00       5.0
CGS
CH3     H               CH2     H2              13.954  0.00     15.100
CGS
CH3O            M       CH2O    H       M       14.000  0.00       25.0
CGS
CH2OH           M       CH2O    H       M       14.000  0.00       25.0
CGS
CH3O    H               CH2O    H2              13.301  0.00       0.0
CGS
CH2OH   H               CH2O    H2              13.301  0.00       0.0
CGS
CH3O    OH              CH2O    H2O             13.000  0.00       0.0
CGS
CH2OH   OH              CH2O    H2O             13.000  0.00       0.0
CGS
CH3O    O               CH2O    OH              13.000  0.00       0.0
CGS
CH2OH   O               CH2O    OH              13.000  0.00       0.0
CGS
CH3O    O2              CH2O    HO2             10.799  0.00       2.6
CGS
CH2OH   O2              CH2O    HO2             13.170  0.00       1.5
CGS
CH2     H               CH      H2              18.000  -1.56      0.0
CGS
CH2     OH              CH      H2O              7.053  2.00       3.0
CGS
CH2     OH              CH2O    H               13.398  0.00       0.0
CGS
CH      O2              HCO     O               13.519  0.00       0.0
CGS
CH      O               CO      H               13.756  0.00       0.0
CGS
CH      OH              HCO     H               13.477  0.00       0.0
CGS
CH      CO2             HCO     CO              12.531  0.00      0.69
CGS
CH      H               C       H2              14.176  0.00       0.0
CGS
CH      H2O             CH2O    H               15.068  -0.75      0.0
CGS
```

```
CH      CH2O            CH2CO   H               13.976  0.00    -0.515
CGS
CH      C2H2            C3H2    H               14.000  0.00       0.0
CGS
CH      CH2             C2H2    H               13.602  0.00       0.0
CGS
CH      CH3             C2H3    H               13.477  0.00       0.0
CGS
CH      CH4             C2H4    H               13.778  0.00       0.0
CGS
C       O2              CO      O               13.301  0.00       0.0
CGS
C       OH              CO      H               13.699  0.00       0.0
CGS
C       CH3             C2H2    H               13.699  0.00       0.0
CGS
C       CH2             C2H     H               13.699  0.00       0.0
CGS
CH2     CO2             CO      CH2O            11.041  0.00       1.0
CGS
CH2     O               CO      H       H       13.699  0.00       0.0
CGS
CH2     O               CO      H2              13.477  0.00       0.0
CGS
CH2     O2              CO2     H       H       12.204  0.00       1.0
CGS
CH2     O2              CH2O    O               13.699  0.00       9.0
CGS
CH2     O2              CO2     H2              11.839  0.00       0.5
CGS
CH2     O2              CO      H2O             10.279  0.00      -1.0
CGS
CH2     O2              CO      OH      H       10.934  0.00      -0.5
CGS
CH2     O2              HCO     OH              10.633  0.00      -0.5
CGS
CH2O    OH              HCO     H2O              9.535  1.18    -0.447
CGS
CH2O    H               HCO     H2               8.340  1.77       3.0
CGS
CH2O            M       HCO     H       M       16.520  0.00     81.00
CGS
CH2O    O               HCO     OH              13.255  0.00      3.08
CGS
HCO     OH              CO      H2O             14.000  0.00       0.0
CGS
HCO             M       CO      H       M       14.398  0.00    16.802
CGS
H2O 5.0 CO2 3.0 H2  1.9 CO  1.9 CH4 2.8
3BOD
HCO     H               CO      H2              13.076  0.25       0.0
CGS
```

```
HCO     O               CO      OH              13.477  0.00       0.0
CGS
HCO     O               CO2     H               13.477  0.00       0.0
CGS
HCO     O2              CO      HO2             13.519  -.40       0.0
CGS
CO      O       M       CO2             M       14.790  0.00       3.0
CGS
CO      OH              CO2     H                7.179  1.30    -0.758
CGS
CO      O2              CO2     O               13.204  0.00      41.0
CGS
CO      HO2             CO2     OH              13.763  0.00    22.934
CGS
C2H6    CH3             C2H5    CH4             -0.260  4.00       8.3
CGS
C2H6    H               C2H5    H2               2.732  3.50      5.21
CGS
C2H6    O               C2H5    OH               7.477  2.00     5.115
CGS
C2H6    OH              C2H5    H2O              9.940  1.05      1.81
CGS
C2H4    H               C2H3    H2              14.041  0.00       8.5
CGS
C2H4    O               HCO     CH3              9.204  1.20     0.746
CGS
C2H4    OH              C2H3    H2O             13.305  0.00     5.955
CGS
CH3     CH2             C2H4    H               13.477  0.00       0.0
CGS
C2H4    H       M       C2H5            M       13.344  0.00     2.066
CGS
LINDCGS 0.0000  0.00000 0.00000 0.000           27.804  -2.8    -0.054
PRES
H2O 5.0 CO2 3.0 H2  2.0 CO  2.0
3BOD
C2H5    H               CH3     CH3             14.000  0.00       0.0
CGS
C2H5    O2              C2H4    HO2             11.926  0.00     3.875
CGS
C2H2    O               CH2     CO               7.009  2.00       1.9
CGS
C2H2    O               HCCO    H                7.009  2.00       1.9
CGS
C2H     H2              C2H2    H                5.613  2.39     0.864
CGS
C2H2    H       M       C2H3            M       12.744  0.00     2.410
CGS
LINDCGS 0.0000  0.00000 0.00000 0.000           27.427  -3.5     2.410
PRES
H2O 5.0 CO2 3.0 H2  2.0 CO  2.0
3BOD
```

```
C2H3    H               C2H2    H2              13.602  0.00       0.0
CGS
C2H3    O               CH2CO   H               13.477  0.00       0.0
CGS
C2H3    O2              HCO     CH2O            12.602  0.00     -0.25
CGS
C2H3    OH              C2H2    H2O             12.699  0.00       0.0
CGS
C2H3    CH2             C2H2    CH3             13.447  0.00       0.0
CGS
C2H3    C2H             C2H2    C2H2            13.477  0.00       0.0
CGS
C2H3    CH              CH2     C2H2            13.699  0.00       0.0
CGS
C2H2    OH              C2H     H2O              7.528  2.00      14.0
CGS
OH      C2H2            HCCOH   H                5.702  2.30      13.5
CGS
C2H2    OH              CH2CO   H               -3.662  4.50      -1.0
CGS
OH      C2H2            CH3     CO              -3.316  4.00      -2.0
CGS
HCCOH   H               CH2CO   H               13.000  0.00       0.0
CGS
C2H2    O               C2H     OH              15.500  -.60      15.0
CGS
CH2CO   O               CO2     CH2             12.243  0.00      1.35
CGS
CH2CO   H               CH3     CO              13.053  0.00     3.428
CGS
CH2CO   H               HCCO    H2              13.699  0.00       8.0
CGS
CH2CO   O               HCCO    OH              13.000  0.00       8.0
CGS
CH2CO   OH              HCCO    H2O             12.875  0.00       2.0
CGS
CH2CO           M       CH2     CO      M       14.477  0.00    70.980
CGS
LINDCGS 0.0000  0.00000 0.00000 0.000           15.556  0.00    59.270
PRES
C2H     O2              CO      CO      H       13.699  0.00      1.5
CGS
C2H     C2H2            C4H2    H               13.477  0.00       0.0
CGS
HCCO    H               CH2(S)  CO              14.000  0.00       0.0
CGS
HCCO    O               CO      CO      H       14.000  0.00       0.0
CGS
HCCO    O2              CO      CO      OH      12.204  0.00     0.854
CGS
CH      HCCO            C2H2    CO              13.699  0.00       0.0
CGS
```

```
HCCO    HCCO            C2H2    CO      CO      13.000  0.00        0.0
CGS
CH2(S)          M       CH2             M       13.000  0.00        0.0
CGS
H   0.0
3BOD
CH2(S)  CH4             CH3     CH3             13.602  0.00        0.0
CGS
CH2(S)  C2H6            CH3     C2H5            14.079  0.00        0.0
CGS
CH2(S)  O2              CO      OH      H       13.477  0.00        0.0
CGS
CH2(S)  H2              CH3     H               13.845  0.00        0.0
CGS
CH2(S)  H               CH2     H               14.301  0.00        0.0
CGS
C2H     O               CH      CO              13.699  0.00        0.0
CGS
C2H     OH              HCCO    H               13.301  0.00        0.0
CGS
CH2     CH2             C2H2    H2              13.602  0.00        0.0
CGS
HCCO    CH2             C2H3    CO              13.477  0.00        0.0
CGS
CH2     C2H2            C3H3    H               13.079  0.00        6.6
CGS
C4H2    OH              C3H2    HCO             12.823  0.00      -0.41
CGS
C3H2    O2              HCO     HCCO            13.000  0.00        0.0
CGS
C3H3    O2              CH2CO   HCO             10.477  0.00      2.868
CGS
C3H3    O               CH2O    C2H             13.301  0.00        0.0
CGS
C3H3    OH              C3H2    H2O             13.301  0.00        0.0
CGS
C2H2    C2H2            C4H3    H               12.301  0.00       45.9
CGS
C4H3            M       C4H2    H       M       16.000  0.00       59.7
CGS
CH2(S)  C2H2            C3H3    H               13.477  0.00        0.0
CGS
C4H2    O               C3H2    CO              12.079  0.00        0.0
CGS
C2H2    O2              HCCO    OH               8.301  1.50       30.1
CGS
C2H2            M       C2H     H       M       16.623  0.00      107.0
CGS
C2H4            M       C2H2    H2      M       15.176  0.00       55.8
CGS
C2H4            M       C2H3    H       M       16.146  0.00      82.36
CGS
```

```
H2      O2              OH      OH              13.230  0.00     47.78
CGS
H2      OH              H2O     H                9.068  1.30    3.6260
CGS
O       OH              O2      H               14.602  -0.5       0.0
CGS
O       H2              H       OH               4.704  2.67    6.2900
CGS
H       O2      M       HO2             M       17.558  -0.72      0.0
CGS
H2O 19. CO2 4.2 H2  2.9 CO  2.1 N2  1.3
3BOD
HO2     OH              H2O     O2              12.875  0.00       0.0
CGS
HO2     H               OH      OH              14.146  0.00     1.073
CGS
HO2     O               OH      O2              13.146  0.00     1.073
CGS
OH      OH              H2O     O                8.778  1.30       0.0
CGS
H       H       M       H2              M       18.000  -1.0       0.0
CGS
H2O 0.0 CO2 0.0 H2  0.0
3BOD
H       H       H2      H2      H2              16.964  -0.6       0.0
CGS
H       H       H2O     H2      H2O             19.778  -1.25      0.0
CGS
H       H       CO2     H2      CO2             20.740  -2.0       0.0
CGS
H       OH      M       H2O             M       22.204  -2.0       0.0
CGS
H2O 5.0
3BOD
H       O       M       OH              M       16.792  -0.6       0.0
CGS
H2O 5.0
3BOD
O       O       M       O2              M       13.276  0.0     -1.788
CGS
HO2     H               H2      O2              13.097  0.00       0.0
CGS
HO2     HO2             H2O2    O2              12.301  0.00       0.0
CGS
H2O2            M       OH      OH      M       17.114  0.00      45.5
CGS
H2O2    H               HO2     H2              12.204  0.00       3.8
CGS
H2O2    OH              H2O     HO2             13.000  0.00       1.8
CGS
WH2O                    H2O                      3.310  0.00      11.5
CGS
```

```
WH2O                    H2O                   -10.00  0.00       0.0
REVE
WH2                     H2                     3.310  0.00      11.5
CGS
WH2                     H2                    -10.00  0.00       0.0
REVE
WOH                     OH                     3.310  0.00      11.5
CGS
WOH                     OH                    -10.00  0.00       0.0
REVE
WA1                     CH2O                   3.510  0.00      12.9
CGS
WA1                     CH2O                  -10.00  0.00       0.0
REVE
WA2                     CH2O                   5.800  0.00      21.3
CGS
WA2                     CH2O                  -10.00  0.00       0.0
REVE
WC3                     C2H4                  11.200  0.00      42.8
CGS
WC3                     C2H4                  -10.00  0.00       0.0
REVE
WC1                     CH4                    4.530  0.00      16.5
CGS
WC1                     CH4                   -10.00  0.00       0.0
REVE
WCO                     CO                     4.530  0.00      16.5
CGS
WCO                     CO                    -10.00  0.00       0.0
REVE
WCO2                    CO2                    4.530  0.00      16.5
CGS
WCO2                    CO2                   -10.00  0.00       0.0
REVE
WC2                     C2H4                   4.530  0.00      16.5
CGS
WC2                     C2H4                  -10.00  0.00       0.0
REVE
WTCO                    TCO                    4.530  0.00      16.5
CGS
WTCO                    TCO                   -10.00  0.00       0.0
REVE
WTCD                    TCO2                   4.530  0.00      16.5
CGS
WTCD                    TCO2                  -10.00  0.00       0.0
REVE
WTC1                    TC1                    4.530  0.00      16.5
CGS
WTC1                    TC1                   -10.00  0.00       0.0
REVE
WTC2                    TC2                    4.530  0.00      16.5
CGS
```

```
WTC2                    TC2                    -10.00  0.00       0.0
REVE
WTH2                    TH2                     4.530  0.00      16.5
CGS
WTH2                    TH2                    -10.00  0.00       0.0
REVE
WTHCN                   THCN                    4.530  0.00      16.5
CGS
WTHCN                   THCN                   -10.00  0.00       0.0
REVE
TCO                     CO                      7.660  0.00     21.03
CGS
TCO                     CO                     -10.00  0.00       0.0
REVE
TCO2                    CO2                     5.550  0.00     11.72
CGS
TCO2                    CO2                    -10.00  0.00       0.0
REVE
TC1                     CH4                     7.890  0.00     22.54
CGS
TC1                     CH4                    -10.00  0.00       0.0
REVE
TC2                     C2H4                    8.880  0.00     26.55
CGS
TC2                     C2H4                   -10.00  0.00       0.0
REVE
TH2                     H2                       9.64  0.00     30.86
CGS
TH2                     H2                     -10.00  0.00       0.0
REVE
THCN                    HCN                     7.980  0.00      22.3
CGS
THCN                    HCN                    -10.00  0.00       0.0
REVE

MB MECHANISM
NFLOL  =
      6  /
PATM   =
     1.0  /
TA     =
     116  /
TF     =
     77.0   /
TF2    =
     77.0 /
TF3    =
     77.0 /
FLOELM =
    1,2,8,4,2,6 /
WF     =
   0.007282695,0.,0.,0. /
WF2    =
```

```
    0.000 /
WF3    =
    0.0000 /
WA     =
    0.002,0.,0.,0.032,0.032,0.1465 /
AREA   =
    100.,100.,414.,414.,100.,414. /
DELX   =
    1.,2.3,23,10.,0.1,1. /
NODIN  =
      1,2,3,4,5,6 /
NODOUT =
      2,3,4,5,6,7 /
FF     =
      1.,1.,1.,1.,1.,1. /
IDEBUG =
      0  /
NQSS   =
      2  /
TOL    =
    1.0E-03  /
IKREV  =
      1  /
RXNS   =
      0 /
NPFR   =
      30 /
END

REACTANTS-F1
C 1.     O 1.                          WTCO      0.372          G
C 1.     O 2.                          WTCD      0.055          G
C 1.     H 4.                          WTC1      0.082          G
C 2.     H 4.                          WTC2      0.104          G
H 2.                                   WTH2      0.002          G
H 2.     O 1.                          WH2O      0.271          G
H 2.                                   WH2       0.008          G
O 1.     H 1.                          WOH       0.002          G
C 1.     H 2.     O 1.                 WA1       0.016          G
C 1.     H 2.     O 1.                 WA2       0.011          G
C 2.     H 4.                      WC3       0.003          G
C 1.     O 2.                          WCO2      0.033          G
C 1.     O 1.                          WCO       0.033          G
C 1.     H 4.                          WC1       0.003          G
C 2.     H 4.                      WC2       0.002          G

REACTANTS-F2
C 1.     H 4.                      CH4       1.000          G

REACTANTS-F3
H 2.     O 1.                      WH2O      1.000          G

REACTANTS-AIR
```

```
N 2.                          N2        79.0   M         G        AIR
O 2.                          O2        21.0   M         G        AIR
```

A.8.2 Output File

The following is an output file for the Dec 12th burn (input file above) with PFT1 at 500 K.

The residence time for the PSR2 element is 5 milliseconds.

```
*** INPUT DATA ***
 ELEM NODE NODE ELEM   AREA    LENGTH
   #   IN   OUT TYPE (SQ. IN) (INCHES)
   1    1    2   MIX 1.00E 1.00E
   2    2    3   PSR 1.00E 2.30E
   3    3    4   PFT 4.14E 1.70E
   4    4    5   PSX 4.14E 1.59E-02
   5    5    6   PSR 1.00E 1.00E-01
   6    6    7   PFR 4.14E 1.00E

 ELEM INLET AIR INLET FUEL1 INLET FUEL2 INLET FUEL3 INLET FLOW
   #   (LBM/S)    (LBM/S)     (LBM/S)     (LBM/S)    FRACTION
   1   2.00E-03   7.28E-03    0.00E    0.00E   1.00E
   2   0.00E   0.00E    0.00E    0.00E   1.00E
   3   0.00E   0.00E    0.00E    0.00E   1.00E
   4   3.20E-02   0.00E    0.00E    0.00E   1.00E
   5   3.20E-02   0.00E    0.00E    0.00E   1.00E
   6   1.47E-01   0.00E    0.00E    0.00E   1.00E

  AIR TEMP =  1.1600E F      COMBUSTOR PRESSURE =  1.0000E ATM
FUEL1 TEMP =  7.7000E F              FUEL2 TEMP =  7.7000E F
FUEL3 TEMP =  7.7000E F

*** OUTPUT ***

MB MECHANISM

TEMP AND COMPOSITION FOR MARK-II MODEL:
PRESSURE  =   1.0000E ATM       OVERALL E.R. =   1.5505E-01
FUEL FLOW =   2.6218E LBM/HR      AIR FLOW   =   2.1250E-01 LBM/SEC



ELEMENT NO.        1         2         3         4         5         6
ELEMENT TYPE      MIX       PSR       PFT       PSX       PSR       PFR
EQUIV RATIO   1.647E 1.647E 1.647E 9.691E-01 4.992E-01 1.550E-01
RES TIME, SEC 3.552E-01 8.169E-01 1.511E 5.000E-03 4.710E-03 7.117E-02
TTL TIME, SEC 1.672E 1.753E 3.264E 3.265E 3.265E 3.273E
AREA, SQ IN   1.000E 1.000E 4.140E 4.140E 1.000E 4.140E
VELO, FT/SEC  2.346E-01 2.346E-01 9.375E-02 2.642E-01 1.769E 1.171E
FLOW, LBM/SEC 9.283E-03 9.283E-03 9.283E-03 4.128E-02 7.328E-02 2.198E-01
```

```
LENGTH, IN    1.000E 2.300E 1.700E 1.585E-02 1.000E-01 1.000E
ENTH, BTU/LBM-1.747E1.747E1.797E3.967E2.193E6.677E
TEMP EFF     -1.296E-02-1.295E-02 1.328E-01 3.097E-02 2.729E-02 2.482E-02
TEMP, K       3.022E 3.022E 5.000E 3.803E 3.556E 3.323E
MIN. REACTION 9.967E-21 5.569E-15 9.898E-16 9.898E-16 5.569E-15 9.898E-16


ELEMENT NO.       11
ELEMENT TYPE      EQL
EQUIV RATIO   1.550E-01
RES TIME, SEC 0.000E
TTL TIME, SEC 3.273E
AREA, SQ IN   0.000E
VELO, FT/SEC  0.000E
FLOW, LBM/SEC 2.198E-01
LENGTH, IN    0.000E
ENTH, BTU/LBM-6.677E
TEMP EFF     -2.792E
TEMP, K       8.173E
MIN. REACTION 1.000E


MOLE FRACTIONS X(I)
SPECIES "I"        1         2         3         4         5         6
C             0.000E 2.263E-19 2.263E-19 2.717E-19 2.788E-19 2.852E-19
CH            0.000E 2.263E-19 2.263E-19 2.717E-19 2.788E-19 2.852E-19
CH2           0.000E 2.263E-19 2.263E-19 2.717E-19 2.788E-19 2.852E-19
CH2CO         0.000E 2.263E-19 3.899E-13 1.053E-13 6.084E-14 2.076E-14
CH2O          0.000E 9.579E-09 6.692E-04 1.807E-04 1.044E-04 3.562E-05
CH2OH         0.000E 2.263E-19 1.810E-14 3.419E-18 3.360E-19 2.852E-19
CH2(S)        0.000E 2.263E-19 2.263E-19 2.717E-19 2.788E-19 2.852E-19
CH3           0.000E 1.360E-14 2.119E-10 3.714E-11 1.645E-11 1.335E-12
CH3O          0.000E 1.482E-17 1.452E-11 3.809E-13 8.958E-14 2.263E-15
CH4           0.000E 1.073E-10 3.287E-04 8.872E-05 5.128E-05 1.749E-05
CN            0.000E 2.263E-19 2.263E-19 2.717E-19 2.788E-19 2.852E-19
CO            0.000E 2.815E-09 2.447E-03 6.605E-04 3.818E-04 1.302E-04
CO2           0.000E 4.402E-10 1.095E-03 2.956E-04 1.708E-04 5.827E-05
C2H           0.000E 2.263E-19 2.263E-19 2.717E-19 2.788E-19 2.852E-19
C2H2          0.000E 2.263E-19 5.998E-15 1.619E-15 9.359E-16 3.192E-16
C2H3          0.000E 2.263E-19 3.268E-15 7.512E-19 2.788E-19 2.852E-19
C2H4          0.000E 4.089E-11 6.876E-05 1.856E-05 1.073E-05 3.659E-06
C2H5          0.000E 2.263E-19 1.109E-11 2.345E-14 1.301E-16 1.433E-18
C2H6          0.000E 2.263E-19 3.412E-10 9.211E-11 5.324E-11 1.816E-11
C2N2          0.000E 2.263E-19 2.263E-19 2.717E-19 2.788E-19 2.852E-19
C3H2          0.000E 2.263E-19 2.263E-19 2.717E-19 2.788E-19 2.852E-19
C3H3          0.000E 2.263E-19 2.263E-19 2.717E-19 2.788E-19 2.852E-19
C4H2          0.000E 2.263E-19 2.263E-19 2.717E-19 2.788E-19 2.852E-19
C4H3          0.000E 2.263E-19 2.263E-19 2.717E-19 2.788E-19 2.852E-19
H             0.000E 4.278E-16 3.516E-11 2.115E-14 2.590E-15 1.929E-16
HCCO          0.000E 2.263E-19 2.263E-19 2.717E-19 2.788E-19 2.852E-19
HCCOH         0.000E 2.263E-19 2.263E-19 2.717E-19 2.788E-19 2.852E-19
```

HCN	0.000E	2.263E-19	2.842E-19	2.717E-19	2.788E-19	2.852E-19
HCNO	0.000E	2.263E-19	2.263E-19	2.717E-19	2.788E-19	2.852E-19
HCO	0.000E	5.461E-16	9.072E-12	1.185E-14	1.933E-15	1.745E-16
HNCO	0.000E	2.263E-19	2.263E-19	2.717E-19	2.788E-19	2.852E-19
HNO	0.000E	2.263E-19	2.263E-19	2.717E-19	2.788E-19	2.852E-19
HOCN	0.000E	2.263E-19	2.263E-19	2.717E-19	2.788E-19	2.852E-19
HO2	0.000E	1.606E-09	5.554E-07	1.387E-07	7.661E-08	2.083E-08
H2	0.000E	5.671E-07	1.760E-02	4.750E-03	2.745E-03	9.364E-04
H2CN	0.000E	2.263E-19	2.263E-19	2.717E-19	2.788E-19	2.852E-19
H2O	0.000E	2.153E-06	6.766E-02	1.826E-02	1.056E-02	3.601E-03
H2O2	0.000E	6.442E-09	2.339E-04	6.314E-05	3.650E-05	1.245E-05
N	0.000E	2.263E-19	2.263E-19	2.717E-19	2.788E-19	2.852E-19
NCO	0.000E	2.263E-19	2.263E-19	2.717E-19	2.788E-19	2.852E-19
NH	0.000E	2.263E-19	2.263E-19	2.717E-19	2.788E-19	2.852E-19
NH2	0.000E	2.263E-19	2.263E-19	2.717E-19	2.788E-19	2.852E-19
NH3	0.000E	2.263E-19	2.263E-19	2.717E-19	2.788E-19	2.852E-19
NNH	0.000E	2.263E-19	2.263E-19	2.717E-19	2.788E-19	2.852E-19
NO	0.000E	2.263E-19	2.263E-19	2.717E-19	2.788E-19	2.852E-19
NO2	0.000E	2.263E-19	2.263E-19	2.717E-19	2.788E-19	2.852E-19
N2	1.335E-01	1.335E-01	1.335E-01	6.128E-01	6.876E-01	7.551E-01
N2O	0.000E	2.263E-19	2.263E-19	2.717E-19	2.788E-19	2.852E-19
O	0.000E	2.059E-11	3.139E-14	6.968E-16	6.680E-17	8.084E-19
OH	0.000E	1.116E-09	1.570E-10	4.764E-12	1.614E-12	4.995E-13
O2	3.549E-02	3.549E-02	3.526E-02	1.628E-01	1.827E-01	2.007E-01
WH2O	2.679E-01	2.679E-01	2.008E-01	5.420E-02	3.133E-02	1.069E-02
WH2	7.067E-02	7.067E-02	5.297E-02	1.430E-02	8.265E-03	2.819E-03
WOH	2.094E-03	2.094E-03	1.570E-03	4.237E-04	2.449E-04	8.353E-05
WA1	9.490E-03	9.490E-03	8.485E-03	2.290E-03	1.324E-03	4.515E-04
WA2	6.524E-03	6.524E-03	6.495E-03	1.753E-03	1.013E-03	3.456E-04
WC1	3.330E-03	3.330E-03	3.228E-03	8.713E-04	5.036E-04	1.718E-04
WC2	1.270E-03	1.270E-03	1.231E-03	3.322E-04	1.920E-04	6.549E-05
WC3	1.904E-03	1.904E-03	1.905E-03	5.141E-04	2.972E-04	1.014E-04
WCO	2.098E-02	2.098E-02	2.034E-02	5.489E-03	3.173E-03	1.082E-03
WCO2	1.335E-02	1.335E-02	1.294E-02	3.494E-03	2.019E-03	6.888E-04
WCR1	0.000E	2.263E-19	2.263E-19	2.717E-19	2.788E-19	2.852E-19
WCR2	0.000E	2.263E-19	2.263E-19	2.717E-19	2.788E-19	2.852E-19
WCR3	0.000E	2.263E-19	2.263E-19	2.717E-19	2.788E-19	2.852E-19
WCR4	0.000E	2.263E-19	2.263E-19	2.717E-19	2.788E-19	2.852E-19
WCR5	0.000E	2.263E-19	2.263E-19	2.717E-19	2.788E-19	2.852E-19
WCR6	0.000E	2.263E-19	2.263E-19	2.717E-19	2.788E-19	2.852E-19
WCR7	0.000E	2.263E-19	2.263E-19	2.717E-19	2.788E-19	2.852E-19
WTCD	2.226E-02	2.226E-02	2.157E-02	5.823E-03	3.366E-03	1.148E-03
WTCO	2.365E-01	2.365E-01	2.292E-01	6.188E-02	3.577E-02	1.220E-02
WTC1	9.102E-02	9.102E-02	8.823E-02	2.382E-02	1.377E-02	4.695E-03
WTC2	6.602E-02	6.602E-02	6.399E-02	1.727E-02	9.984E-03	3.405E-03
WTH2	1.767E-02	1.767E-02	1.712E-02	4.623E-03	2.672E-03	9.113E-04
WTHCN	0.000E	2.263E-19	2.263E-19	2.717E-19	2.788E-19	2.852E-19
TCO	0.000E	7.620E-09	5.858E-03	1.581E-03	9.140E-04	3.118E-04
TCO2	0.000E	7.164E-10	1.678E-05	4.528E-06	2.617E-06	8.921E-07
TC1	0.000E	2.933E-09	2.583E-03	6.974E-04	4.031E-04	1.375E-04
TC2	0.000E	2.127E-09	2.008E-03	5.421E-04	3.134E-04	1.069E-04
TH2	0.000E	5.693E-10	5.448E-04	1.471E-04	8.501E-05	2.899E-05
THCN	0.000E	2.263E-19	2.263E-19	2.717E-19	2.788E-19	2.852E-19

RH2O	0.000E	2.263E-19	2.263E-19	2.717E-19	2.788E-19	2.852E-19
RA1	0.000E	2.263E-19	2.263E-19	2.717E-19	2.788E-19	2.852E-19
RHCN	0.000E	2.263E-19	2.263E-19	2.717E-19	2.788E-19	2.852E-19
CHR1	0.000E	2.263E-19	2.263E-19	2.717E-19	2.788E-19	2.852E-19
CHR2	0.000E	2.263E-19	2.263E-19	2.717E-19	2.788E-19	2.852E-19
CHR3	0.000E	2.263E-19	2.263E-19	2.717E-19	2.788E-19	2.852E-19
CHR4	0.000E	2.263E-19	2.263E-19	2.717E-19	2.788E-19	2.852E-19
CHR5	0.000E	2.263E-19	2.263E-19	2.717E-19	2.788E-19	2.852E-19
CHR6	0.000E	2.263E-19	2.263E-19	2.717E-19	2.788E-19	2.852E-19
CHR7	0.000E	2.263E-19	2.263E-19	2.717E-19	2.788E-19	2.852E-19
WOOD	8.310E-01	8.310E-01	7.301E-01	1.971E-01	1.139E-01	3.885E-02
TAR	0.000E	1.397E-08	1.101E-02	2.972E-03	1.718E-03	5.860E-04
CHAR	0.000E	1.584E-18	1.584E-18	1.902E-18	1.952E-18	1.996E-18
NOx 0%O2dry	0.000E	1.313E-19	1.313E-19	5.849E-19	1.040E-18	3.146E-18
NOx 0%O2wet	0.000E	1.176E-19	1.176E-19	4.689E-19	9.233E-19	3.028E-18
NOx #/MMBTU	0.000E	1.437E-16	1.437E-16	6.392E-16	1.135E-15	3.403E-15
NOx #/TON DF	0.000E	2.346E-15	2.346E-15	1.043E-14	1.852E-14	5.554E-14
ProNO	0.000E	0.000E	0.000E	0.000E	0.000E	0.000E
DesNO	0.000E	0.000E	0.000E	0.000E	0.000E	0.000E
NetNO	0.000E	0.000E	0.000E	0.000E	0.000E	0.000E
ProNO2	0.000E	0.000E	0.000E	0.000E	0.000E	0.000E
DesNO2	0.000E	0.000E	0.000E	0.000E	0.000E	0.000E
NetNO2	0.000E	0.000E	0.000E	0.000E	0.000E	0.000E

MOLE FRACTIONS X(I)

SPECIES "I"	11
C	2.879E-19
CH	2.879E-19
CH2	2.879E-19
CH2CO	2.879E-19
CH2O	2.879E-19
CH2OH	2.879E-19
CH2(S)	2.879E-19
CH3	2.879E-19
CH3O	2.879E-19
CH4	2.879E-19
CN	2.879E-19
CO	2.095E-15
CO2	2.911E-02
C2H	2.879E-19
C2H2	2.879E-19
C2H3	2.879E-19
C2H4	2.879E-19
C2H5	2.879E-19
C2H6	2.879E-19
C2N2	2.879E-19
C3H2	2.879E-19
C3H3	2.879E-19
C4H2	2.879E-19
C4H3	2.879E-19
H	5.894E-19

HCCO	2.879E-19
HCCOH	2.879E-19
HCN	2.879E-19
HCNO	2.879E-19
HCO	2.879E-19
HNCO	2.879E-19
HNO	6.616E-17
HOCN	2.879E-19
HO2	1.884E-11
H2	1.022E-14
H2CN	2.879E-19
H2O	3.763E-02
H2O2	2.333E-12
N	2.879E-19
NCO	2.879E-19
NH	2.879E-19
NH2	2.879E-19
NH3	2.879E-19
NNH	2.879E-19
NO	2.750E-06
NO2	6.324E-07
N2	7.621E-01
N2O	2.282E-10
O	7.284E-14
OH	8.935E-10
O2	1.712E-01
WH2O	2.879E-19
WH2	2.879E-19
WOH	2.032E-10
WA1	2.879E-19
WA2	2.879E-19
WC1	2.879E-19
WC2	2.879E-19
WC3	2.879E-19
WCO	2.879E-19
WCO2	2.879E-19
WCR1	2.879E-19
WCR2	2.879E-19
WCR3	2.879E-19
WCR4	2.879E-19
WCR5	2.879E-19
WCR6	2.879E-19
WCR7	2.879E-19
WTCD	2.879E-19
WTCO	2.879E-19
WTC1	2.879E-19
WTC2	2.879E-19
WTH2	2.879E-19
WTHCN	2.879E-19
TCO	2.879E-19
TCO2	2.879E-19
TC1	2.879E-19
TC2	2.879E-19

TH2	2.879E-19
THCN	2.879E-19
RH2O	2.879E-19
RA1	2.879E-19
RHCN	2.879E-19
CHR1	2.879E-19
CHR2	2.879E-19
CHR3	2.879E-19
CHR4	2.879E-19
CHR5	2.879E-19
CHR6	2.879E-19
CHR7	2.879E-19
WOOD	2.032E-10
TAR	1.727E-18
CHAR	2.015E-18
NOx 0%O2dry	1.848E-05
NOx 0%O2wet	1.779E-05
NOx #/MMBTU	1.999E-02
NOx #/TON DF	3.263E-01
ProNO	0.000E
DesNO	0.000E
NetNO	0.000E
ProNO2	0.000E
DesNO2	0.000E
NetNO2	0.000E

Bibliography

[1] "Biomass Thermal Efficiencies" [Online]. Available: http://www.nrel.gov/docs/fy00osti/26946.pdf. [Accessed: 16-Aug-2014].

[2] "Fossil Fule Plant Efficiencies - EIA" [Online]. Available: http://www.eia.gov/electricity/annual/html/epa_08_01.html. [Accessed: 16-Aug-2014].

[3] 2012, The Handbook of Biomass Combustion and Co-firing, Earthscan.

[4] Malte, P., 2012, "Renewable Energy - Introduction to Bio-Energy" [Online]. Available: https://courses.washington.edu/enenv442/Notes/2013/44213_L5_Bio1.pdf. [Accessed: 06-Jun-2014].

[5] "NSF MUSES: Cellulosic Ethanol: A Future Fuel from Forests" [Online]. Available: http://www.sfi.mtu.edu/FutureFuelfromForest/LignocellulosicBiomass.htm. [Accessed: 06-Jun-2014].

[6] Processing, T., 2011, Thermochemical Processing of Biomass, John Wiley & Sons, Ltd, Chichester, UK.

[7] "What is Lignin? | Lignoworks" [Online]. Available: http://www.lignoworks.ca/content/what-lignin. [Accessed: 19-Jul-2014].

[8] "Biofuels production drives growth in overall biomass energy use over past decade - Today in Energy - U.S. Energy Information Administration (EIA)" [Online]. Available: http://www.eia.gov/todayinenergy/detail.cfm?id=15451. [Accessed: 07-Jun-2014].

[9] "Residential Energy Consumption Survey (RECS) - Data - U.S. Energy Information Administration (EIA)" [Online]. Available: http://www.eia.gov/consumption/residential/data/2009/index.cfm?view=characteristics. [Accessed: 09-Jun-2014].

[10] 2013, Biomass Combustion Science, Technology and Engineering, Elsevier Science.

[11] 1981, Wood Combustion: Principles, Processes, and Economics [Hardcover], Academic Pr.

[12] Park, H. J., Park, Y.-K., Dong, J.-I., Kim, J.-S., Jeon, J.-K., Kim, S.-S., Kim, J., Song, B., Park, J., and Lee, K.-J., 2009, "Pyrolysis characteristics of Oriental white oak: Kinetic study and fast pyrolysis in a fluidized bed with an improved reaction system," Fuel Process. Technol., **90**(2), pp. 186–195.

[13] "GRI-Mech Home Page" [Online]. Available: http://www.me.berkeley.edu/gri-mech/. [Accessed: 20-Jul-2014].

[14] "Stephen R. Turns An Introduction to Combustion- Concepts and Applications 2000.pdf."

[15] Glassman, I., 2012, Combustion, Elsevier Science.

[16] Di Blasi, C., 2008, "Modeling chemical and physical processes of wood and biomass pyrolysis," Prog. Energy Combust. Sci., **34**(1), pp. 47–90.

[17] Prakash, N., and Karunanithi, T., 2008, "Kinetic Modeling in Biomass Pyrolysis – A Review," J. Appl. Sci. Res., **4**(12), pp. 1627–1636.

[18] Novosselov, I. V, 2001, "Eight-Step Global Kinetic Mechanism on Methane Oxidation with Nitric Oxide Formation for Lean- Premixed Combustion Turbines."

[19] Novosselov, I. V, 2006, "Chemical Reactor Networks for Combustion Systems Modeling," Phd Diss.

[20] Nr, E. F., and Nussbaumer, T., 1997, "Furnace Design and Combustion Control to Reduce Emissions and Avoid Ash Siagging," (194010).

[21] Sustainable, M., Technology, E., Eindhoven, T. U., and Technology, S. C., 2009, "SOOT FORMATION OF LIGNIN DERIVED FUELS IN A LAMINAR CO-FLOW DIFFUSION FLAME," (July).

[22] Mba, M., 2010, "Techno- - Economic and Environmental Opportunities for Biomass Heat and Power Generation," (319).

[23] Skreiberg, Ø., and universitet, N. teknisk-naturvitenskapelige, 1997, Theoretical and Experimental Studies on Emissions from Wood Combustion, Norwegian University of Science and Technology, Faculty of Mechanical Engineering, Department of Thermal Energy and Hydropower.

[24] Johansson, L. S., Leckner, B., Gustavsson, L., Cooper, D., Tullin, C., and Potter, A., 2004, "Emission characteristics of modern and old-type residential boilers fired with wood logs and wood pellets," Atmos. Environ., **38**(25), pp. 4183–4195.

[25] Klason, T., 2006, Modelling of Biomass Combustion in Furnaces, Media Tryck AB.

[26] Vassilev, S. V., Baxter, D., Andersen, L. K., and Vassileva, C. G., 2010, "An overview of the chemical composition of biomass," Fuel, **89**(5), pp. 913–933.

[27] Nicol, D. G., 1995, A Chemical Kinetic and Numerical Study of NOx and Pollutant Formation in Low-emission Combustion, University of Washington.

[28] Nunn, T. R., Howard, J. B., Longwell, J. P., and Peters, W. A., 1985, "Product Compositions and Kinetics in the Rapid Pyrolysis of MiHed Wood Lignin," pp. 844–852.

[29] Boroson, M. L., Howard, J. B., Longwell, J. P., and Peters, W. a., 1989, "Heterogeneous cracking of wood pyrolysis tars over fresh wood char surfaces," Energy & Fuels, **3**(6), pp. 735–740.

[30] 1995, Combustion Fundamentals of Fire, Academic Press.

[31] Monaghan, R. F. D., Cuoci, A., Bourque, G., Fu, M., Gordon, R. L., Faravelli, T., Frassoldati, A., and Curran, H. J., 2012, "Detailed Multi-dimensional Study of Pollutant Formation in a Methane Diffusion Flame."

[32] Walsh, A. R., and Phd, "CFD MODELING OF WASTE-FUEL BOILER," p. 2.

[33] Ranzi, E., Cuoci, A., Faravelli, T., Frassoldati, A., Migliavacca, G., Pierucci, S., and Sommariva, S., 2008, "Chemical Kinetics of Biomass Pyrolysis," **4**(5), pp. 4292–4300.

[34] Gauthier, G., Melkior, T., Salvador, S., and Corbetta, M., 2013, "Pyrolysis of Thick Biomass Particles : Experimental and Kinetic Modelling," **32**, pp. 601–606.

[35] Hosoya, T., Kawamoto, H., and Saka, S., 2007, "Cellulose–hemicellulose and cellulose–lignin interactions in wood pyrolysis at gasification temperature," J. Anal. Appl. Pyrolysis, **80**(1), pp. 118–125.

[36] Sharp, 2014, "Sharp GP2Y1010AU0F Datasheet" [Online]. Available: https://www.sparkfun.com/datasheets/Sensors/gp2y1010au_e.pdf. [Accessed: 21-Aug-2014].

[37] Hulst, H. C., and Hulst, H. C. van de, 1957, Light Scattering by Small Particles, Courier Dover Publications.

[38] Scientific, V., 1998, "Mie Scattering Software" [Online]. Available: http://www.scattport.org/index.php/light-scattering-software?start=100. [Accessed: 21-Aug-2014].

[39] E2v, "MOS CO & HC Sensor" [Online]. Available: http://datasheet.octopart.com/MICS-5521-E2V-datasheet-8616644.pdf. [Accessed: 21-Aug-2014].

[40] Motech, "Technology / Sensors / MOS" [Online]. Available: http://www.uta.edu/rfmems/BMC/0720/AppliedSensor/Sensors_MOSpdf.pdf. [Accessed: 21-Aug-2014].

[41] Brockmann, J. E., Liu, B. Y. H., and McMurry, P. H., 1984, "A Sample Extraction Diluter for Ultrafine Aerosol Sampling," Aerosol Sci. Technol., **3**(4), pp. 441–451.

[42] 2011, Aerosol Measurement: Principles, Techniques, and Applications (Google eBook), John Wiley & Sons.

[43] "TSI Aerosol Diluter 3302A" [Online]. Available: http://www.tsi.com/uploadedFiles/_Site_Root/Products/Literature/Spec_Sheets/3302A.pdf. [Accessed: 17-Jun-2014].

[44] McMaster-Carr, "McMaster-Carr - High-Pressure Precision Stainless Steel Tubing, Type 304, 1/16' OD, 0.012' ID, .025" Wall, 1' Long" [Online]. Available: http://www.mcmaster.com/#51755k19/=tdmh26. [Accessed: 21-Aug-2014].

[45] Incropera, F. P., 2011, Introduction to Heat Transfer, John Wiley & Sons.

[46] "Solids - Specific Heats" [Online]. Available: http://www.engineeringtoolbox.com/specific-heat-solids-d_154.html. [Accessed: 06-Jul-2014].

[47] "Heating Value of Common Wood Species" [Online]. Available: http://www.hearth.com/econtent/index.php/articles/heating_value_wood. [Accessed: 06-Jul-2014].

[48] Simpson, W., and TenWolde, A., "Physical properties and moisture relations of wood," **113**.

[49] Pope, S. B., 2000, Turbulent Flows, Cambridge University Press.